NASA CR 72298, 1969
PWA-3470

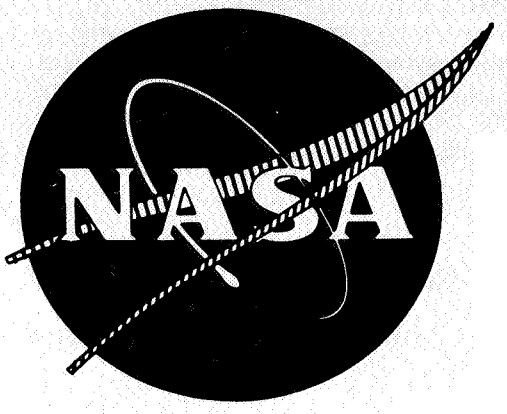

EXPERIMENTAL EVALUATION OF TRANSONIC STATORS

FINAL REPORT

PREPARED FOR

NATIONAL AERONAUTICS AND SPACE ADMINISTRATION

CONTRACT NAS3-7614

Pratt & Whitney Aircraft
DIVISION OF UNITED AIRCRAFT CORPORATION
EAST HARTFORD CONNECTICUT

NOTICE

This report was prepared as an account of Government sponsored work. Neither the United States, nor the National Aeronautics and Space Administration (NASA), nor any person acting on behalf of NASA:

A.) Makes any warranty or representation, expressed or implied, with respect to the accuracy, completeness, or usefulness of the information contained in this report, or that the use of any information, apparatus, method, or process disclosed in this report may not infringe privately owned rights; or

B.) Assumes any liabilities with respect to the use of, or for damages resulting from the use of any information, apparatus, method or process disclosed in this report.

As used above, "person acting on behalf of NASA" includes any employee or contractor of NASA, or employee of such contractor, to the extent that such employee or contractor of NASA, or employee of such contractor prepares, disseminates, or provides access to, any information pursuant to his employment or contract with NASA, or his employment with such contractor.

Requests for copies of this report should be referred to

National Aeronautics and Space Administration
Office of Scientific and Technical Information
P.O. Box 33
College Park, Maryland 20740

NASA CR-72298, 1969

EXPERIMENTAL EVALUATION OF TRANSONIC STATORS

FINAL REPORT

by

M. J. Keenan and J. A. Bartok

prepared for

NATIONAL AERONAUTICS AND SPACE ADMINISTRATION

CONTRACT NAS3-7614

Technical Management
NASA Lewis Research Center
Cleveland, Ohio
Lewis Project Manager: William L. Beede
Lewis Research Advisor: Calvin L. Ball

Pratt & Whitney Aircraft
DIVISION OF UNITED AIRCRAFT CORPORATION
EAST HARTFORD, CONNECTICUT

FOREWORD

The research described herein which was conducted by the Pratt & Whitney Aircraft Division of United Aircraft Corporation, was performed under NASA Contract NAS3-7614. Work was done under the project management of Mr. William L. Beede, Fluid System Components Division, NASA-Lewis Research Center, with Mr. Calvin L. Ball, Fluid System Components Division, NASA-Lewis Research Center, as research advisor.

ABSTRACT

Blade element performance of compressor stators designed to operate in the transonic Mach number range was investigated. Two multiple-circular-arc (MCA) stators, one double-circular-arc (DCA) stator and one slotted multiple-circular-arc stator with design diffusion factors in the range of 0.6 at the hub to 0.5 at the tip were tested to determine the effects of blade airfoil shape and slots on performance.

Total pressure loss levels in end regions for all stators were predominantly higher than those at midspan. It is believed that the high end wall losses overshadowed differences in loss levels due to different profile shapes.

The loss level measured in the mid-span region of the multiple-circular-arc stators when operated at the transonic Mach number range was lower than that of the double-circular-arc stator.

Slotting of the MCA Stator A to discharge high-energy air at the point of shock impingement on the suction surface showed no reduction of loss or increase in turning over the unslotted configuration.

TABLE OF CONTENTS

LIST OF ILLUSTRATIONS

LIST OF ILLUSTRATIONS (cont'd)

LIST OF ILLUSTRATIONS (cont'd)

LIST OF ILLUSTRATIONS (cont'd)

LIST OF TABLES

I. SUMMARY

The objective of this investigation was to obtain blade element data on a family of blade shapes which are considered suitable for stator blade sections that operate at high-flow Mach numbers. This new family of blade shapes, which has been designated multiple-circular-arc (MCA), is defined as two double-circular-arc blade segments joined at a common transition point. The forward and rearward portions of the blade are circular-arc sections of different radii. These blade shapes are intended to minimize the flow-turning over the forward portion of the blade consistent with flow choking limitations in order to reduce the losses associated with flow shocks.

The program included testing three different stator airfoil shapes. Two stators were designed with multiple-circular-arc airfoil elements with supersonic turning of 0.6 of an equivalent double-circular-arc airfoil. One multiple-circular-arc design (MCA Stator A) has the transition point between the low-curvature forward section and the high-curvature rearward section at the assumed shock position. The second design (MCA Stator B) has the transition point located to the rear of the shock. A third stator with double-circular-arc airfoils (DCA) provides a basis for comparison. A fourth stator consisted of the MCA Stator A vanes with a radial slot added in order to eject high-energy flow at the assumed point of shock impingement (MCA Stator A Slotted). The slot was added in an attempt to energize the suction-surface boundary layer and thereby to minimize the tendency toward flow separation.

Design stator inlet Mach numbers varied from 1.11 at the hub to 0.84 at the tip. Stator inlet flow was generated by an inlet guide vane and a flow-generating rotor. For all four stators, overall performance data and blade element data were obtained. Data on the inlet guide vanes and the rotor blade performance were obtained during the test of the first stator configuration (MCA-A). Distortions of flow caused by probe blockage at the stator inlet were significant. Also the inlet guide vanes and stators both caused significant circumferential distortions in total temperature, total pressure, and static pressure. These flow distortions were taken into account by the calculation procedure employed and by averaging the data obtained at various circumferential positions.

Data from all stator configurations showed high stator losses near the end walls, but at design speed mid-span losses were lower than the predicted design values. At mid-span, the stator minimum total pressure loss coefficient, $\overline{\omega}$, ranged from 0.056 to 0.075 at design speed for all four configurations. At 5

percent of span from the tip, the stator minimum total pressure loss coefficients ranged from 0.205 to 0.220; at 95 percent of span, they ranged from 0.238 to 0.250, compared with the design values of 0.070 at 5 percent span and 0.135 at 95 percent span.

Increased transonic acceleration of the airflow along the highly cambered forward portion of the DCA stator, as indicated in the design analysis and test results, leads to higher surface Mach numbers and consequently higher losses.

Reduced shock losses in the MCA stators gave a significant improvement in stage performance over the DCA stator configuration at 110 and 120 percent of design speed. At 50 and 100% of design speed losses were about the same for MCA and DCA stators.

At design speed the DCA stator had minimum loss at incidence angles 1 to 3 degrees lower than the MCA stators. At high incidence angles, the losses for the DCA stator were higher than those for the MCA stators. At low incidence angles, the losses for the DCA stator were lower than those for the MCA stators. This gave the stage with the DCA stator more flow capacity at design speed than the MCA stator configurations; but the MCA stators, with their lower losses at positive incidence, gave higher pressure ratios at stall than the DCA stator. At lower speeds (lower Mach numbers), the minimum loss incidence angle and loss level were approximately the same for all configurations, thus the stage performances were nearly equal. Above 100% of design speed the maximum attainable flow for the DCA stator was less than that for the MCA stators. The reduced flow capacity is believed to be caused by choking at the stator trailing edge where boundary layer displacement thicknesses occupied so much of the stator exit annulus area that free-stream flow was choked.

Deviation angles were higher near end walls than at mid span for all stators. The level of MCA deviation angles was higher than that of the DCA stator. The MCA stators had greater deviation angles than design estimates. In contrast, the DCA deviations were lower than design, except near the end walls. The increased deviation near blade ends appears to be a secondary flow effect.

Blade element losses were higher for the slotted MCA stator A than for the unslotted stator at higher transonic Mach numbers except at 10% of span where minimum loss for the slotted stator was inexplicably lower. At subsonic Mach numbers, there was little difference between minimum loss values for slotted and unslotted stators. At 110% of design speed, the slotted stator had minimum loss at higher incidence angles near the hub, but losses at positive incidences were

no lower than for the unslotted stator. This resulted in lower flow capacity for the stage with the slotted stator. Pressure ratio at stall was the same for both stages, but stall occurred at a lower weight flow for the stage with the slotted stator. No significant differences in deviation were apparent between the slotted and unslotted stators.

II. INTRODUCTION

For future turbine power plants, higher stage pressure ratios are desired and adequate stage flow range must be achieved at these increased work levels. Increased stage pressure ratio can lead to increased stator blade inlet Mach numbers. The objective of this investigation was to obtain data on a new family of blade shapes considered suitable for stators operating at high flow Mach numbers. Airfoil sections of this family of blade shapes, designated as multiple-circular-arc (MCA) blading are defined by two double-circular-arc blade segments joined at a common transition point. Forward and rearward segments of the blade are double-circular-arc (DCA) segments of different radii. These blade shapes are aimed at controlling the flow turning over the forward portion of the blade with respect to total turning to minimize losses associated with flow shocks. A parallel experimental program on this new family of blade shapes was conducted on rotor blading (Reference 1).

Four stator configurations, one DCA, two MCA, and a slotted MCA, were tested in combination with an inlet guide vane and a flow generation rotor. Complete design information except for the slot design is given in Reference 2. The DCA airfoil stator was designed and tested to provide a basis for comparing the performance of the MCA stators. The performance data obtained on this stator is given in Reference 3. The two MCA stators had supersonic turning equal to 0.6 of that for an equivalent DCA stator. Performance of the MCA Stator A which had the transition point between the low curvature forward section and the rearward section at the assumed passage shock position is presented in Reference 4. Inlet guide vane and rotor performance are also given in Reference 4. Performance of the MCA Stator B with its transition point aft of the shock position, is given in Reference 5.

The MCA Stator A was slotted to energize the suction surface boundary layer at the shock impingement point with high energy air bled from the pressure surface. The slot was added in an attempt to minimize the effect of shock-boundary layer interaction and permit efficient diffusion along the rearward portion of the blade. The slot design and the slotted stator performance are presented in Reference 6.

This report presents a comparison of the performance of the four stator configurations.

III. COMPRESSOR DESIGN

A. General Design Approach

Research stators were designed for an inlet relative Mach number of 1.1 at the hub and an inlet flow angle of 48°. The stator blading was designed to turn the flow back to the axial direction at all radii. These stator inlet flow conditions approximated those for a highly-loaded, high-pressure-ratio stage with axial flow into the rotor. The flow-generation rotor was designed to be compatible with stator specifications. To keep the rotor design within current technology, guide vanes were used to develop part of the stator inlet swirl. The rotor was designed to produce a constant total pressure ratio from hub to tip of 1.55, which ensured that test stand duct losses would not limit rig operation at high flow rates.

A constant outer diameter was selected in order to simplify fabrication, reduce rotor-tip clearance problems, and to provide a smooth platform from which to mount interstage instrumentation probes. The outer diameter of 31 inches was selected because it was large enough to permit application of the results to future gas turbine engine designs without regard for scale effects and because it was compatible with the size limitations of the test facility. A rotor root inlet diameter of 16.6 inches was also selected.

The absolute velocity vector at the rotor root exit was determined by stator inlet requirements and was variable only as a function of wheel speed. The relative velocity vector was set at 16 degrees past axial, resulting in a wheel speed of 643 ft/sec at the rotor root exit.

With exit swirl and wheel speed established for the rotor root section, Euler's equation was used to calculate the rotor inlet swirl required to meet the pressure ratio requirement. A free-vortex rotor inlet swirl was selected to define the radial variation of turning for the inlet guide vane.

Inlet flow per unit of annulus area was 36.0 $lb/ft^2/sec$. Lower values of inlet flow per unit of annulus area would require increased camber on the inlet guide vane and rotor as well as increased flowpath curvatures. The selected flow was well within the state of the art and provided acceptable values for camber and flowpath curvature.

The design corrected weight flow for the rotor was 135 lbs per second and the design tip speed was 1197 ft per second.

Axial spacing between blade rows was larger than that which might be used in an actual engine in order to provide space for instrumentation. A spacing equal

to fifty percent of the inlet guide vane chord (1.75 inches) was provided between the inlet guide vane and rotor. A spacing of 1.5 inches was provided between the rotor and the test stator. A cross-section of the test compressor is shown in Figure 1.

Mechanical design included a structural and vibratory analysis. Combined stresses produced by centrifugal force, gas bending, and untwist were well within the capability of the AMS titanium alloy used for the rotor blades. The fatigue characteristics of the alloy appeared to be adequate for the anticipated vibratory stress. All critical speeds were outside the operating range. (See Reference 2 for complete details of aerodynamic and mechanical design.)

B. Stator Designs

Details of the stator designs are given in Reference 2, with the exception of the slotted stator design, which is given in Reference 6. A summary of the stator designs is presented herein.

The stators were designed to operate in the transonic Mach number range with design diffusion factors of 0.5 at the tip to 0.6 at the hub. Stator losses were estimated by the method presented in Reference 2, which accounted for a shock loss plus the diffusion loss. The shock-loss calculation method of Reference 7 was modified in accordance with Reference 2 to permit calculation of shock losses for high subsonic inlet Mach numbers as well as for supersonic inlet Mach numbers. The diffusion loss was calculated in accordance with Reference 8. Design inlet Mach number and the estimated suction surface Mach number ahead of the passage shock for three sets of stators are shown in Figure 2. The average of the suction surface Mach number and the inlet Mach number was used to calculate a shock loss. Design values of the total pressure loss coefficient ($\bar{\omega}$) and the diffusion factor are presented in Figures 3 and 4. The MCA stators had a slightly higher diffusion factor over most of the span than the DCA stator because of the slight reduction in axial velocity at the stator outlet for the MCA stators resulting from their lower estimated losses. The deviation angles for the three stators were estimated using Carter's rule, modified in accordance with Reference 9 to account for changes in camber distribution.

Multiple-Circular-Arc Stator A

A cross-section of a multiple-circular-arc blade, showing blade element geometry, may be found in Figure 5. The transition point between the forward and rearward double-circular-arc sections for the MCA-A airfoil was located at the assumed shock location, as was the maximum thickness point. The supersonic suction-surface camber was set at 0.6 of that of the a DCA stator. The 0.6 value was selected based upon a minimum value which was considered

consistent with flow choking limitations. Rear-section camber for the MCA stators was selected to obtain axial exit flow. Figure 6 is a photograph of the multiple-circular-arc stator A blade. Blade geometry for eight streamlines is summarized in Table I.

TABLE I

DESIGN DATA, MCA STATOR A

(Station 8 - Station 9)

	Percent of Stator Leading Edge Span From O.D.							
	5*	10	30	50	70	80*	90	95*
Inlet Dia.	30.54	30.02	28.18	26.35	24.52	23.60	22.69	22.30
Exit Dia.	30.60	30.05	28.38	26.74	25.11	24.32	23.53	23.24
β_8	41.63	41.46	41.57	42.55	44.02	45.04	46.89	48.08
β_9	0.0	0.0	0.0	0.0	0.0	0.0	0.0	0.0
σ	1.412	1.437	1.525	1.627	1.740	1.803	1.870	1.896
t/c	0.078	0.076	0.068	0.060	0.052	0.048	0.044	0.042
c	2.155	2.155	2.155	2.155	2.155	2.155	2.155	2.155
i_m	11.2	11.1	10.3	9.3	7.9	7.1	6.2	5.8
$\delta°$	9.5	9.2	8.6	8.5	8.7	9.0	9.7	9.8
ϕ_m	39.9	39.56	39.87	41.76	44.84	46.92	50.13	52.30
ϕ_{sps}	10.90	10.57	9.88	9.61	9.70	9.84	10.34	10.82
$\gamma°$	17.40	17.38	17.95	18.67	19.28	19.88	20.60	21.05

* Blade element data was not obtained at these spanwise locations during MCA Stator A (unslotted) tests.

Multiple-Circular-Arc Stator B

The MCA Stator B differed from the MCA Stator A in that the transition point was located behind the assumed shock location by rotating a line through an angle (Z) of 12 degrees as shown in Figure 5. The maximum-thickness point and the transition point are coincident, but locating the transition point behind the assumed shock reduces the rate of turning immediately behind the shock. It was thought that the reduced rate of turning immediately behind the shock would tend to reduce the effects of boundary layer interaction and the tendency towards flow separation behind the shock, resulting in lower losses. A summary of the stator design geometry for the eight streamlines at which blade element data were obtained is given in Table II.

TABLE II

DESIGN DATA, MCA STATOR B

(Station 8 - Station 9)

	Percent of Stator Leading Edge Span From O.D.							
	5	10	30	50	70	80	90	95
Inlet Dia.	30.54	30.02	28.18	26.35	24.52	23.60	22.69	22.30
Exit Dia.	30.60	30.05	28.38	26.74	25.11	24.32	23.53	23.24
β_8	41.63	41.46	41.57	42.55	44.02	45.04	46.89	48.08
β_9	0.0	0.0	0.0	0.0	0.0	0.0	0.0	0.0
σ	1.412	1.437	1.525	1.627	1.740	1.803	1.870	1.896
t/c	0.078	0.076	0.068	0.060	0.052	0.048	0.044	0.042
c	2.155	2.155	2.155	2.155	2.155	2.155	2.155	2.155
i_m	8.1	8.0	8.0	6.9	6.0	5.5	5.0	4.5
$\delta°$	12.4	11.8	10.5	10.0	10.1	10.2	10.8	11.1
ϕ_m	45.65	45.12	44.49	45.6	47.98	49.68	52.53	54.30
ϕ_{sps}	10.92	10.60	9.90	9.60	9.68	9.86	10.33	10.80
$\gamma°$	18.20	18.19	18.42	19.00	20.15	21.04	22.12	22.75

Double-Circular-Arc Stator

The double-circular-arc stator, which has been used extensively for transonic blading, is an airfoil in which the transition point and the maximum-thickness point are at mid-chord, and the forward and rearward portions of the blade are circular-arc sections of the same radii. The DCA blade sections were designed for the same stator inlet flow conditions and the same outlet flow angle as the MCA Stators A and B. The DCA stator was designed and tested to provide a reference for evaluating the performance of the two stators using the MCA blade shapes. It has 1.67 times the supersonic suction surface camber of the MCA blades, giving higher acceleration in the supersonic flow region ahead of the shock. A summary of the DCA stator design geometry for the eight streamlines at which blade element data were obtained is presented in Table III.

TABLE III

DESIGN DATA, DCA STATOR

(Station 8 - Station 9)

	Percent of Stator Leading Edge Span From O. D.							
	5	10	30	50	70	80	90	95
Inlet Dia.	30.54	30.02	28.18	26.35	24.52	23.60	22.69	22.30
Exit Dia.	30.60	30.05	28.38	26.74	25.11	24.32	23.53	23.24
β_8	41.63	41.46	41.57	42.55	44.02	45.04	46.89	48.08
β_9	0.0	0.0	0.0	0.0	0.0	0.0	0.0	0.0
σ	1.412	1.437	1.525	1.627	1.740	1.803	1.870	1.896
t/c	0.078	0.076	0.068	0.060	0.052	0.048	0.044	0.042
c	2.155	2.155	2.155	2.155	2.155	2.155	2.155	2.155
i_m	7.5	7.3	6.4	5.5	4.6	4.2	3.8	3.6
$\delta°$	8.1	8.0	7.7	7.7	7.9	8.2	8.6	8.8
ϕ_m	42.00	42.06	43.00	44.73	47.36	49.04	51.60	53.40
ϕ_{sps}	18.29	17.71	16.48	16.01	16.15	16.50	17.28	18.06
$\gamma°$	13.10	13.20	13.72	14.80	15.72	16.20	16.90	17.35

Multiple-Circular-Arc Stator A (Slotted)

After the MCA Stator A had been tested, two stator slots were machined, one from the tip to 40 percent of span and the second from 60 percent of the span to the hub. Airflow entered the slot on the pressure surface and was ejected into the flow stream at the assumed point of shock impingement. Typical blade spacing and a typical slot location are shown in Figure 7. A summary of the stator design geometry for the eight streamlines at which blade element data were obtained is presented in Table I. A summary of the stator slot design geometry for four percentages of span is presented in Table IV. Slot geometry nomenclature is given in Figure 8. Photographs of the MCA Stator A (Slotted) are presented in Figure 9.

TABLE IV

DESIGN DATA, MCA STATOR A (SLOTTED)

	Percent of Stator Leading Edge Span From O. D.			
	10	30	70	90
Inlet Dia., Inches	30.02	28.18	24.52	22.69
Wedge Angle, Degrees	10	10	10	10
Slot Throat, Inches	0.038	0.038	0.036	0.036
*Discharge Angle, Degrees	20	19	23	21
Front Coanda Radius, Inches	0.275	0.275	0.181	0.181
Rear Coanda Radius, Inches	0.122	0.122	0.082	0.082
X/c at Slot Inlet	0.169	0.155	0.195	0.204
X/c at Slot Exit	0.339	0.320	0.308	0.316
Trailing Edge Radius of Front Section, Inches	0.005	0.005	0.005	0.005
Leading Edge Radius of Rear Section, Inches	0.015	0.015	0.010	0.010

*Angle between slot centerline and a line tangent to blade suction surface at the point of intersection

IV. TEST FACILITY AND INSTRUMENTATION

A. Compressor Test Facility

The compressor test facility (Figure 10) was equipped with a gas-turbine-drive engine using a 2.1:1 gearbox for optimum speed-range capability. Air entered through a nozzle calibrated for flow measurements and flowed through a straight 72-foot section of 42-inch-diameter pipe to an inlet plenum 90 inches in diameter. A wire-mesh screen and an "egg-crate" structure located midway through the plenum ensured uniform pressure to the compressor.

The compressor airflow exhausted into a toroidal collector before entering a discharge stack six feet in diameter. A valve, also six feet in diameter, in the stack provided back pressure for the compressor. Two smaller valves, one 24-inch and one 12-inch located in bypass lines provided vernier control of back pressure.

B. Instrumentation

Airflow was measured with a flow nozzle designed to ISA specifications (Reference 10). Compressor speed was measured with an impulse-type pickup (an electromagnetic device that counts the number of gear teeth passing within a prescribed time interval and converts the count to rpm). Figure 11 shows the axial position of the instrumentation stations and their number designations. Figure 12 shows the circumferential positions of the instrumentation.

Instrumentation was located to balance out the effects of the inlet guide vane wakes, which shadow downstream through the rotor and stator, and to account partially for the effect of local back-pressuring of the rotor by the stator. The magnitude of these effects is discussed in the Procedure section of this report.

Three high-frequency-response total pressure probes with quartz crystal transducers as sensors were located behind the rotor near the outer case at Station 6 (Figure 12). These probes were spaced circumferentially to determine the number of rotating stall cells and their rotating speed. After MCA Stator A had been tested, these probes were removed because there was no evidence of rotating stall as back-pressure was increased to the point were a rapid fall-off in flow occurred indicating a stalled condition. This rapid fall-off in flow was used to define the stalled condition for the follow-on tests.

Two total-pressure wake rakes (Figure 13a), each with thirteen impact tubes equally spaced across a stator gap, were traversed radially behind the stator. These were spaced circumferentially so as to average out the effects of the inlet guide vane wakes. Five total-temperature radial rakes (Figure 13b) with

shielded thermocouples were located downstream of the stator on an extension of the stator mid-channel streamline and were spaced circumferentially to average-out the effects of the inlet guide vane wakes.

Following the testing of the MCA Stator A, one circumferential temperature rake (Figure 13c), consisting of six shielded thermocouples equally spaced across a stator gap, was installed at Station 10. This temperature rake was traversed radially behind the stator to determine the circumferential variation in the total temperature across a stator gap at five radial positions. These data were used to adjust the temperature measured at the stator mid-gap to account for the temperature variation across the gap. The information obtained from the circumferential temperature rake during the test on MCA Stator B was applied to the MCA Stator A analysis. (See Reference 4 for details.)

There were four static pressure taps on the hub and case at each instrumentation plane. At Station 7, ten additional taps equally spaced across a stator vane gap were added. For reducing the data, four of the 14 OD and ID wall static pressures, which would average out any circumferential distortions caused by inlet guide vane wakes or stator blockage effects, were used.

Disk probes (Figure 13d) were used to measure the radial distributions of static and total pressure and air angle. There were two disk probes at the stator inlet and exit stations located on extensions of the stator mid-channel streamlines and spaced circumferentially to average out any inlet guide vane wake effects. All disk probes were calibrated for their expected Mach number operating range.

Before the slotted stator was tested, four static pressure taps were installed at the throat of the stator slot at 30 percent and 70 percent of span to measure the slot flow.

Stator surfaces were instrumented with static pressure taps at 10 and 90 percent of blade height from the tip, and additional static pressure taps were installed at the stator hub mid-channel surface. The surface taps were used to determine surface pressure coefficients, and the hub mid-channel taps were used to determine the channel static pressure gradient. The airfoil slot of the slotted stator configuration interrupted the leads of the blade surface taps forward of 35 percent of chord.

Chromel-alumel type "K" wire, calibrated over full operating temperature ranges, was used for all temperature-measuring rakes and for the lead wire. Recovery calibrations for Mach number were based on test measurements. Pressure corrections were applied as noted in Reference 11.

Disk-probe pressures were measured with transducers; all other pressures were measured with precision-bore manometer tubes of 0-80 inches range. Water, acetylene tetrabromide, and mercury were used as manometer liquids.

Stationary and rotating parts were instrumented with strain gages to determine the levels of vibratory stress over the operating range of the compressor.

V. PROCEDURE

A. Test Procedure

Over-all and blade element performance tests for the rotor and MCA Stator A were run at 50, 70, 90, 95, 100 and 110 percent of design speed. Five data points were obtained at each speed from open throttle to near-stall.

In the original test plan, tests were scheduled at 95 percent of design speed to obtain data at an inlet Mach number of approximately 1.0 at the stator hub. However, analysis of the data from MCA Stator A showed that inlet Mach numbers were lower than design values, and tests of all other configurations used 120 percent of design speed in place of 95 percent to obtain the higher Mach number data.

For all stator configurations, five complete data points and one near-stall point were obtained except at 120 percent speed. For the MCA Stator B and the DCA Stator, the near-stall point at 120 percent speed was not run because a severe stall, with the small tip clearances, might have damaged the test rig. During the MCA Stator A (Slotted) test, only one data point was obtained at 120 percent of design speed due to a rotor blade failure.

Complete data points included radial traverse measurements of total pressure, static pressure, and air angle before and after the stator. Wake-rake traverses of stator exit total temperature and pressure were also taken. Near-stall points were run without traversing ahead of the stator.

Vibratory stress of the rotor and stator was surveyed during the testing of MCA Stator A up to 110 percent of design speed and over a range of flows from wide-open throttle to near-stall. During the MCA Stator B test program, this survey was extended to 120 percent of design speed. Vibratory stress was monitored on open-throttle and near-stall operating lines between 110 and 120 percent of design speed, and on the 120 percent-speed line between open throttle and near-stall. Mechanical limitations were not evident during these tests.

At the start of the MCA stator A tests the stress survey was followed by a survey of rotating stall, in which rapid-response transducers were used to record rotor exit total pressure as a function of time. There was no evidence of rotating stall as the back-pressure was increased to the point where a rapid fall-off in flow occurred indicating a stalled condition. This rapid fall-off in flow was used to define the stall condition for the follow-on tests.

Shakedown testing showed that full immersion of a traverse probe at the stator inlet at high speeds caused large circumferential distortions, and these affected the readings of most fixed instrumentation and of the other traverse probes in the airstream. This was attributed to the probes causing local flow choking as

a result of the high flow Mach numbers. Traverse probes at the stator inlet were consequently run independently of other instrumentation for all speeds. The data obtained from these surveys was not used in the evaluation of blade element performance, but at the lower Mach numbers was used to check the streamline calculation procedure.

Shakedown testing also showed that full immersion of a traverse probe at the stator inlet reduced flow by approximately three percent. This reduction made it necessary to set the "near-stall" point three percent above stall flow in order to avoid stall while taking data.

Analysis of data from MCA Stator A tests showed that loss coefficients near the stator hub were still decreasing as stall was approached. To define more complete plots of total pressure loss versus incidence, additional data points were added within one percent of stall flow in all subsequent tests. To prevent stall, no stator inlet traverses were made for these points.

B. Calculation Procedure

Circumferential variations in total temperature were measured at the stator exit. Data from the MCA stator B tests are presented to illustrate this effect. Figure 14 shows the temperatures measured at 90 percent of span at 110 percent speed with wide-open throttle. Temperature is plotted versus position relative to inlet guide vanes in Figure 14a. Fixed rake temperatures were measured at stator mid-gap, and variation in these temperatures is an inlet guide vane effect. The difference between the curve drawn through fixed-rake measurements and the circumferential rake temperatures is a stator effect, and differences are plotted versus position relative to stators in Figure 14b. The temperature variation in Figure 14 is an extreme example and is not typical of all temperature data. As shown in Reference 4, distortions are less pronounced at 10 and 50 percent of span for the same data point. Lowest distortions were measured near minimum stator loss, and the level of variation decreased as Mach number decreased. The cyclic temperature pattern may be explained by a tendency for rotor wake flow to migrate toward stator pressure surfaces, as explained in Reference 12, or by local throttling at the rotor exit caused by stator blockage in high-Mach-number flow. The maximum differences between mid-gap and circumferential rake temperatures were correlated as a function of inlet Mach number (Figure 15). Similar distortions in static pressure and total pressure were also observed.

The calculation procedure used appropriately spaced instrumentation to average out the circumferential distortions in total temperature, total pressure, and static pressure. The magnitude of the distortions of the static pressure and total pressure and the averaging techniques employed at each instrumentation station are discussed in detail in Reference 4.

Because circumferential distortions in total temperature across stator gaps had not been anticipated, stator exit temperatures in the first test (MCA Stator A) were measured with five radial rakes located on extensions of stator mid-channel streamlines. Performance data were inconsistent due to inadequate temperature sampling, and the tests of the remaining stator configurations had additional instrumentation to measure gapwise distributions of temperature. Rotor performance obtained during the testing of MCA Stator B, which included the effect of the stator on mass-average temperature rise, was used in reducing the data from the MCA Stator A tests.

Vector-diagram data and performance parameters were calculated for the inlet guide vane, rotor, and stator at 10, 30, 50, 70, and 90 percent of blade height for the MCA Stator A tests. Stator vector diagram data and performance parameters were calculated at 5, 10, 30, 50, 70, 80, 90, and 95 percent of blade height for all other stator tests. All blade-element performance was calculated along streamlines passing through the stator leading edge at specified percentages of the stator-leading-edge span.

Overall performance was calculated from mass-average values of pressure and temperature for each blade row, for combinations of IGV and rotor, rotor and stator, and for IGV with rotor and stator.

Due to flow disturbances caused by probe blockage, the traverse measurements of stator inlet total pressure, total temperature, static pressure, and flow angle were inaccurate. These inaccuracies were more severe at higher speeds. Full immersion of a traverse probe at design speed reduced airflow by approximately 3 percent, and this reduction was detected on fixed instrumentation 90 degreees from the circumferential position of the probe.

Because measurements of the flow parameters at Station 7 were inaccurate, the data were reduced by a streamline-analysis computer program which calculated all static pressures and flow angles at this station. This program requires as input corrected weight flow, corrected speed, and radial distributions of total pressure, and total temperature ratios, and flow angle behind fixed blade rows. The program calculates static pressure from considerations of mass-flow continuity and full radial equilibrium and also calculates the flow angle behind rotating blade rows. This makes analysis possible without relying on the traverse measurements of static pressure and flow angle between the rotor and the stator, where probe blockage in the transonic flow causes serious inaccuracies.

The free-stream total pressure measured on wake-rakes at station 10 and the total temperature measured at Station 10 were translated forward to the instrument plane between the rotor and the stator along design streamlines.

These translated values should be more representative of the true average conditions at Station 7 than the measured values obtained from the radial traversing of the flow passage at that location.

The streamline-analysis computer program also permitted translating the flow conditions from the instrument planes to the leading and trailing edges of the blades in order to provide a more accurate indication of the blade inlet and outlet flow conditions, such as incidence and deviation. This method of translation accounted for the flow-path convergence and included a calculation for the effect of streamline curvature. Comparisons of calculated and measured values are discussed in detail in Reference 4.

VI. RESULTS AND DISCUSSION

A. Overall Performance

Overall stage performance for each stator configuration in terms of pressure ratio and efficiency versus corrected weight flow is compared for 50, 100 and 110% of design speed in Figures 16a, 16b, and 16c respectively. It should be noted that in observing the overall performance of these stages the low value of stage efficiency can be partially attributed to the fact that the stator loading is high compared to the rotor work input and that the high stator losses result in a high ratio of loss to work input and, therefore, a low efficiency. However, if one assumes that the rotor is not affected by the stator, then the differences in stage efficiency are a measure of stator losses.

At 100% of design speed (Figure 16b) the stage pressure ratios with the multiple-circular-arc stators were generally higher than that with the double-circular-arc stator. The efficiency levels were approximately the same for all stators with the exception of the MCA Stator A which was somewhat higher. The higher indicated efficiency of the stage with the MCA Stator A is in part attributed to the fact that during the test of this stage, data was not obtained at 5% and 95% of stator span where high losses due to end-wall conditions existed. This resulted in a higher calculated pressure ratio, and thus efficiency, than the other configurations for which the end-wall losses were more adequately accounted for through the use of increased sampling of the flow conditions. The flow capacity of the stage with the DCA stator was higher than those observed with the stages with MCA stators. The flow capacity appeared to be controlled by stator throat area with the DCA stator accepting the most flow. This stator is the one with the greater area margin from choke. No definite trends could be established in stall flow as related to stator configuration.

All configurations achieved stall margin over the design pressure ratio at design speed but flows at design pressure ratio were less than the design value. Predicted design point efficiencies were achieved or slightly exceeded by all the stator configurations although peak efficiencies were obtained at lower than design weight flows. The slotted stator configuration just achieved design efficiency, but at a reduced weight flow.

At 110% of design speed (Figure 16c) the pressure ratios for the stages with the MCA stators were higher than with the DCA stator, as was also observed at 100% of design speed. The efficiency levels at 110% of design speed were higher with all MCA stators than that with the DCA stator. Thus, it would appear from the overall performance at 110% of design speed (higher Mach numbers) that the losses for the MCA stators were somewhat lower than that for the DCA stator. The flow capacity of the stage with the double-circular-arc

stator at 110% of design speed was lower than that with the MCA stators which is opposite to that observed at 100% of design speed. This is attributed to high stator losses for the DCA stator operating at the high stator Mach numbers causing choking at the stator trailing edge where boundary layer displacement thickness occupied so much of the stator exit annulus area that freestream flow was choked.

At 50% of design speed (Figure 16a) there was no discernible difference in pressure ratio or flow capacity for any of the stator configurations. Because of data inaccuracy, differences in efficiency are not considered reliable at the 50% speed. The temperature measurement inaccuracy(±1°F) in combination with the low temperature rise (approximately 20°F) at this speed could result in an efficiency error of five percent.

In comparing the overall performance of the stage with the slotted MCA Stator A and that with the unslotted MCA Stator A the primary difference was noted at 110 percent of design speed. At this speed, pressure ratio, efficiency, and flow capacity were somewhat lower for the slotted configuration. The lower flow capacity of the stage with the slotted stator is attributed to the injection of slot flow into the channel throat causing a reduced effective area margin from choke.

In general, MCA stators gave the stage better high-speed performance than the DCA stator, and the improvement at high-speed was made without penalizing low-speed performance. The particular slot design used for MCA Stator A did not improve low-speed performance and reduced performance at high-speed.

B. Stator Blade Element Performance

Loss

Stator loss coefficient versus incidence for 50, 100, 110 and 120 percent of design speed with stator type as a parameter are presented for 5, 10, 30, 50, 70, 80, 90 and 95-percent of span in Figures 17 through 24. Comparison of the minimum loss coefficient versus percent span at 50,100, 110 and 120 percent of design speed for each stator configuration are presented in Figure 25. These minimum loss coefficients were obtained from Figures 17 through 24. Included in Figure 25b (100 percent design speed) are the loss coefficients employed in the stator designs. The lowest curve presents the loss coefficients obtained from the correlation of stator loss based upon the loss parameter ($\varpi \cos \beta_{exit}/2\ \sigma$) versus loading (D-factor) presented in Reference 13. It is referred to as a profile loss and does not include estimated shock loss. The next lowest curve is the total loss used in the design of the MCA stators and includes an estimated shock loss for the MCA stators. The upper curve is the total loss used in the design of the DCA stator and includes an estimated shock loss for this stator. (See Reference 2 for details on the loss calculations.)

At 100% of design speed (Figure 25b) data from all stator configurations showed higher stator losses near the end-walls than the design values but the mid-span losses were lower than the design values. The loss levels were approximately the same for all configurations. Thus, it is concluded that the method of estimating design losses resulted in too high a loss in the mid-span region of the blade and did not adequately account for gradients due to end-wall effects. The overestimation of losses in the mid-span region of the blade may be due to an overestimate of losses associated with flow shocks, an overestimate of profile losses or a combination thereof.

At 50% of design speed (Figure 25a) the end-wall losses remained high but the mid-span losses were significantly lower than those at 100% of design speed. Again the loss levels were approximately the same for all configurations.

At 110 and 120% of design speed (Figures 25c and 25d) the losses in the mid-span region of the blade for the DCA stator increased sharply over that of the MCA stators. In the end-wall regions no differences in losses between the various stator configurations were observed. This may be due, in part, to the high losses associated with the end-wall overshadowing those associated with the blade profiles. The level of loss in the end-wall region remained about the same as that noted at the other speeds. Thus it is concluded that the loss coefficients near end-walls were not strongly affected by compressor speed (Mach number) in contrast to mid-span loss levels, which rose with increasing speed. The sharp increase in loss of the DCA stator over that of the MCA stators as the speed was increased above the design speed indicates a definite advantage of the MCA blade shape for high Mach number operation.

Within the scatter of the data, no discernible differences were noted between the losses for the unslotted and slotted MCA Stator A at all speeds and at all radii.

Comparisons of minimum stator loss coefficient versus stator inlet Mach number, with stator type as a parameter, are presented in Figure 26. The plots show that at the lower Mach number levels associated with the 50% and 100% of design speed (Mach numbers below 0.90) that no appreciable difference in loss level between the stator configuration exists as was noted from Figure 25. At the high Mach numbers (above 0.90) associated with the 110 and 120% of design speed the losses for the DCA stator increased more sharply than those for the MCA blade rows for the mid-span elements. Near the end-walls no appreciable difference in loss level can be noted.

Loss parameters ($\bar{\omega}\cos\beta_9/2\sigma$) for all minimum blade element loss points are presented as a function of loading at 5, 10, 30, 50, 70, 80, 90 and 95-percent span in Figures 27 through 34. Two sets of parameters are presented for each spanwise location: one based on stator blade element total loss and the

other on "profile" losses obtained by subtracting estimated shock losses from total losses. Shock losses were estimated using the method described in Reference 7 and modified in Reference 2 to permit calculating a shock loss at high subsonic inlet Mach numbers. The profile loss parameter versus diffusion factor of Reference 13 which was used in the design is shown for comparison. In general, the plots of profile loss parameter versus diffusion factor revealed that losses in the end-wall regions of the blade were high and were also insensitive to loading. In the mid-span regions the losses were lower than in the end wall regions and increased with loading as expected. The trend of increased loss with increased loading is more apparent in total loss data. The increase in loading was obtained at the higher speeds, and therefore at the higher Mach numbers. Therefore, increased shock losses would be expected at the higher loading levels. The profile loss parameter for the mid-span region tended to agree with the correlation of Reference 13 while those near the end-walls were much higher. The higher losses near the end-walls are probably associated with the end-wall boundary layer and secondary flows. The data used in the correlation of loss versus diffusion factor curve presented in Reference 13 did not show an end-wall effect for stator blade rows.

In general, the profile loss parameter arrived at by subtracting a calculated shock loss from the total loss parameter resulted in a reasonably good correlation of loss versus diffusion factor for the tip regions of all the stators. In the mid-span and hub regions of the blades this resulted in a lower profile loss parameter for the DCA stator than for the MCA stator.

Incidence

In general, the loss-versus-incidence curves in Figures 17 through 24 show a steady trend of increase in minimum loss incidence angle as compressor speed and stator inlet Mach numbers increased. At 50 percent of design speed the minimum loss incidence angles were approximately the same for all stator configurations. At design speed the minimum loss incidence angles for the DCA stator were lower than those for the MCA stators. At 110 and 120 percent of design speed the minimum loss incidence angles for the DCA stator were higher than those for the MCA stators. This increase in minimum loss incidence angle for the DCA stator above that for the MCA stators as speed was increased above design speed is believed to be the result of a flow choking condition at the exit of the DCA stator due to the high losses. These high losses are associated with large stator wakes which tend to reduce the effective flow area. Choking at the exit of the DCA stator at speeds above the design speed would explain the change in overall performance of the stages (see Figure 16) between 100 and 110 percent of design speed, where at 100 percent the stage with the DCA stator showed the highest flow capacity but at 110 percent speed had the lowest flow capacity as compared to the stages with the MCA stators.

The spanwise distribution of minimum loss incidence to the suction surface at design speed is presented in Figure 35. All stators were designed for zero incidence to the suction surface. Near the end-walls minimum loss incidence angles were positive to the suction surface for all stator configurations. Near the mid-span, minimum loss occurred near design incidence for the MCA stators and occurred at negative values for the DCA stator. Thus, the design assumption that minimum loss occurred at zero degrees to the suction surface for all stators at all spanwise positions was not confirmed by the data.

There appears to be a consistent relationship between minimum loss incidence angles and blade element throat area between adjacent blades. The ratio of throat area to capture area as a function of stator inlet Mach number is shown for minimum loss data points at 30, 50, and 70 percent span in Figure 36. "Capture area" is stator inlet gap width multiplied by the cosine of the inlet angle. "Throat area" is the minimum two-dimensional width of the flow channel, modified to account for stream tube convergence. The throat area is fixed by blade geometry. The capture area decreases with increasing incidence angle, thus, the ratio of capture area to throat area also decreases with increasing incidence angle. The lower the ratio of capture area to throat area, the greater the area margin from choking. Most of the data shown in Figure 36 fell within a band corresponding to ±2° in incidence angle. The data shows a gradual increase in required area margin from choke for minimum loss incidence angle as inlet Mach number increases to approximately 0.8 and then a more rapid increase in area margin from choke with further increases in Mach number. This correlation presented in Figure 36 appears to provide a means of estimating the minimum loss incidence angle with respect to throat area and inlet Mach number.

Range

Range was defined as the difference between high and low incidence angles at which $\bar{\omega}$ equaled $\bar{\omega}$ min + 0.05. The range appeared to be about the same for all stator configurations at a given speed (Figures 17 through 24). Range from MCA Stator B was correlated as a function of inlet Mach number (Figure 37). Stagger and camber do not differ greatly across the span and therefore data are presented for the various spanwise locations. Greatest range was obtained near the tip; least range occurred near the hub. The range decreased with increasing Mach number for all spanwise positions.

Deviation

Figure 38 shows deviation angles of each stator versus incidence to the suction surface for design speed data points at 5, 10, 30, 50, 70, 80, 90 and 95 percent of span except for MCA stator A where data were not obtained at 5, 80, and 95 % span. For purposes of comparison, spanwise distributions of deviation angles of the different stators at design speed minimum loss points are compared to design values in Figure 39. Measured deviations are shown

as open symbols; design values by solid and dashed lines. Deviation angles of the DCAstator in the mid-span region are one or two degrees lower than the design estimate. MCA stator deviation angles at mid-span are two to four degrees higher than design estimates. The design estimates were made using a form of Carter's rule, modified to account for camber distribution according to Reference 9. The modifications apparently did not account fully for the camber distribution differences between stator types.

All stators had approximately the same patterns of increased deviation near end walls. This spanwise deviation pattern may be explained as a secondary flow effect. Additional deviation due to secondary flow was calculated using the method reported in Reference 14. The calculation was made assuming a seventh-power velocity profile and a boundary-layer displacement thickness of 0.8-percent of span on both end walls. The spanwise distribution of this additional deviation is shown in Figure 39 .

C. Pressure Coefficients

Pressure coefficient data obtained at the 10 and 90% span locations for the various stator configurations were analyzed to estimate the passage shock location as compared to the design assumption, to compare indicated suction surface Mach numbers to design values, and to estimate the strength of the passage shock and local diffusion level.

The location of the passage shocks are noted by a rapid increase in static pressure and thus pressure coefficient, along the blade suction surface. Their presence was more apparent at the higher speeds where the flow Mach numbers were higher (References 2,3, 4 and 5). A typical plot of pressure coefficient versus percent chord is presented in Figure 40. It is for the DCA stator and was taken at 100% of design speed and at the 90% span location. Plots are shown for wide open throttle, part throttle and near stall conditions. The part throttle condition was near minimum loss for this blade element. The shock locations, as noted in Figure 40, moved toward the blade leading edge as back pressure was increased. The assumed shock location (Figure 5) was at 35-percent of chord for this percent of span. Actual shock locations for open throttle and minimum loss data points straddle the assumed location. This is typical for all stator configurations tested.

Ratios of local static pressure to stator inlet total pressure at 10 and 90 percent of span were used to calculate peak suction surface Mach numbers. Pressure coefficients for design speed data points nearest design incidence at 90 percent span for the three unslotted stators are presented in Figure 41, and peak suction surface Mach numbers are noted. Pressure coefficients for the slotted MCA Stator A are not presented because the flow slot makes data interpretation uncertain. The maximum suction surface Mach number for the DCA Stator is 1.518 as compared to the design estimate of 1.64. Indicated peak

suction surface Mach numbers are 1.380 for the MCA Stator A and 1.275 for the MCA Stator B compared with the design estimate of 1.43. Maximum suction surface Mach numbers for near minimum loss data points are presented as a function of inlet Mach number for MCA Stator A, MCA Stator B, and the DCA Stator in Figure 42. Figure 42a presents data for 10 percent span, Figure 42b for 90 percent span. The figure shows that the DCA Stator has higher peak Mach numbers than the MCA Stators at the higher inlet Mach numbers, and helps to explain rapid increase in loss of the DCA Stator as speed was increased above design speed.

The ratio of maximum velocity to exit velocity was used in an attempt to correlate the loss parameter for minimum loss data points. Figure 43 shows loss parameters as a function of V maximum/V exit at 10 and 90 percent of span for the DCA stator, the MCA Stator A, and MCA Stator B configurations. Exit velocities for data points in Figure 43 were taken from streamline calculations, using circumferentially mass averaged total pressures and temperatures, and static pressures which satisfy continuity for axisymmetric flow. In general, the correlation appears to be no better than that based upon diffusion factor (Figures 28b and 33b).

A multiple shock system was noted in the data obtained on the MCA stators at 10 percent of span while operating with low back pressures at inlet Mach numbers over 0.9. Suction surface Mach numbers for 110 percent of design speed are presented as a function of chord for the DCA stator, MCA Stator A, and MCA Stator B configurations in Figure 44. For the MCA stator configurations it appears that following an initial passage shock at approximately 30 percent of chord the flow reaccelerates followed by a second passage shock in the vicinity of 50 percent of chord. The DCA stator had a much higher suction surface Mach number, but reacceleration after the initial shock is not noted.

VII. SUMMARY OF RESULTS

1. Data from all four stator configurations showed the losses in the end wall regions to be much higher than that assumed in the design, and midspan losses were slightly lower than the design estimates.

2. Near the end walls the high losses for all four stator blade configurations seemed to obscure differences in performance resulting from differences in blade shape. Near the midspan, differences in performance between the MCA stators and the DCA stator were apparent at transonic Mach numbers, where DCA supersonic acceleration and losses were substantially higher than those of the MCA stators. At low inlet Mach numbers there was little difference in performance between the airfoil types.

3. The slotted stator design used in this investigation showed no advantage as to loss or range when compared to the unslotted MCA Stator A .

4. Inlet guide vane wakes pass through rotor and stator blade rows, causing circumferential distortion in exit total temperature and total pressure. A cyclic circumferential temperature variation existed at the stator exit, with one cycle corresponding to a stator gap. This may be explained by a tendency for rotor wake flow to migrate toward stator surfaces, as explained in Reference 12, or by local throttling at the rotor exit caused by stator blockage in high Mach number flow.

5. Camber distribution has a significant effect on optimum incidence angle. At design speed, the DCA stator had minimum loss at incidence angles 1 to 3 degrees lower than the MCA stators. Above design speed however, the DCA stator's greater supersonic acceleration produced higher losses and reduced flow capacity, so that optimum incidence angles became higher than for the MCA stators. At low speeds, optimum incidence angles were approximately the same for all stators.

6. Deviation angles were higher near end walls than at midspan for all stators. The level of MCA stator deviation angles was higher than for the DCA stator. MCA stators had deviation angles greater than design estimates. The DCA stator had lower deviation angles than design, except near end walls. Increased deviation near end walls may be explained as a secondary flow effect.

VIII. REFERENCES

1. Gostelow, J. P., Krabacher, K. W., and Smith, L. H. Jr., "Performance Comparisons of High Mach Number Compressor Rotor Blading," NASA CR 1256, 1968.

2. Keenan, M. J., and Monsarrat, N. T., "Experimental Evaluation of Transonic Stators, Preliminary Analysis and Design Report," NASA CR-54620, 1967 (PWA-2749).

3. Keenan, M. J., and Bartok, J. A., "Experimental Evaluation of Transonic Stators, Data and Performance Report, Double-Circular-Arc Stator," NASA CR-54623, 1968 (PWA-3404).

4. Keenan, M. J., Harley, K. G. and Bogardus, G. A., "Experimental Evaluation of Transonic Stators, Data and Performance Report, Multiple-Circular-Arc Stator A," NASA CR-54621, 1968 (PWA-3260).

5. Keenan, M. J., and Bartok, J. A., "Experimental Evaluation of Transonic Stators, Data and Performance Report, Multiple-Circular-Arc Stator B," NASA CR-54622, 1968 (PWA-3356).

6. Keenan, M. J., and Bartok, J. A., "Experimental Evaluation of Transonic Stators, Data and Performance Report, Multiple-Circular-Arc Stator A (Slotted)," NASA CR-54624, 1968 (PWA-3411).

7. Schwenk, F. C., Lewis, G. W., and Hartmann, M. J., "A Preliminary Analysis of the Magnitude of Shock Losses in Transonic Compressors," NACA RM E57A30, March 1957.

8. Lieblein, S., Schwenk, F. C., and Broderick, R. L., "Diffusion Factor for Estimating Losses and Limiting Blade Loadings in Axial-Flow-Compressor Blade Elements," NACA RM E53D01, June 1953.

9. Shepherd, D. G., "Principles of Turbomachinery," New York: The Macmillan Company, 1965.

10. ASME Research Committee on Fluid Meters., "Fluid Meters - Their Theory and Application," Fifth Edition, American Society of Mechanical Engineers, New York, N.Y., 1959, p. 47.

VIII. REFERENCES (Cont'd)

11. Glawe, George E., Simmons, Frederick S., Stickney, Truman N., "Radiation and Recovery Corrections in Time Constants of Several Chromel-Alumel Thermocouple Probes in High Temperature, High Velocity Gas Streams," NACA Technical Note 3766, October 1956.

12. Mikolajczak, A. A., and Kerrebrock , J. L., "Intra-Stator Transport of Rotor Wakes and its Effect on Compressor Performance," Paper to be presented at the ASME Gas Turbine Division Conference, Brussels, Belgium, May 1970.

13. Robbins, William H., Jackson, Robert J. and Lieblein, Seymour, "Blade Element Flow in Annular Cascades, Aerodynamic Design of Axial-Flow Compressors," NASA SP-36, 1965, ch. VII. pp.227-254.

14. Hawthorne, W. R. "Some Formulae for the Calculation of Secondary Flow in Cascades," ARC 14519, University of Cambridge, March 1955.

APPENDIX A
Symbols

The following symbols are used:

A	- area, ft^2
c	- chord length, in
D	- diffusion factor
i_m	- incidence angle, angle between inlet air direction and line tangent to blade mean camber line at leading edge, degrees
i_s	- incidence angle, angle between inlet air direction and line tangent to blade suction surface at leading edge, degrees
M	- Mach number
N	- rotor speed, rpm
P	- total pressure, psfa
p	- static pressure, psfa
r	- radius, ft
s	- circumferential distance between adjacent blades
T	- total temperature, °R
t/c	- thickness-to-chord ratio
V	- air velocity, ft/sec
W	- weight flow, lbs/sec
X	- distance along chord line, inches
Z	- angle between assumed shock location and line connecting airfoil transitio and leading edge of following blade
β	- air angle, angle between air velocity and axial direction, degrees
γ	- ratio of specific heats

SYMBOLS (Cont'd)

γ° - blade chord angle, angle in cascade projection between blade chord and axial direction, degrees

δ - ratio of inlet total pressure to standard pressure of 2116.22 psfa

δ° - deviation angle, angle between exit air direction and tangent to blade mean camber line at trailing edge, degrees

η - efficiency, %

θ - ratio of inlet total temperature to standard temperature of 518.6°R

ρ - mass density, lbs-sec^2/ft^4

σ - solidity, ratio of chord to spacing

ϕ_{aft} - airfoil mean line camber aft of transition, degrees

ϕ_{fwd} - airfoil mean line camber forward of transition, degrees

ϕ_m - airfoil mean line camber, degrees

ϕ_{sp} - airfoil mean line camber forward of assumed shock location, degrees

ϕ_{sps} - airfoil suction surface camber forward of assumed shock location, degrees

$\overline{\omega}$ - total pressure loss coefficient

Superscripts:

* - designates blade geometry

Subscripts:

ad - adiabatic

r - radial direction

z - axial direction

θ - tangential direction

0 - plenum chamber

SYMBOLS (Cont'd)

1	- instrument plane upstream of inlet guide vane (IGV)
2	- station at IGV leading edge
3	- station at IGV trailing edge
4	- instrument plane upstream of rotor
5	- station at rotor inlet
6	- station at rotor exit
7	- instrument plane upstream of stator
8	- station at stator leading edge
9	- station at stator trailing edge
10	- instrument plane downstream of stator

APPENDIX B
Performance Parameter Equations

Performance parameters are defined as follows:

a. Stator incidence angle based on mean camber line

$$i_m = \beta_8 - \beta^*_{8m}$$

b. Stator incidence angle based on blade suction surface

$$i_s = \beta_8 - \beta^*_{8s}$$

c. Stator deviation

$$\delta^\circ = \beta_9 - \beta^*_9$$

d. Stator diffusion factor

$$D = 1 - \frac{V_9}{V_8} + \frac{r_8 V_{\theta 8} - r_9 V_{\theta 9}}{(r_8 + r_9)\,\sigma\, V_8}$$

e. Stator loss coefficient

$$\overline{\omega} = \frac{P_8 - P_9}{P_8 - p_8}$$

f. Stator loss parameter

$$\frac{\overline{\omega} \cos \beta_9}{2\sigma}$$

g. Adiabatic efficiency (stage)

$$\eta_{ad} = \frac{\left(\frac{P_{10}}{P_0}\right)^{\frac{\gamma - 1}{\gamma}} - 1}{\left(\frac{T_{10}}{T_0}\right) - 1}$$

h. Pressure Coefficients

$$C_p = \frac{p_{(local)} - p_8}{\frac{1}{2} \rho_8 V_8^2}$$

Note: Leading edge values of local static pressure for Cp were set equal to the inlet stagnation pressure; trailing edge values for Cp were based on calculated static pressure at the stator exit plane.

ILLUSTRATIONS

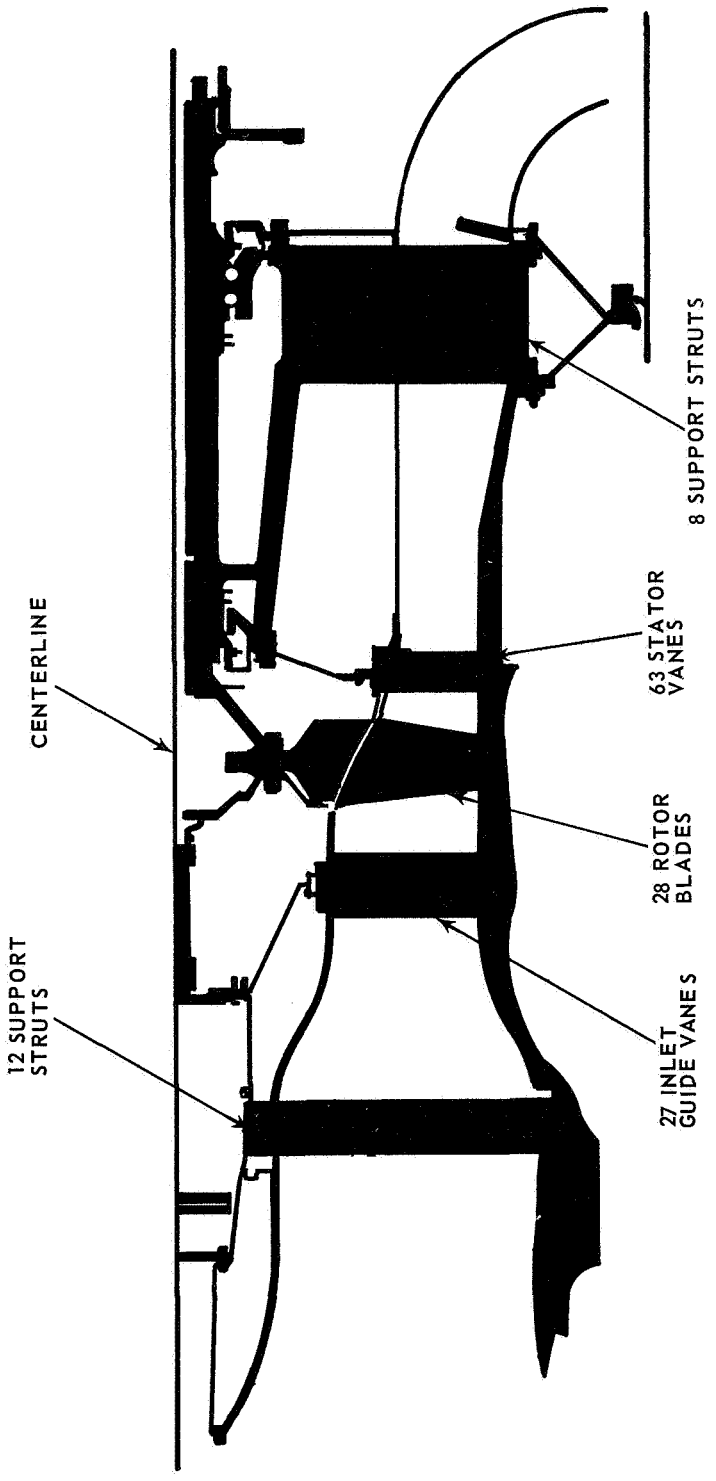

Figure 1 Cross-Section of Test Compressor

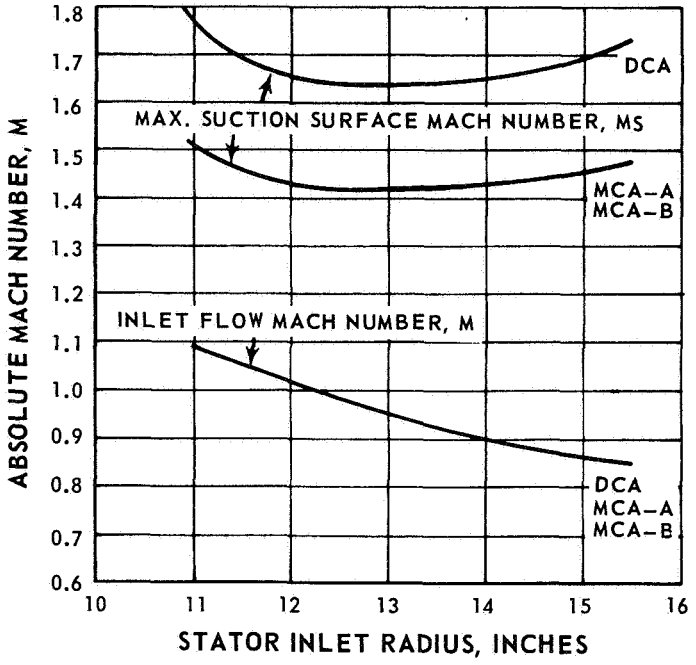

Figure 2 Inlet Flow Mach Number and Estimated Maximum Suction Surface Mach Number for DCA and MCA Stator Blade Rows

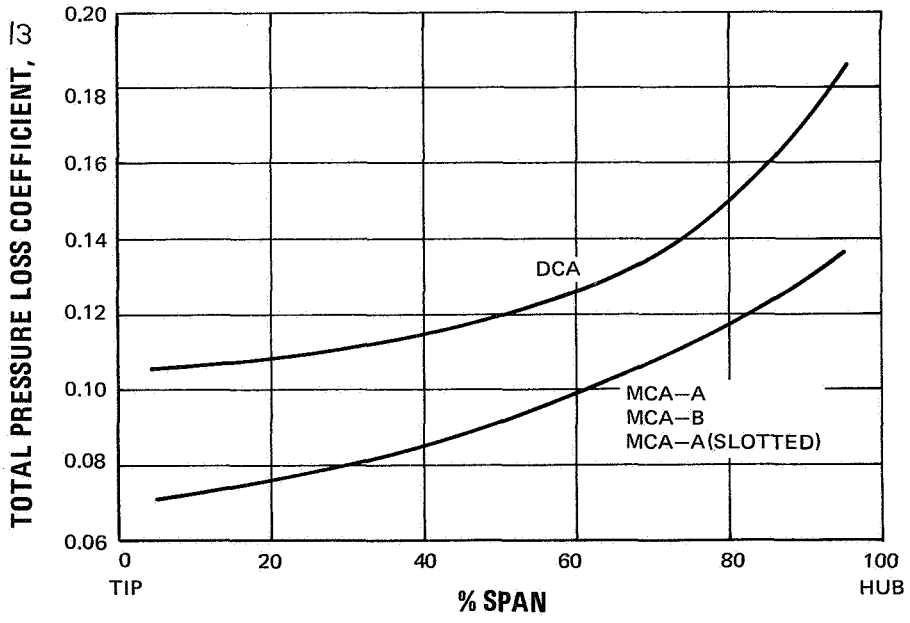

Figure 3 Design Total Pressure Loss for DCA and MCA Stators

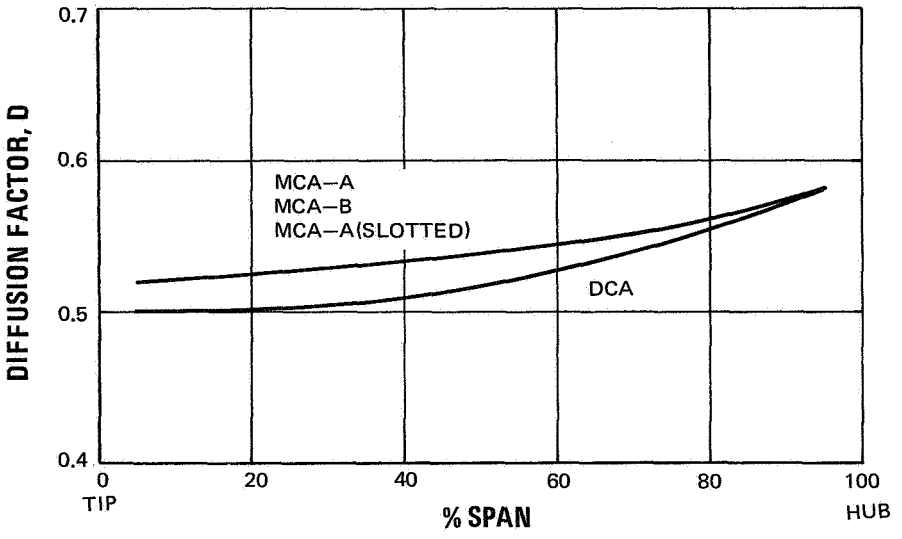

Figure 4 Design Blade Loading Parameter for DCA and MCA Stators

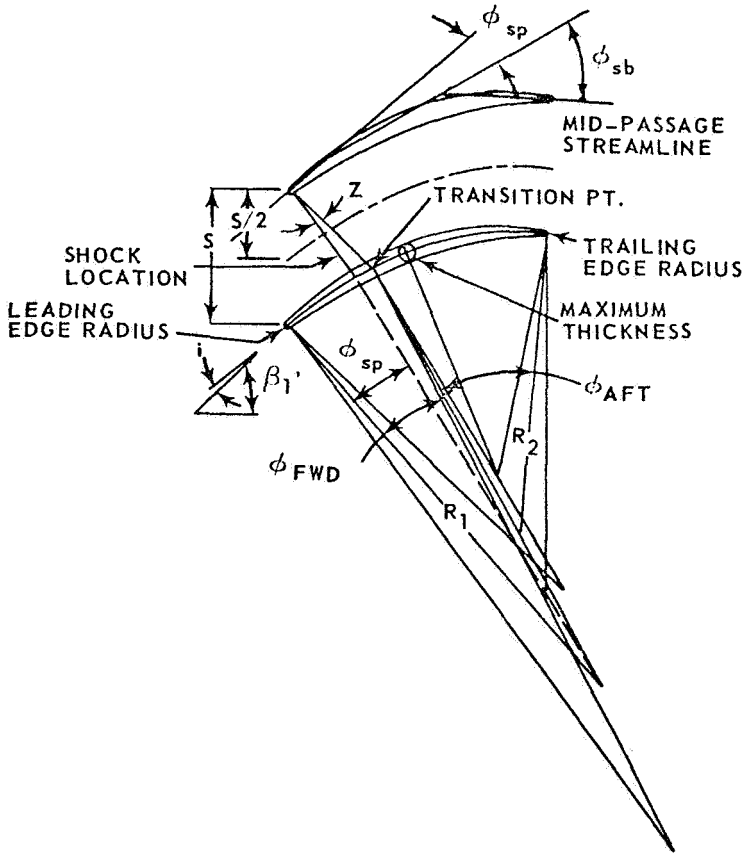

Figure 5 Multiple-Circular-Arc Blade Geometry

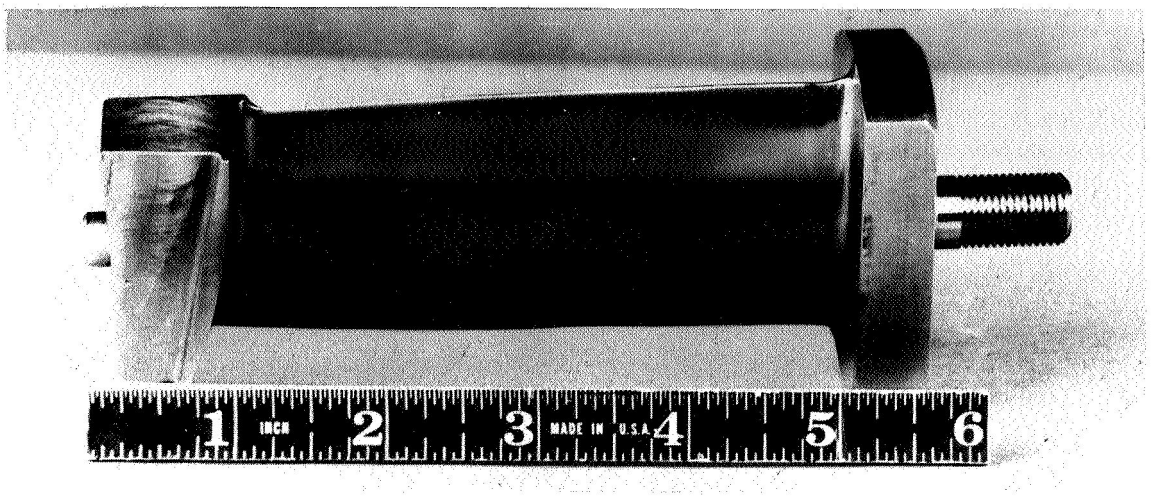

Figure 6 Multiple-Circular-Arc Stator A

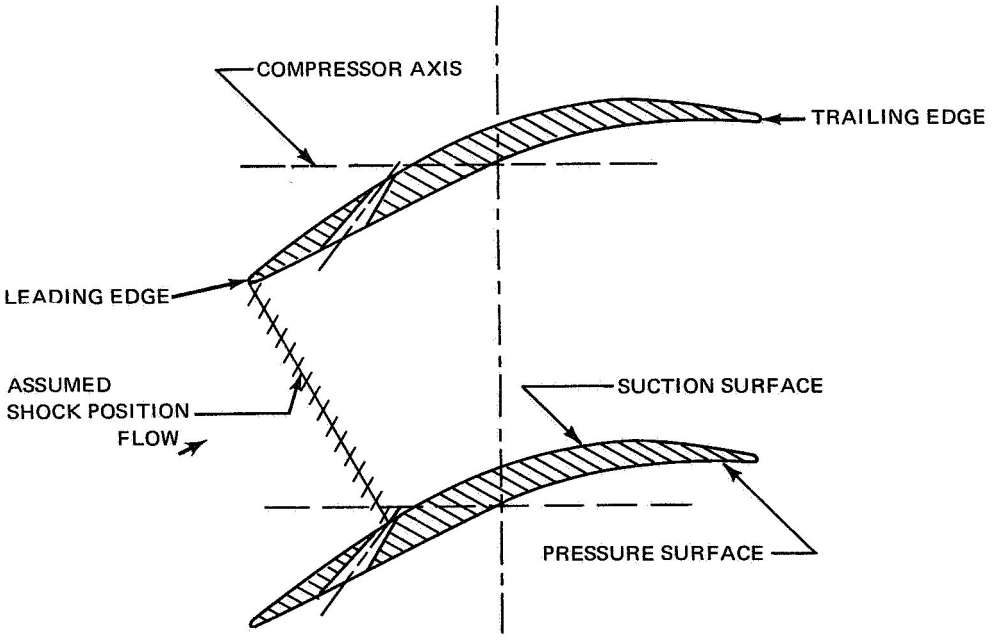

Figure 7 Cross-Sectional View of Multiple-Circular-Arc Stator A (Slotted), Showing Typical Blade Spacing and Slot Location

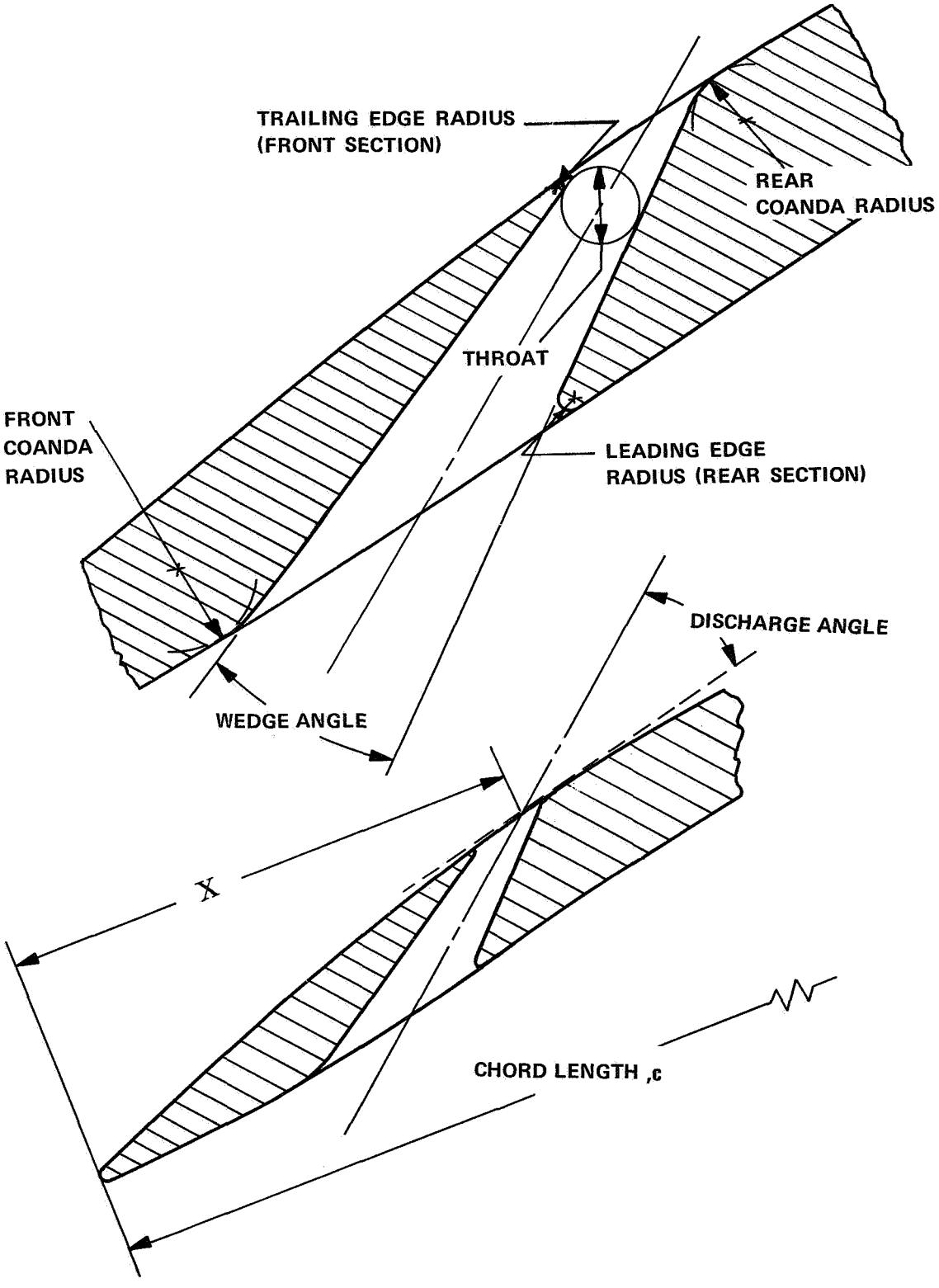

Figure 8 Partial Cross-Section of MCA Stator A (Slotted) Showing Slot Geometry Nomenclature

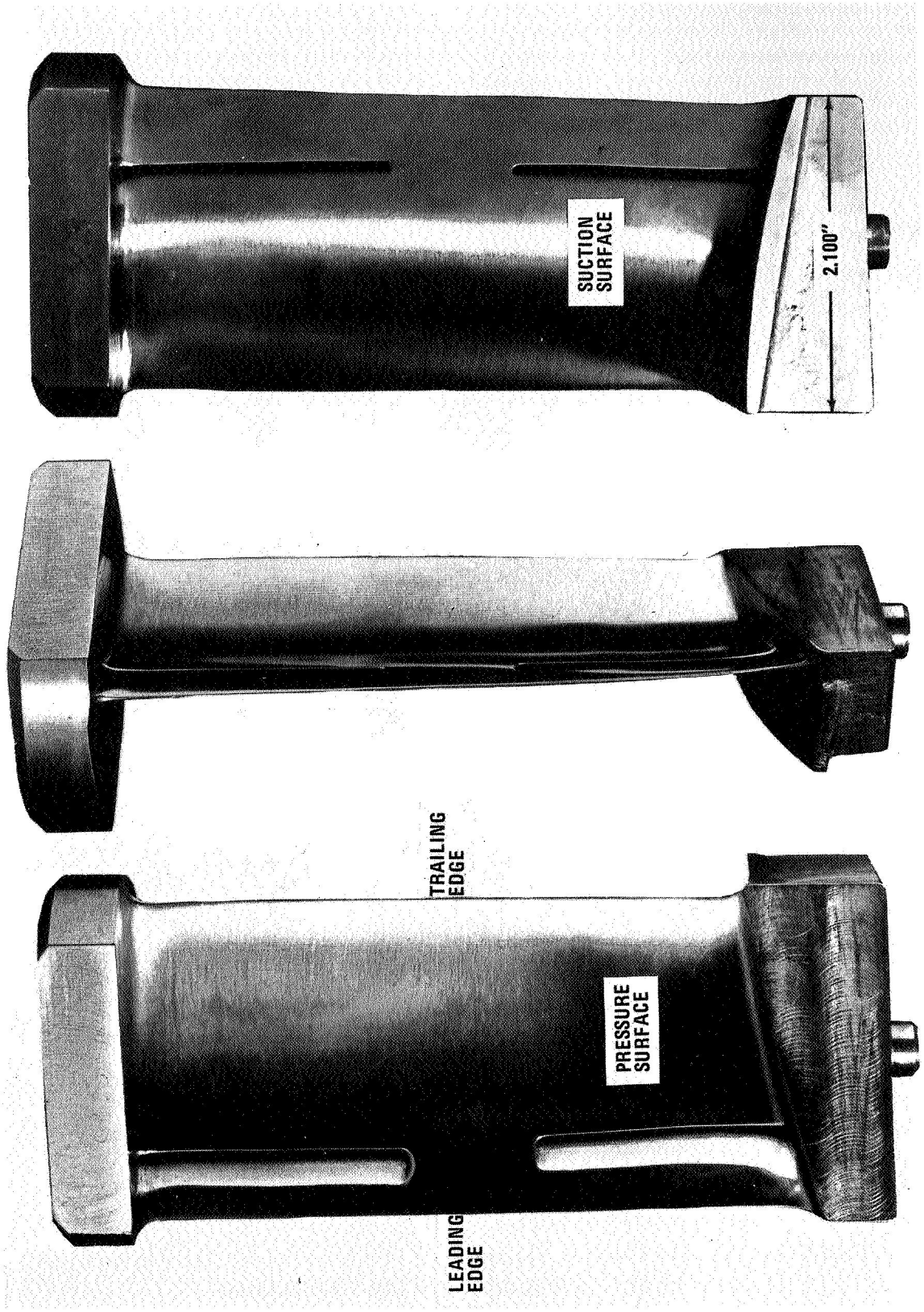

Figure 9 Multiple-Circular-Arc Stator A (Slotted)

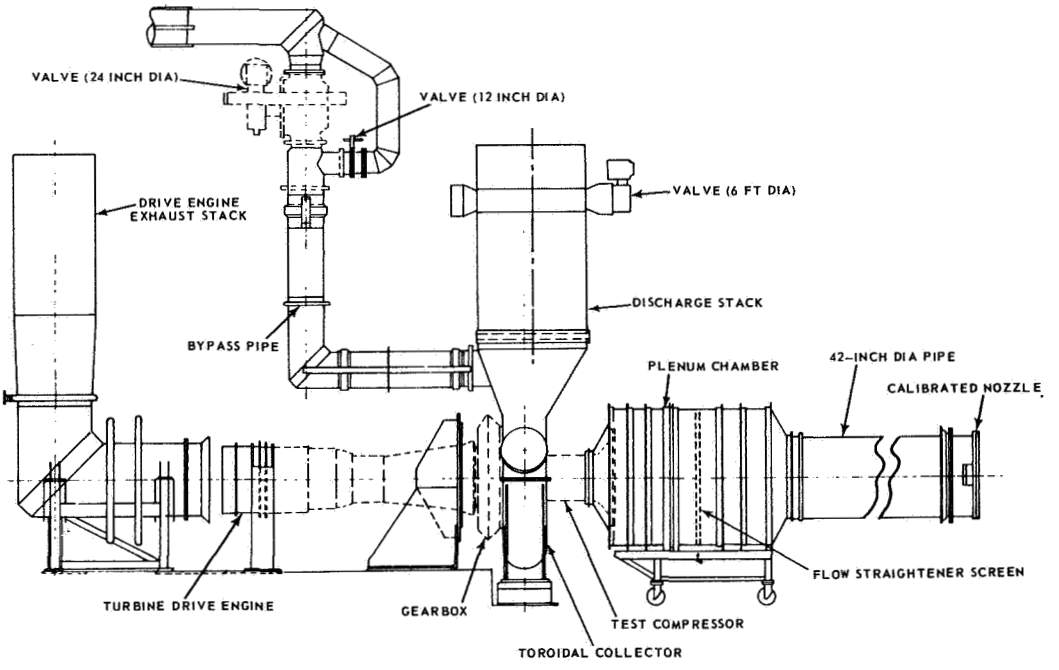

Figure 10 Schematic of Compressor Test Facility

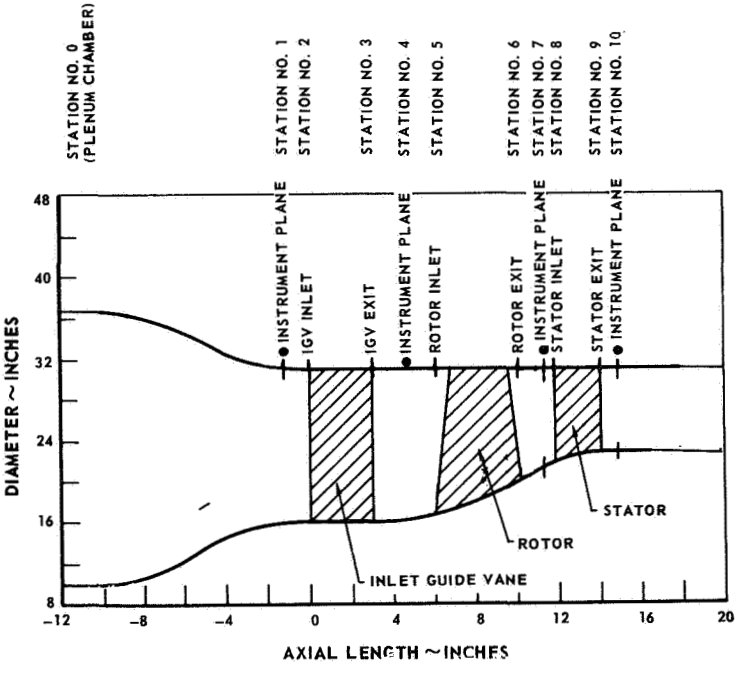

Figure 11 Station Number Designation and Location of Instrumentation and Blade Leading and Trailing Edge Planes

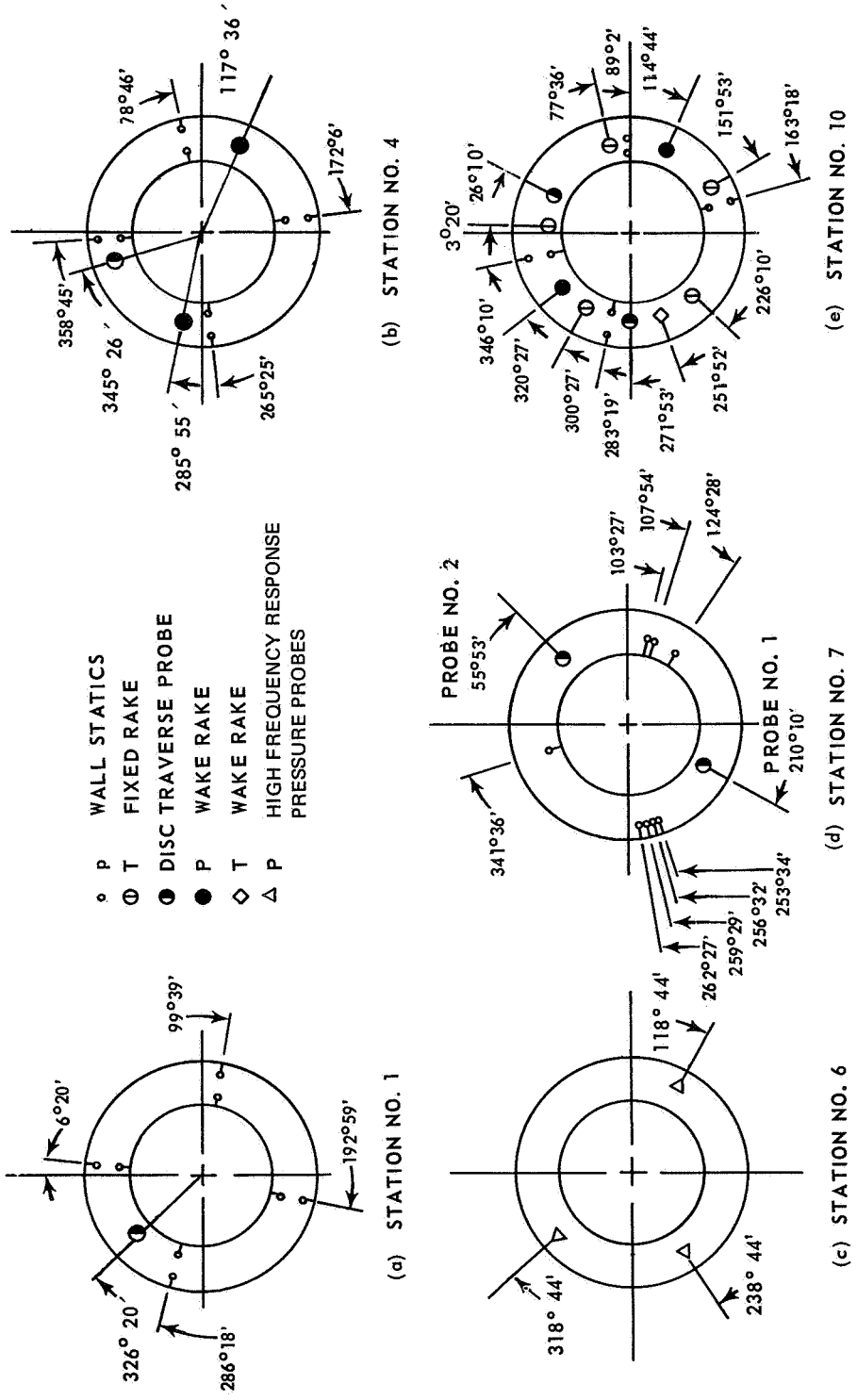

Figure 12 Circumferential Position of Instrumentation

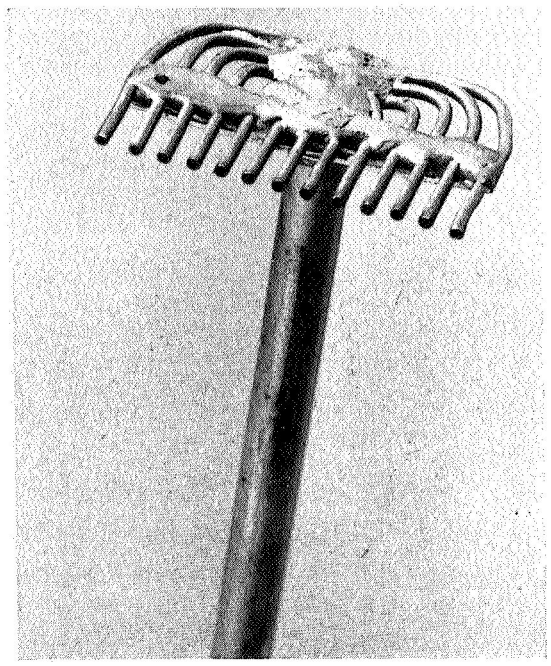

(a) Pressure Wake Rake

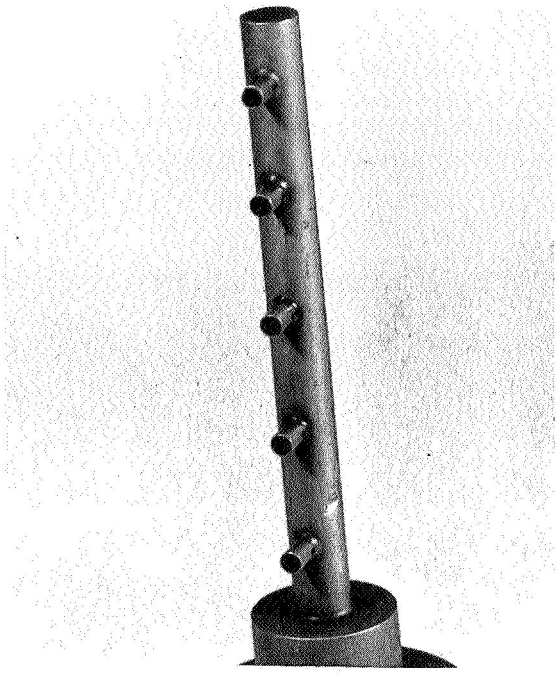

(b) Radial Temperature Rake

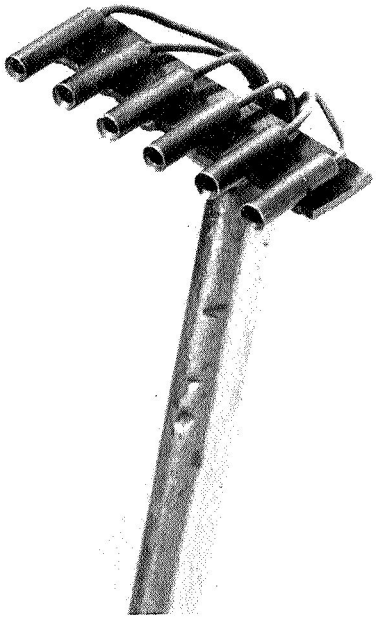

(c) Circumferential Temperature Rake

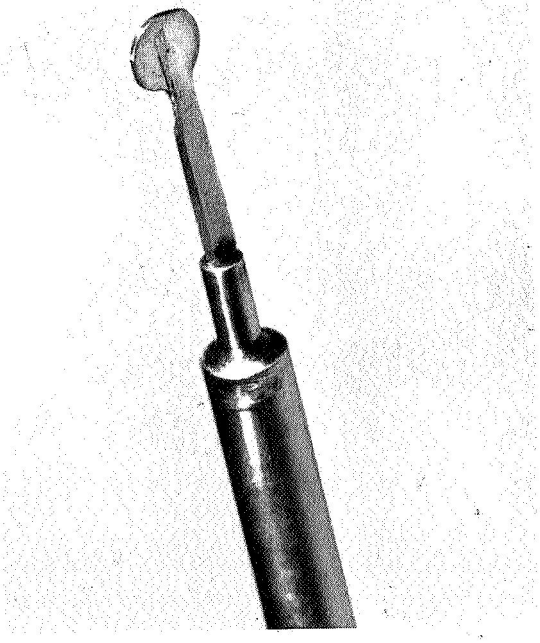

(d) Disk Probe

Figure 13 Compressor Instrumentation

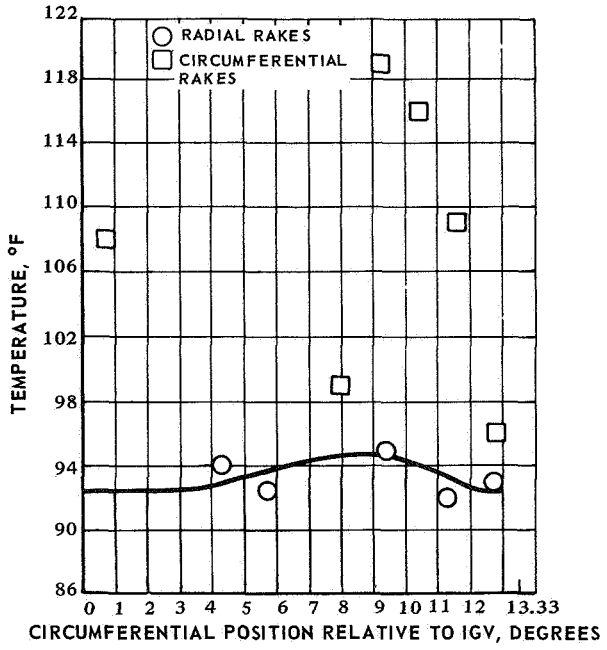

(a) OVERALL CIRCUMFERENTIAL TEMPERATURE DISTORTION

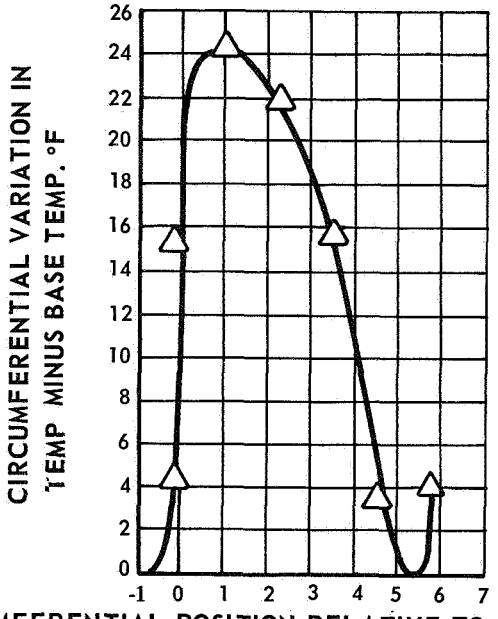

(b) TEMPERATURE DISTORTION ATTRIBUTED TO STATOR

Figure 14 Circumferential Variation in Total Temperature, 90% Span, 110% Design Speed, Wide Open Throttle, Station 10 (MCA Stator B)

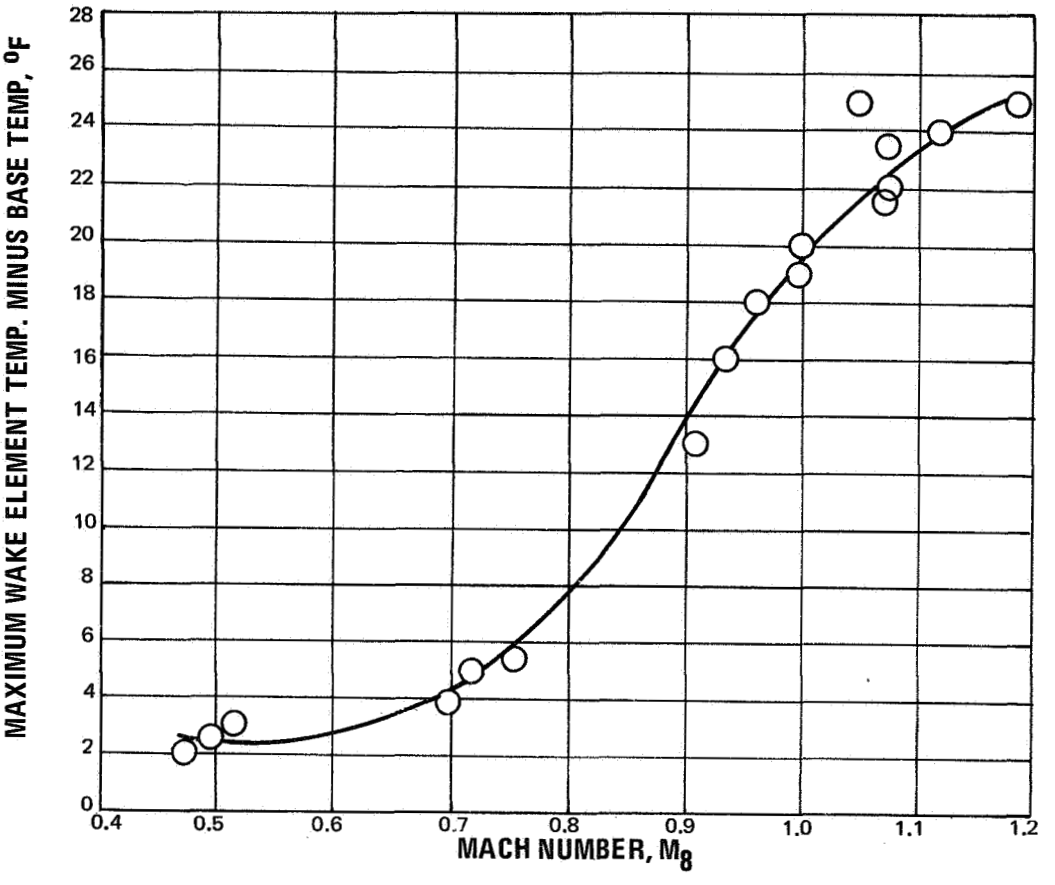

Figure 15 Maximum Circumferential Variation in Total Temperature Attributed to Stator vs. Mach Number, 90% Span, (MCA Stator B)

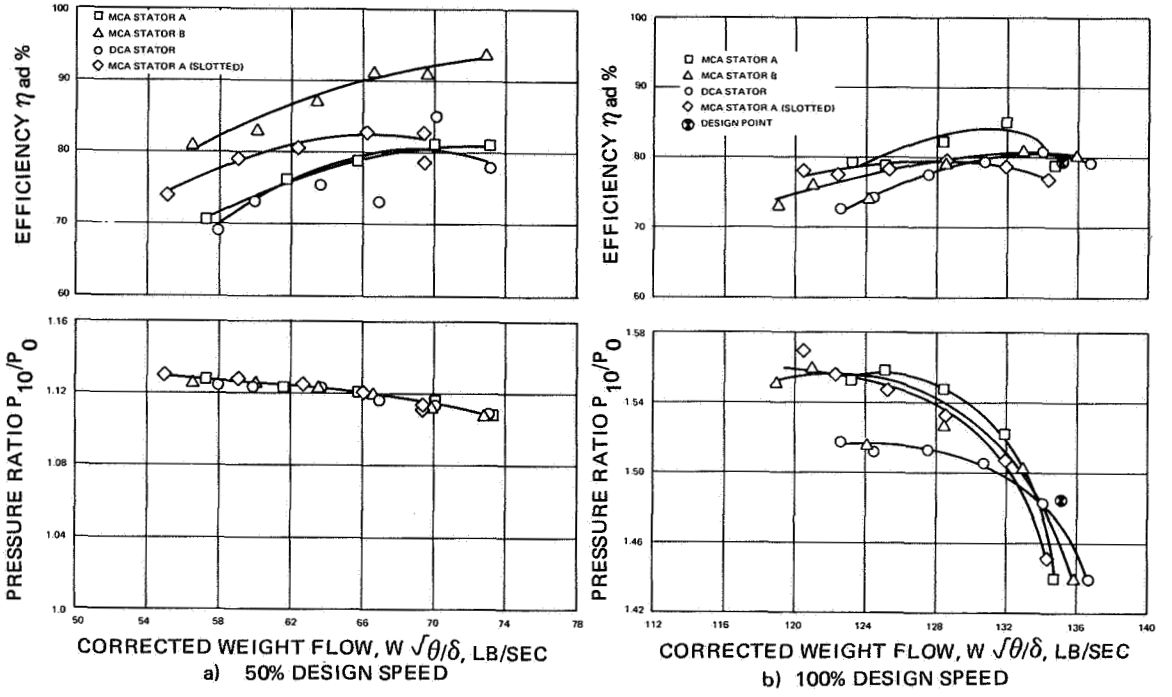

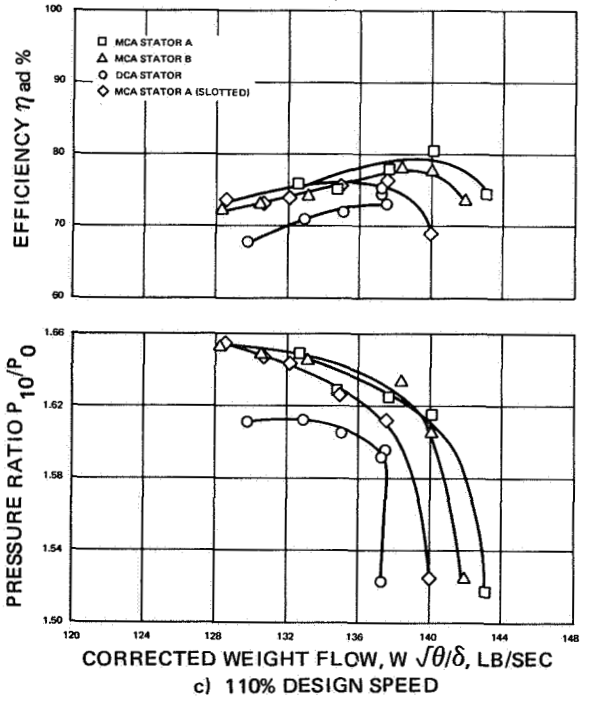

Figure 16 Overall Performance of Inlet Guide Vane, Rotor, and Stator

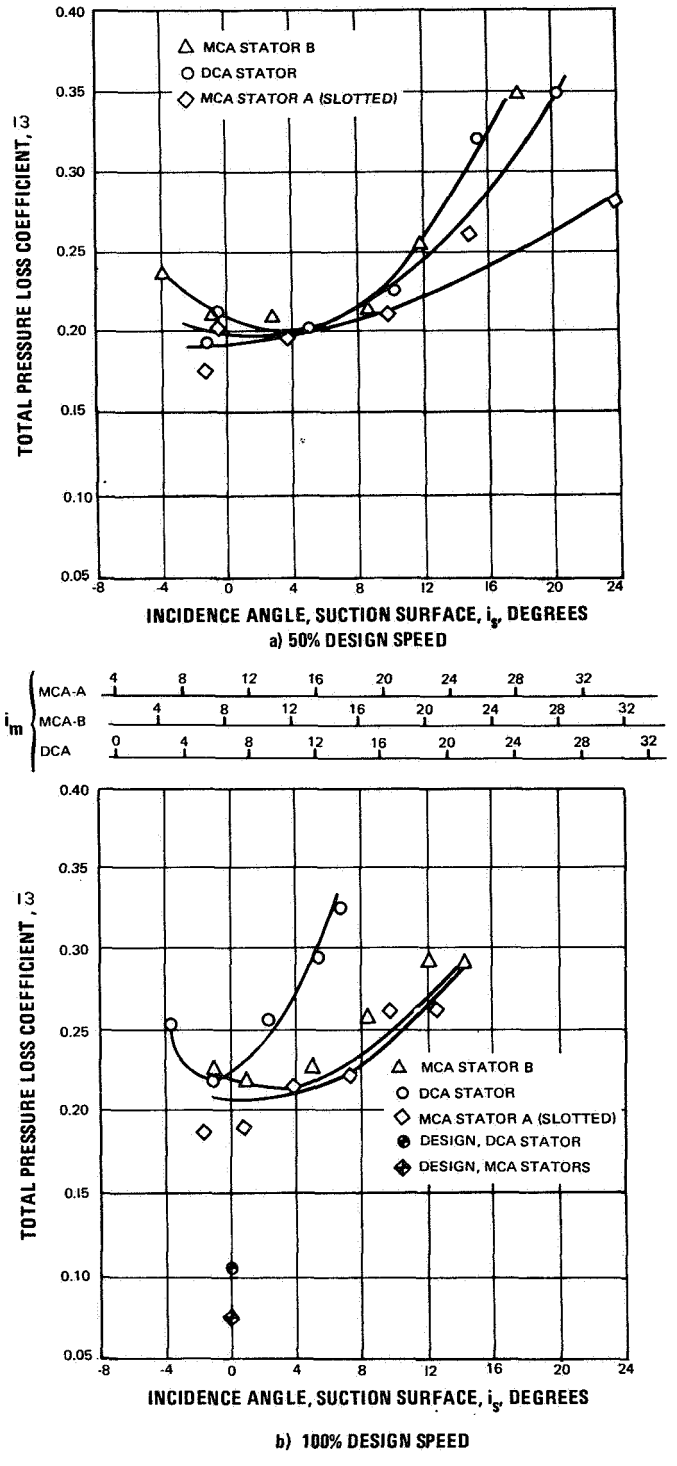

Figure 17 Stator Total Pressure Loss Coefficient vs. Incidence Angle, 5% Span

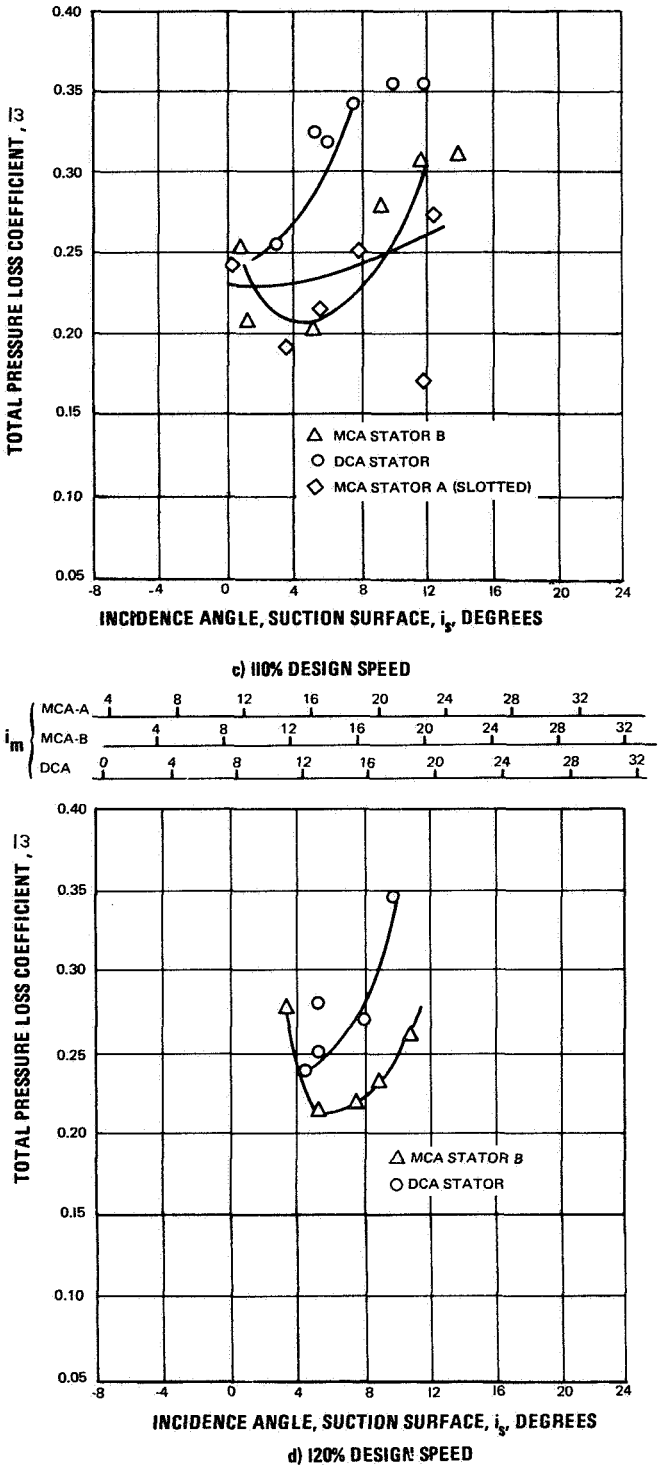

Figure 17 Stator Total Pressure Loss Coefficient vs. Incidence Angle, 5% Span

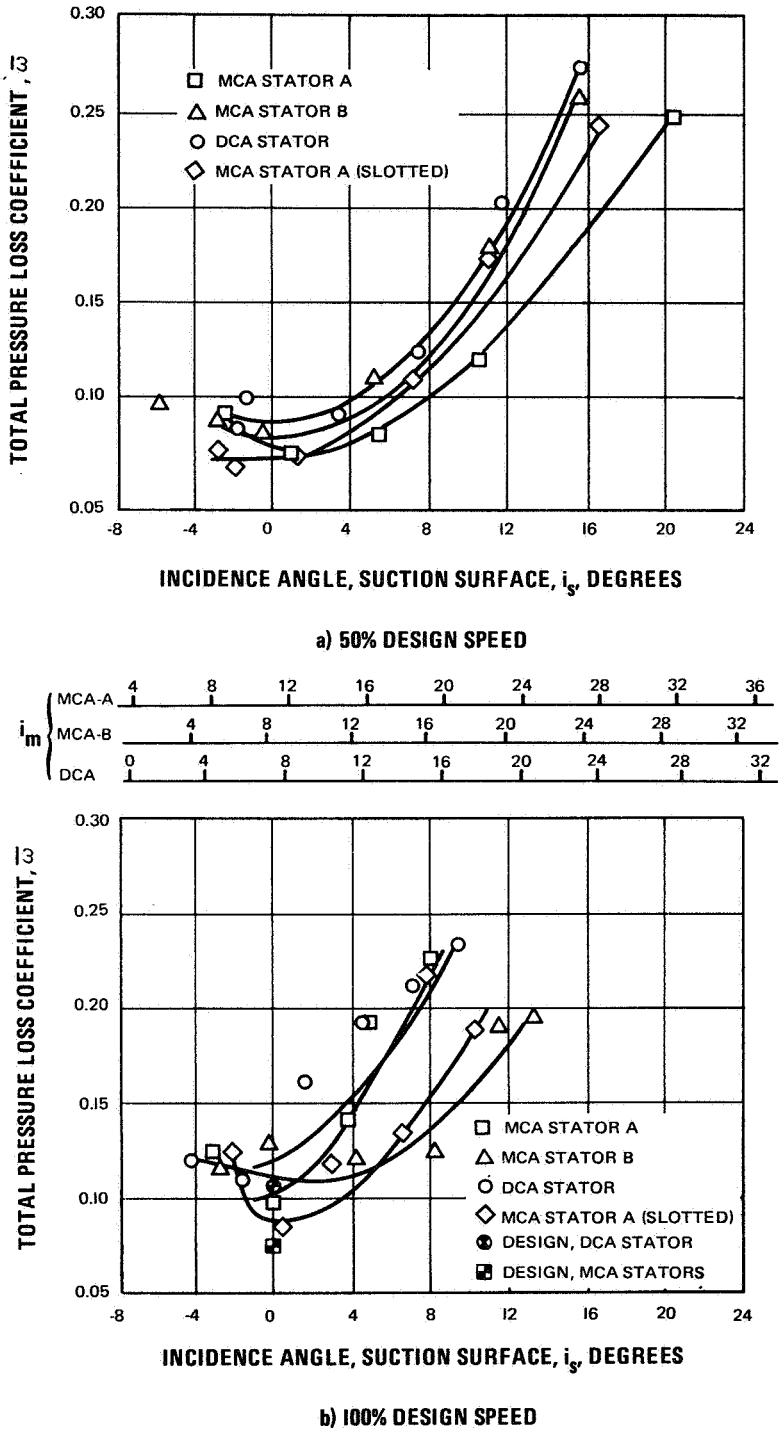

Figure 18 Stator Total Pressure Loss Coefficient vs. Incidence Angle, 10% Span

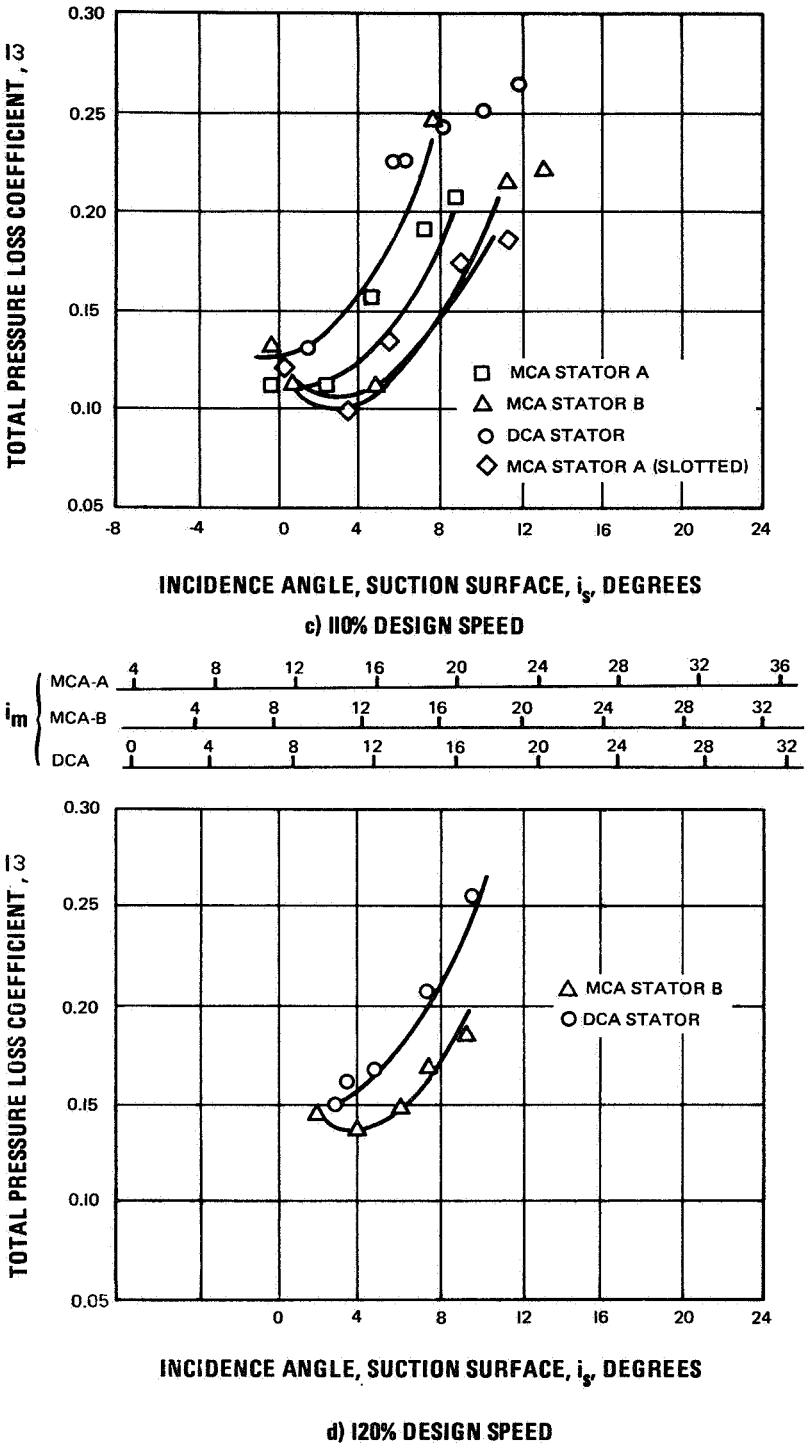

Figure 18 Stator Total Pressure Loss Coefficient vs. Incidence Angle, 10% Span

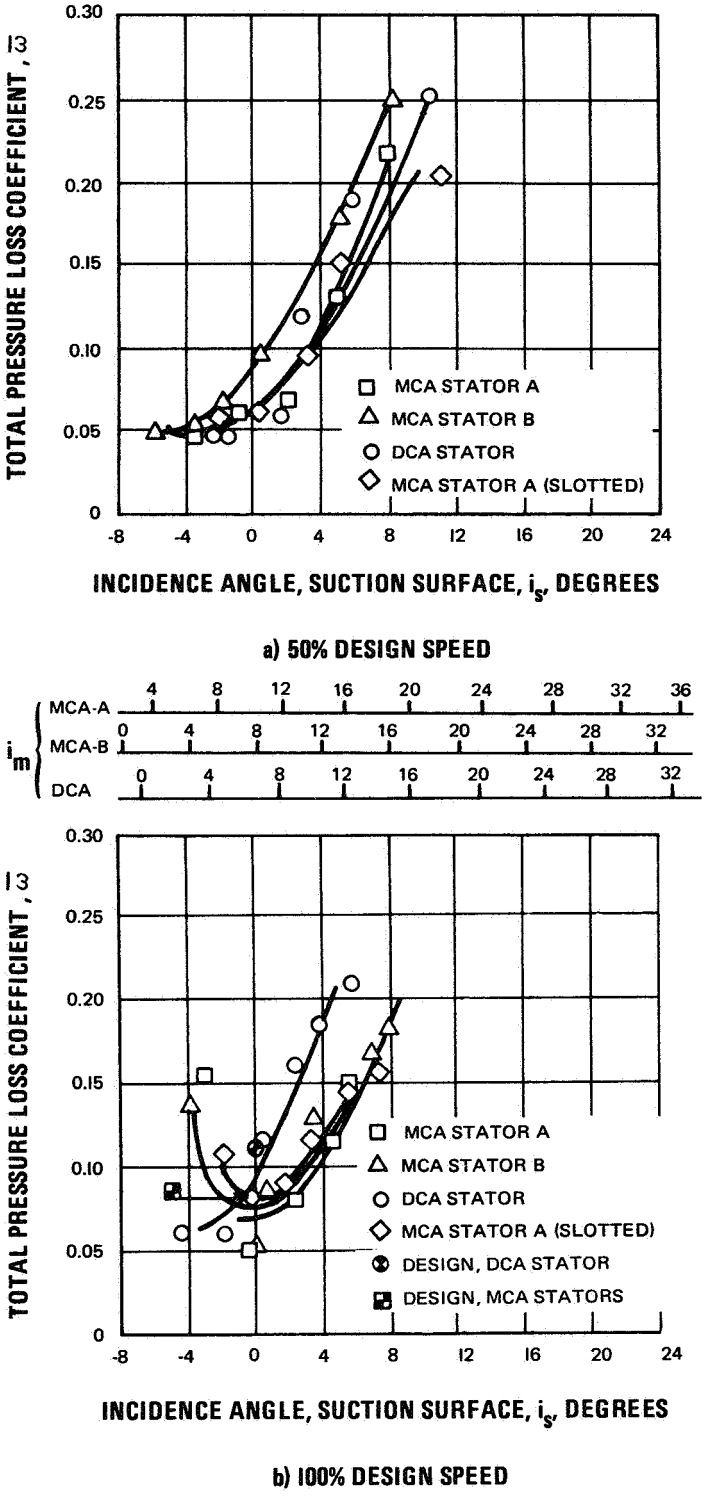

Figure 19 Stator Total Pressure Loss Coefficient vs. Incidence Angle, 30% Span

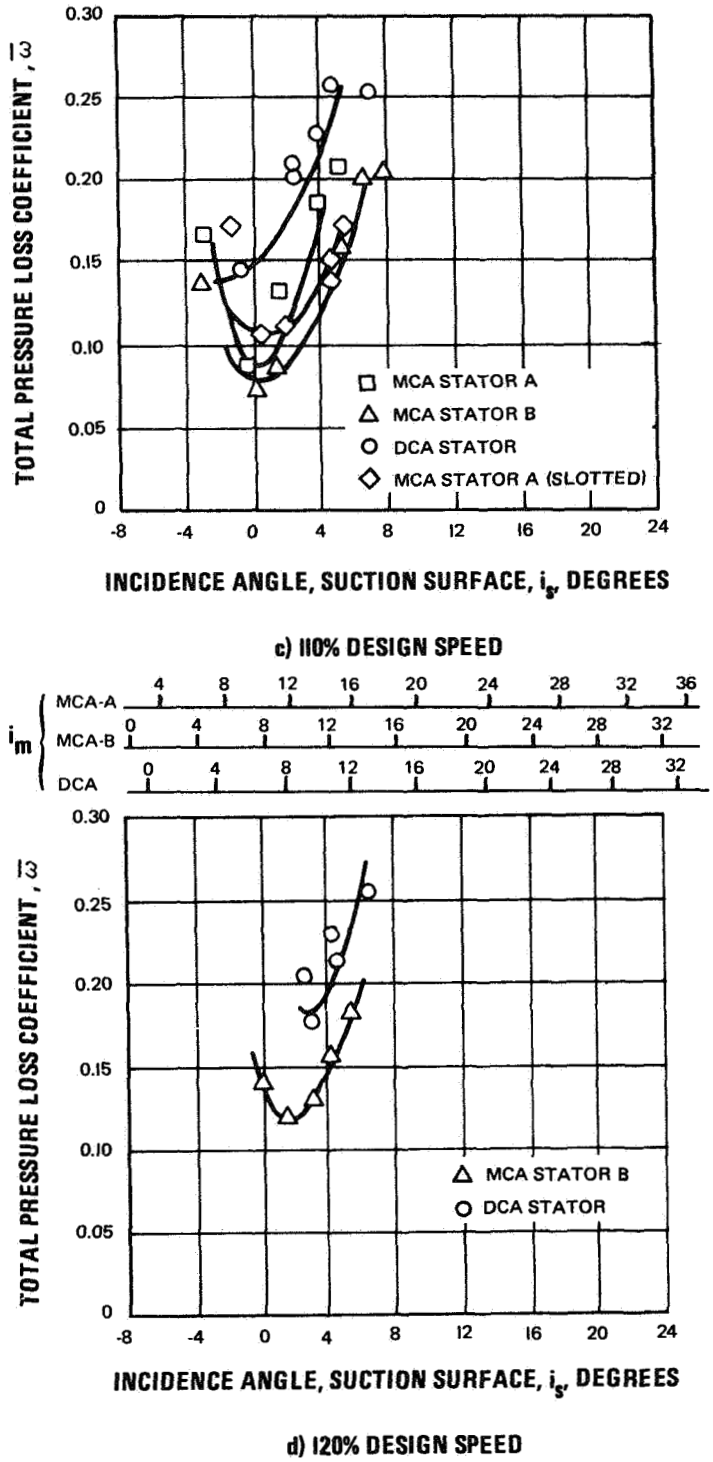

Figure 19 Stator Total Pressure Loss Coefficient vs. Incidence Angle, 30% Span

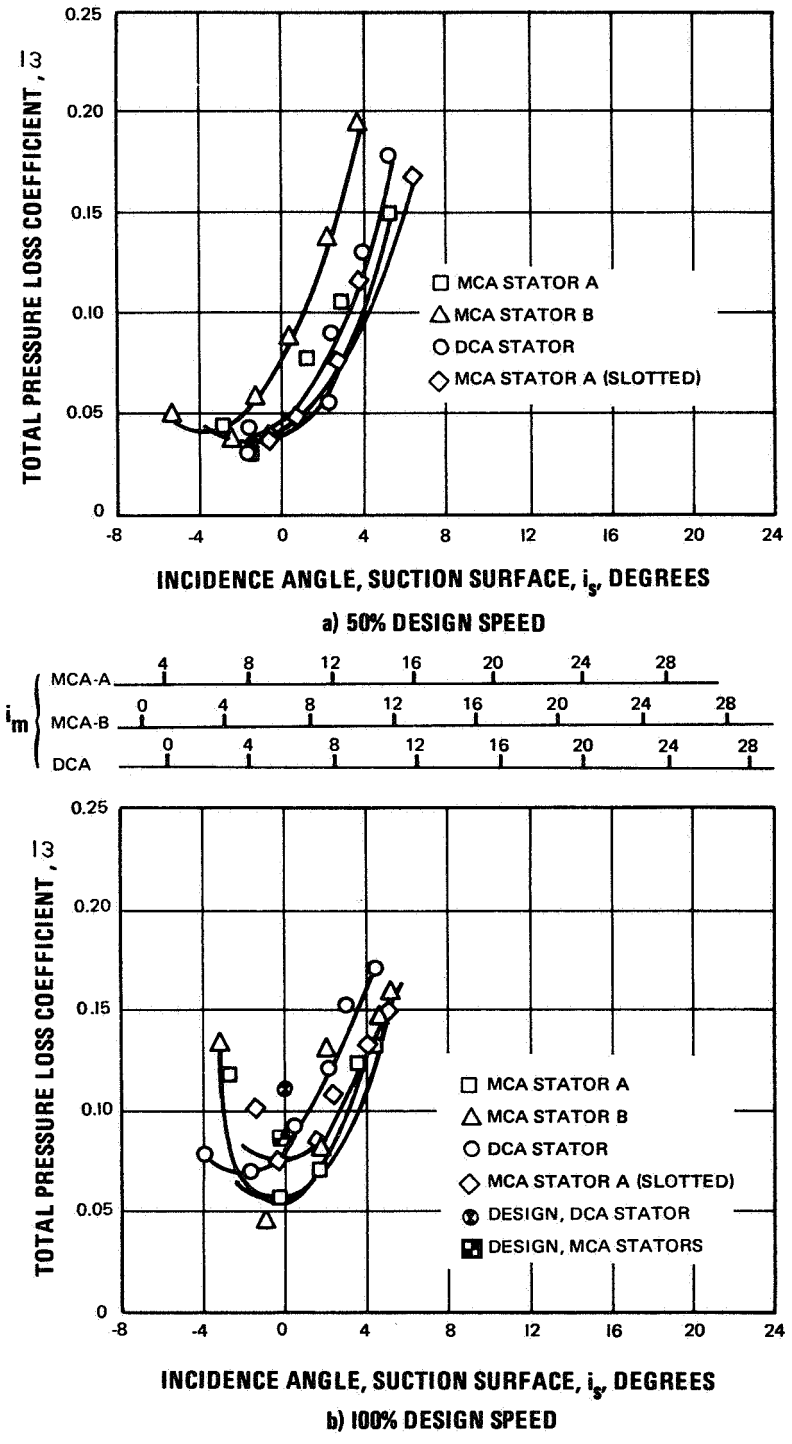

Figure 20 Stator Total Pressure Loss Coefficient vs. Incidence Angle, 50% Span

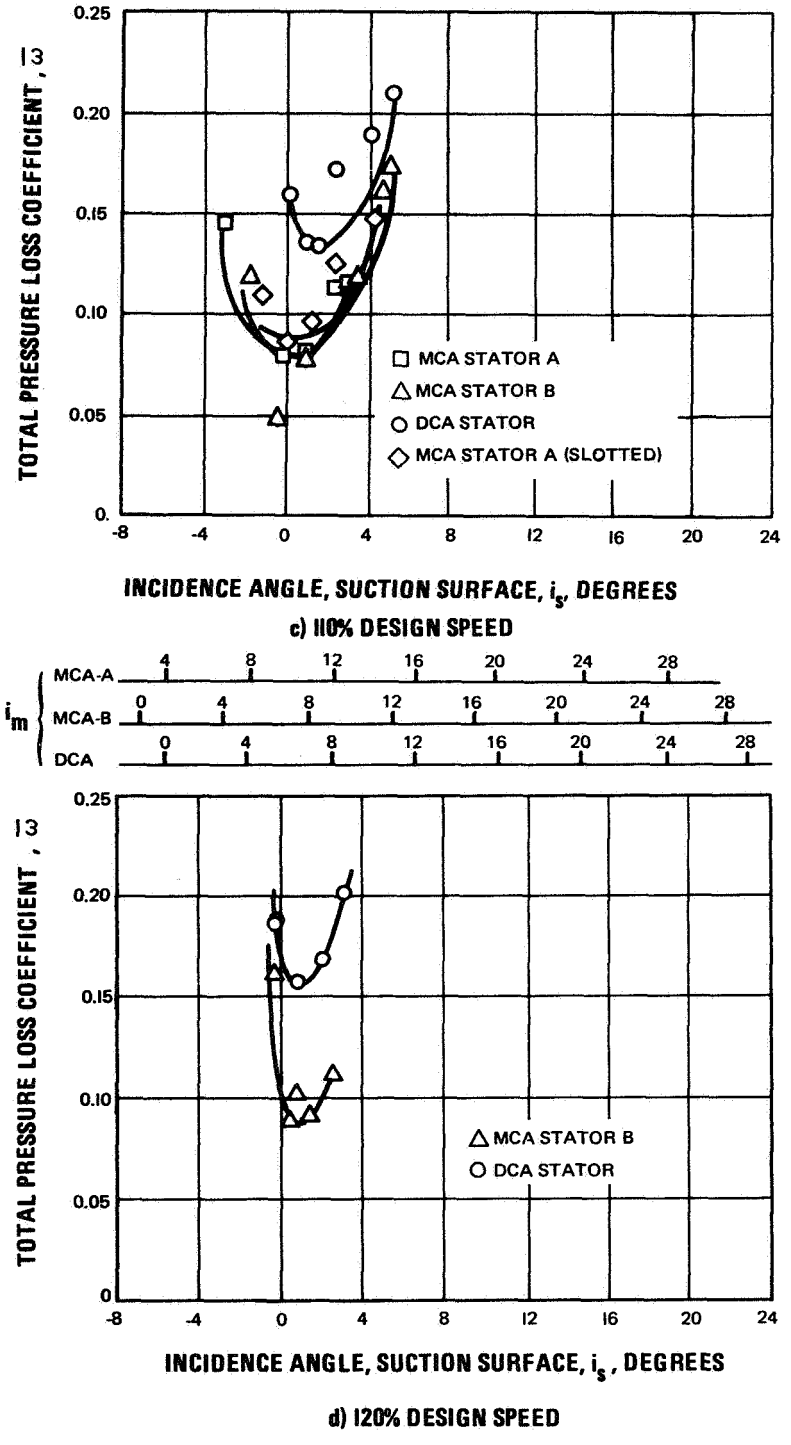

Figure 20 Stator Total Pressure Loss Coefficient vs. Incidence Angle, 50% Span

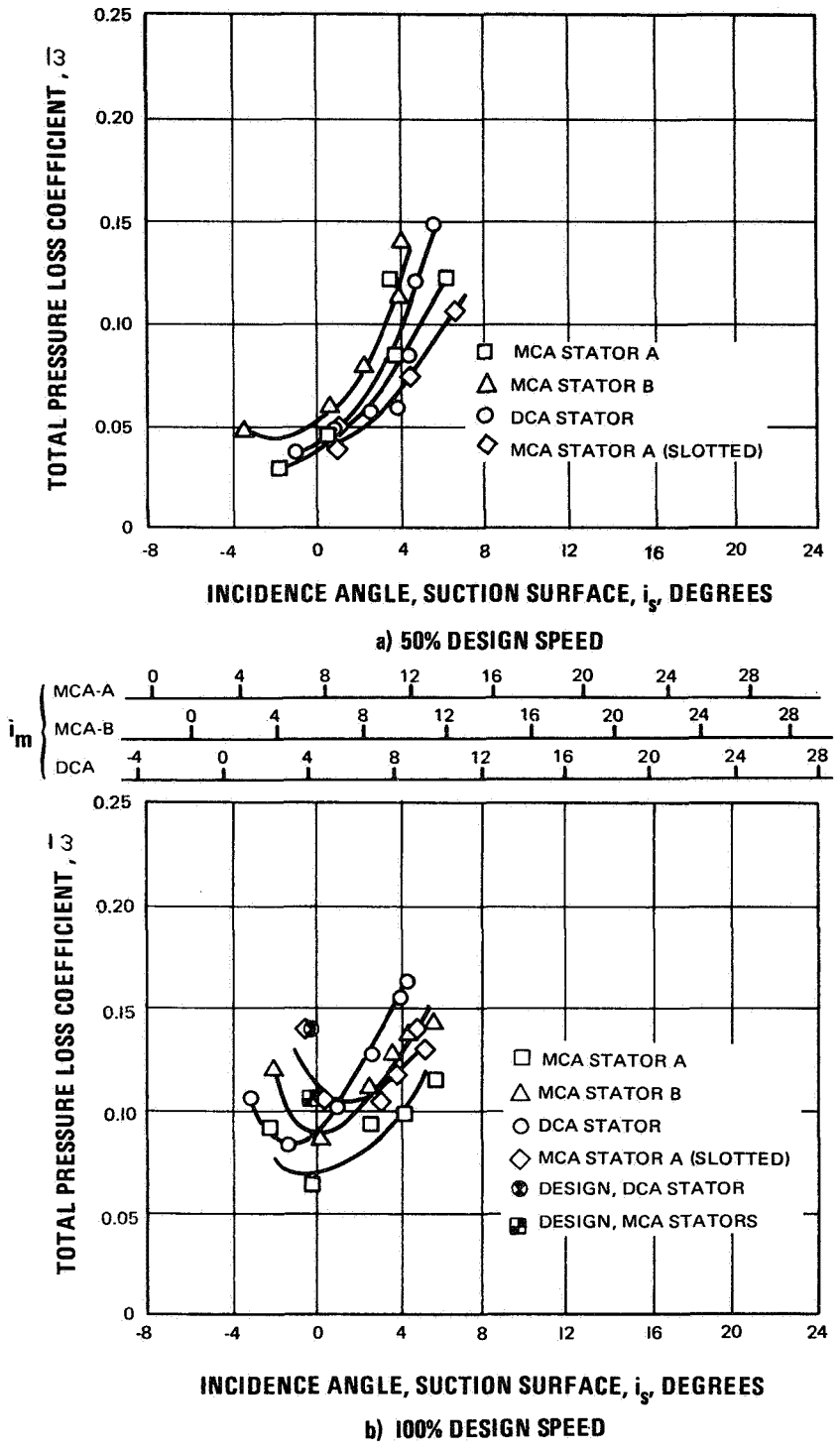

Figure 21 Stator Total Pressure Loss Coefficient vs. Incidence Angle, 70% Span

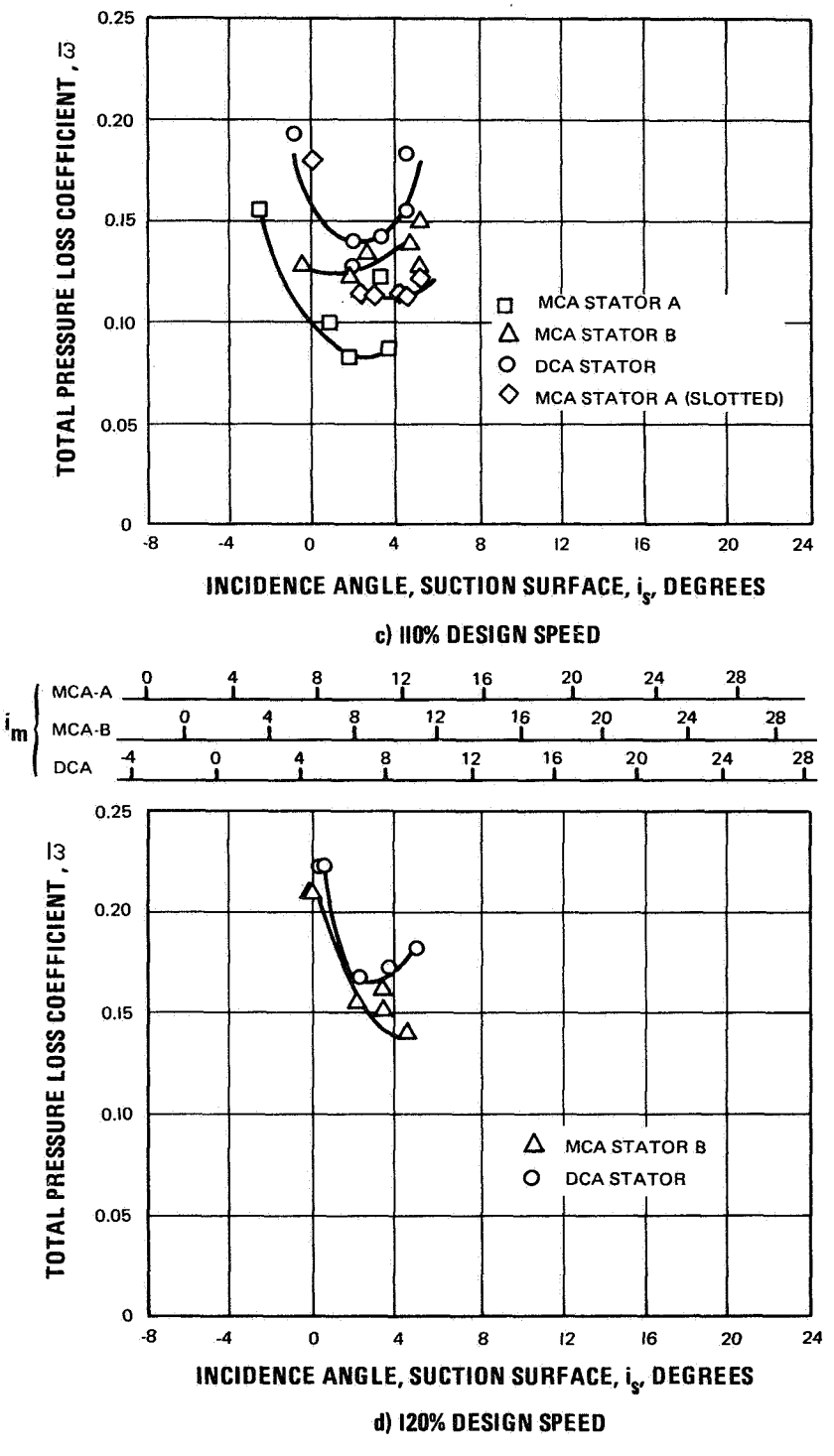

Figure 21 Stator Total Pressure Loss Coefficient vs. Incidence Angle, 70% Span

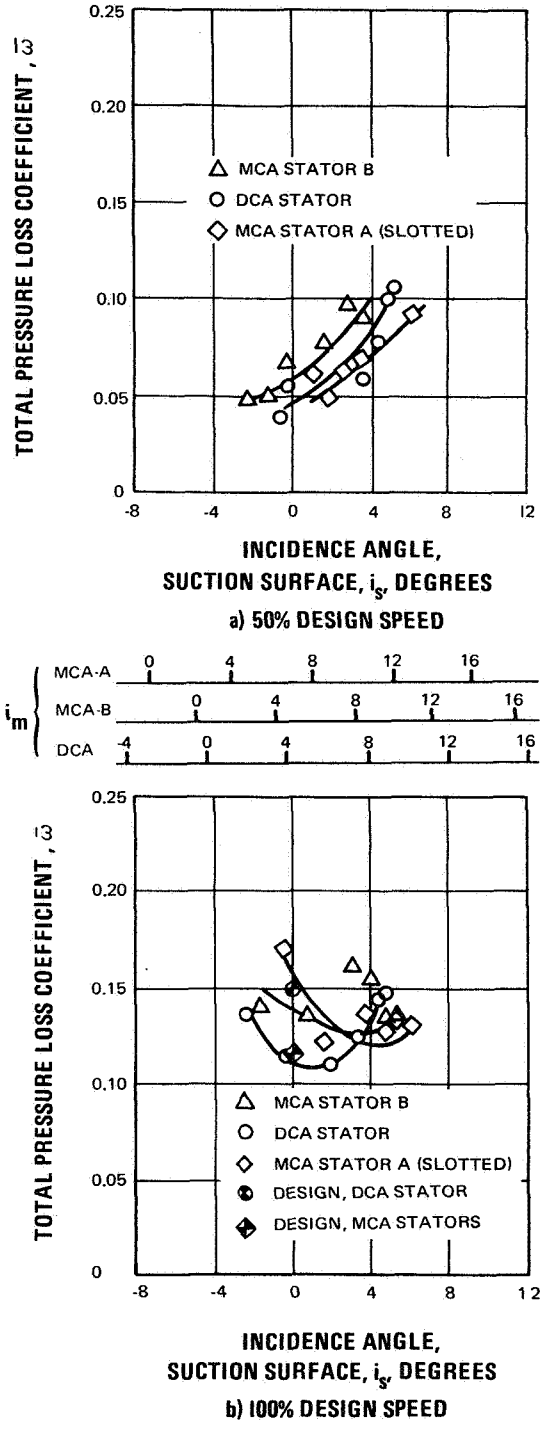

Figure 22 Stator Total Pressure Loss Coefficient vs. Incidence Angle, 80% Span

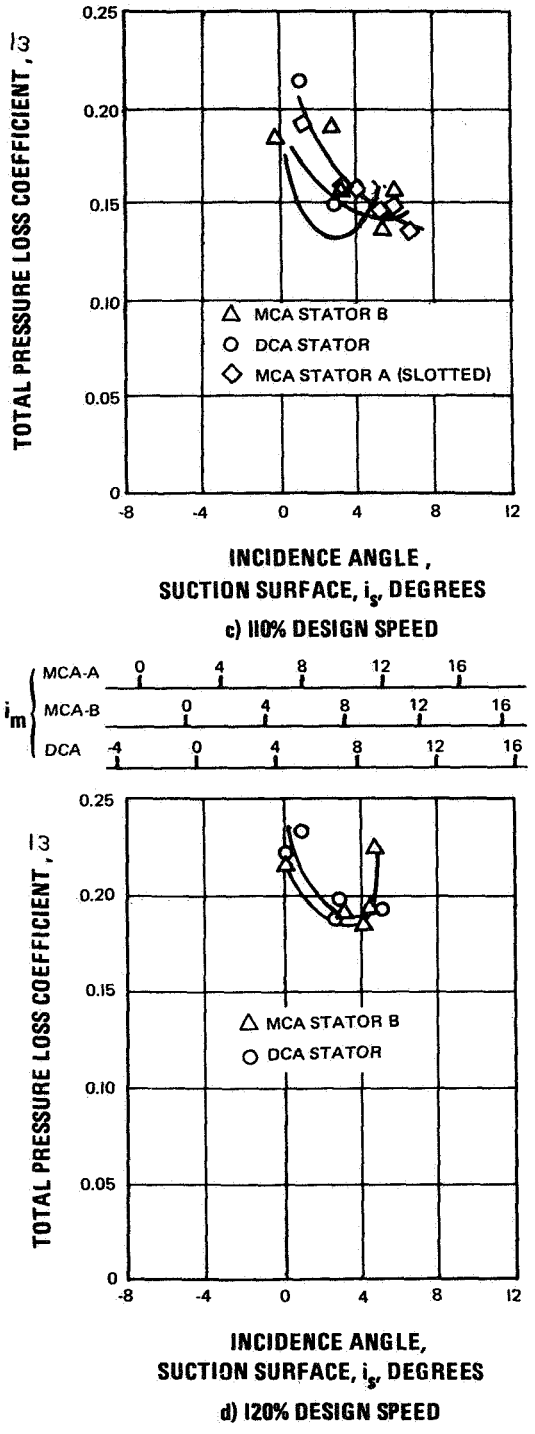

Figure 22 Stator Total Pressure Loss Coefficient vs. Incidence Angle, 80% Span

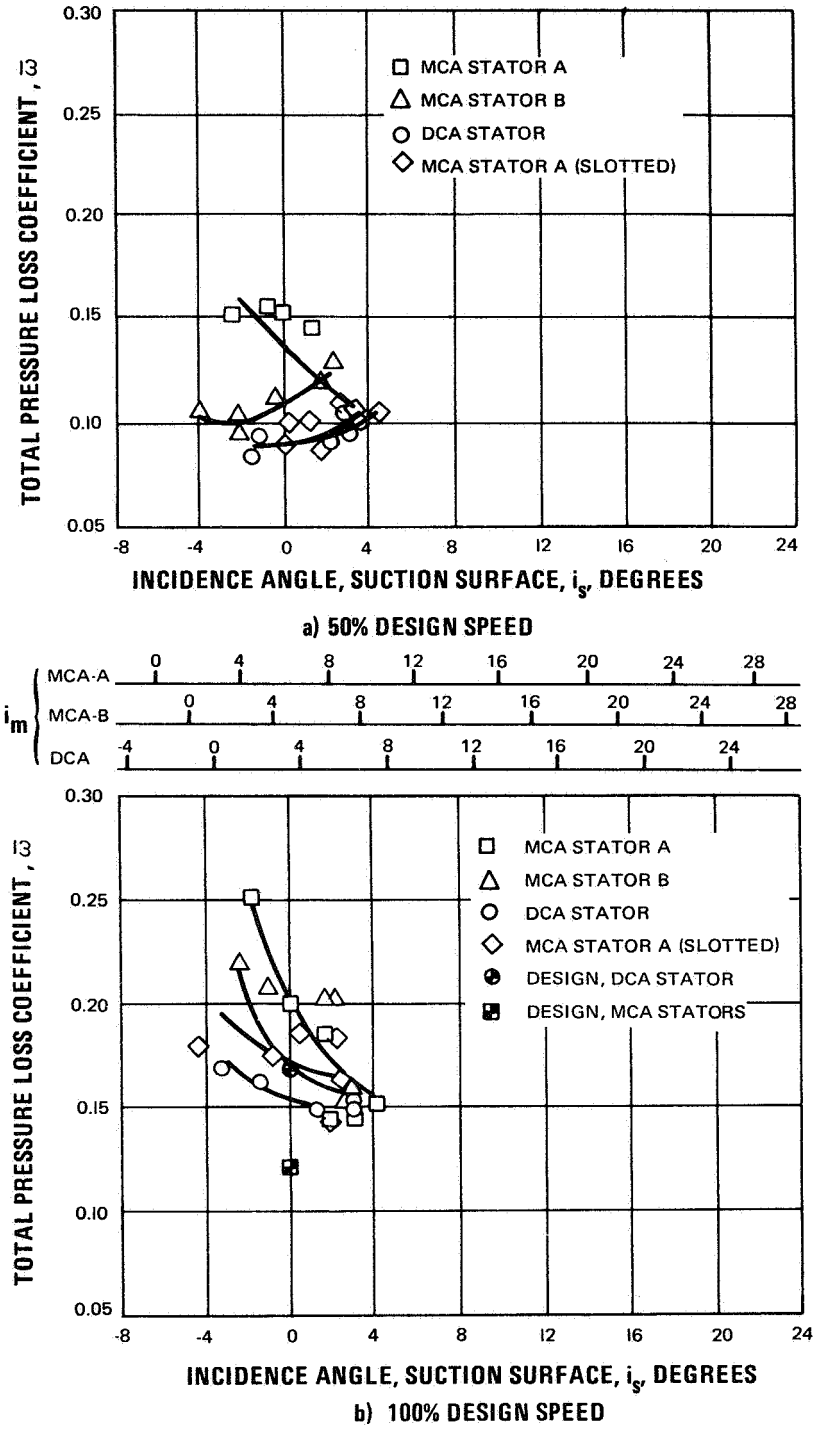

Figure 23 Stator Total Pressure Loss Coefficient vs. Incidence Angle, 90% Span

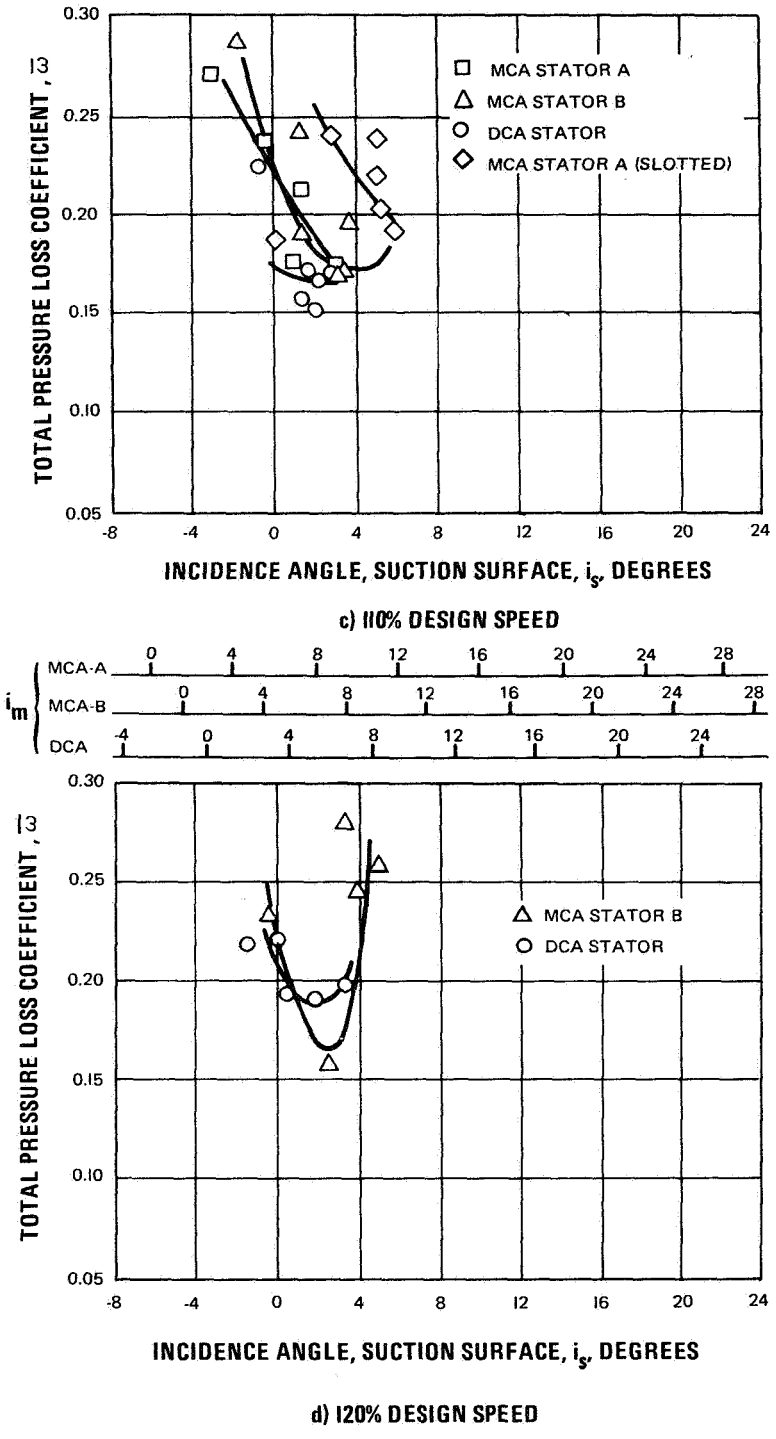

Figure 23 Stator Total Pressure Loss Coefficient vs. Incidence Angle, 90% Span

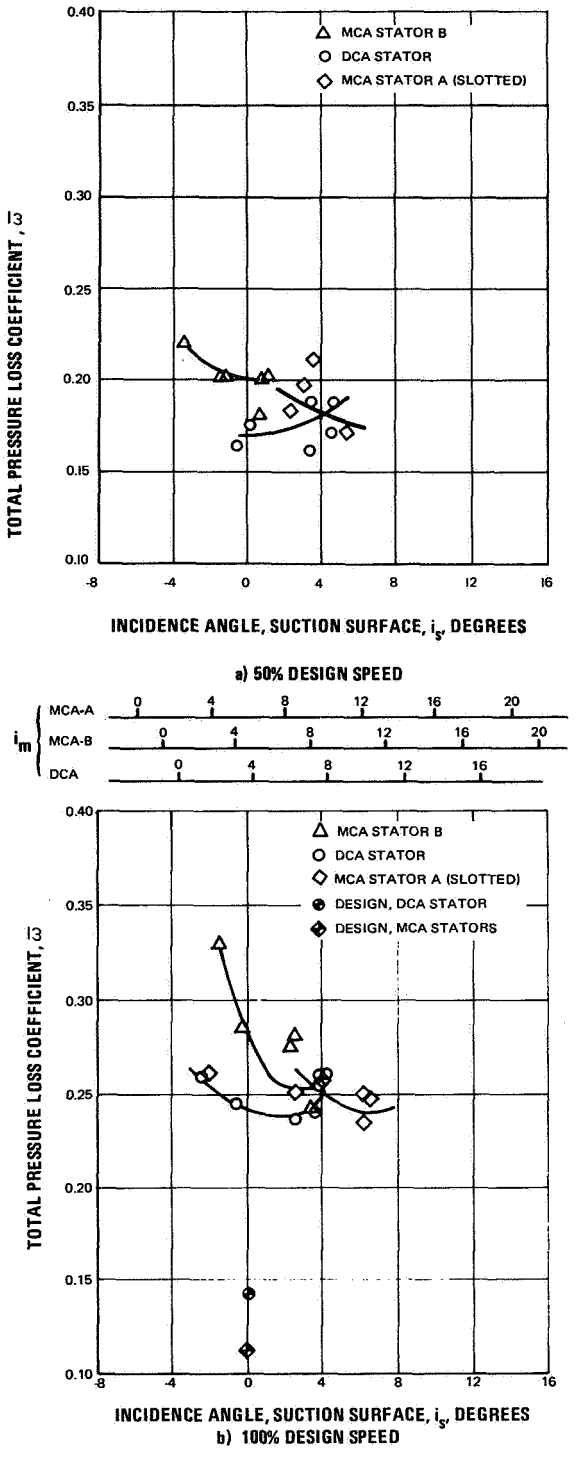

Figure 24 Stator Total Pressure Loss Coefficient vs. Incidence Angle, 95% Span

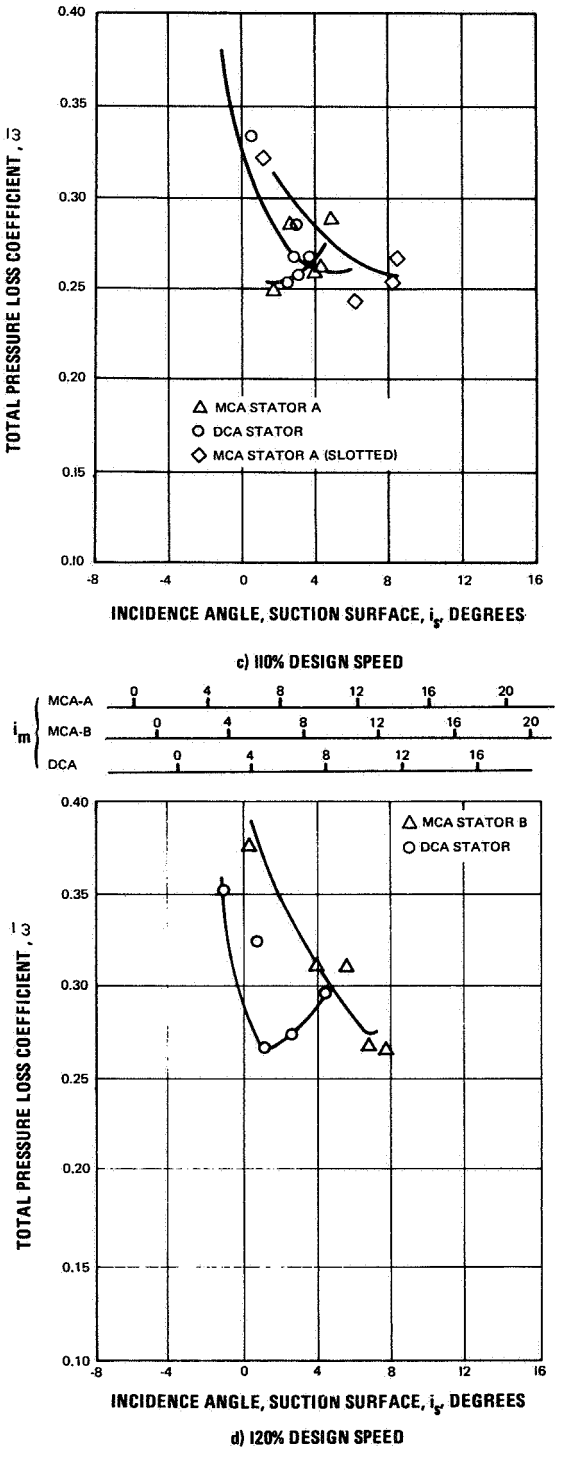

Figure 24 Stator Total Pressure Loss Coefficient vs. Incidence Angle, 95% Span

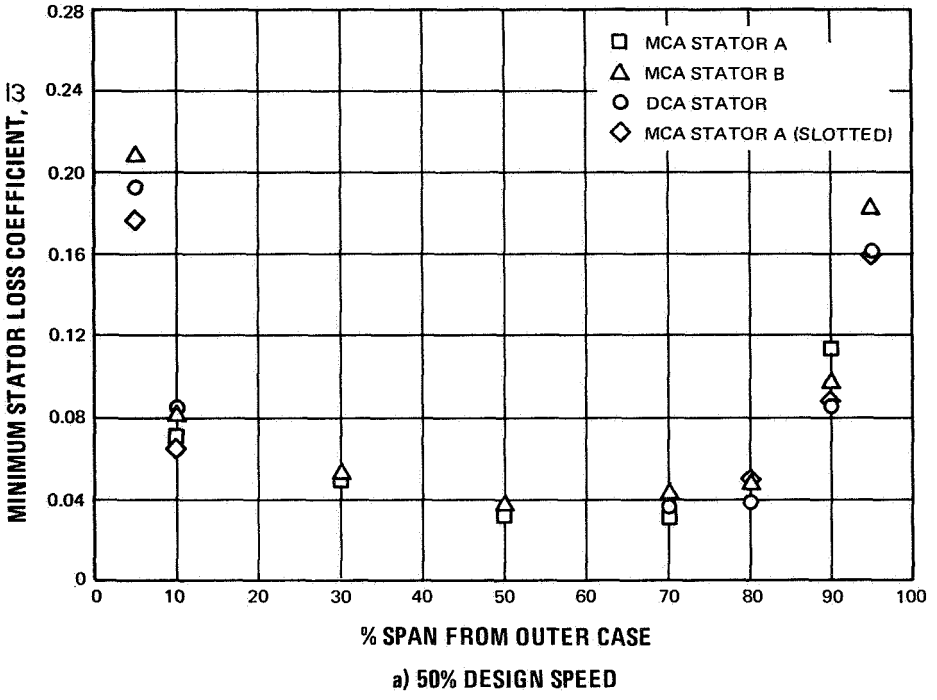

a) 50% DESIGN SPEED

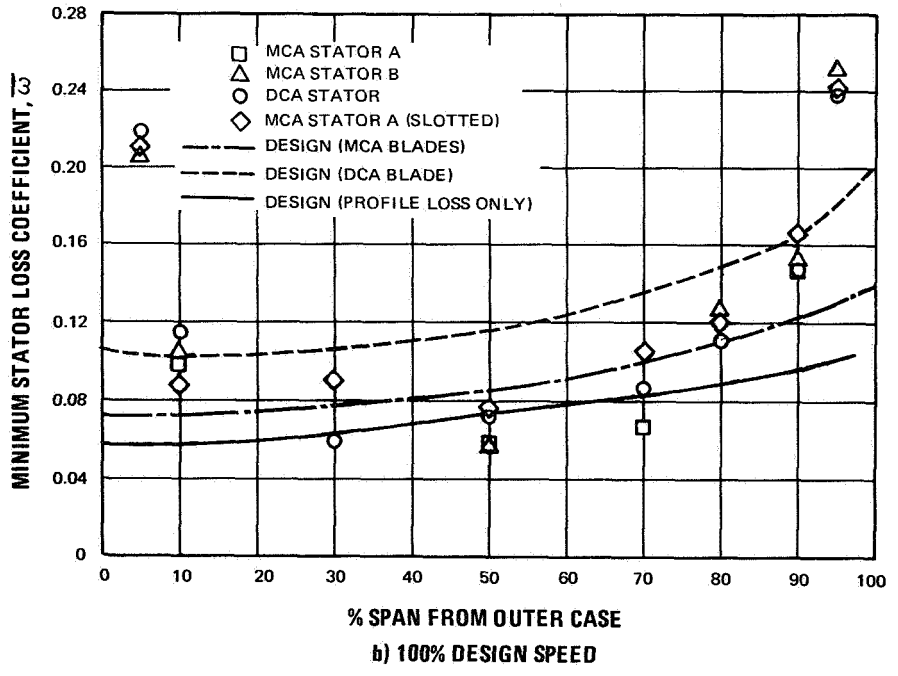

b) 100% DESIGN SPEED

Figure 25 Minimum Stator Loss Coefficient vs. Percent Span

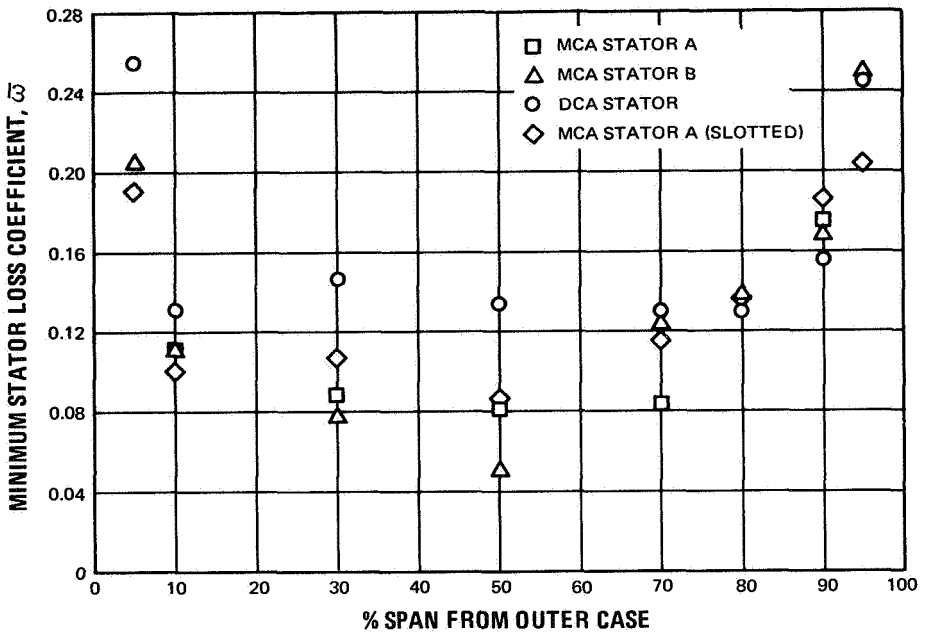

c) 110% DESIGN SPEED

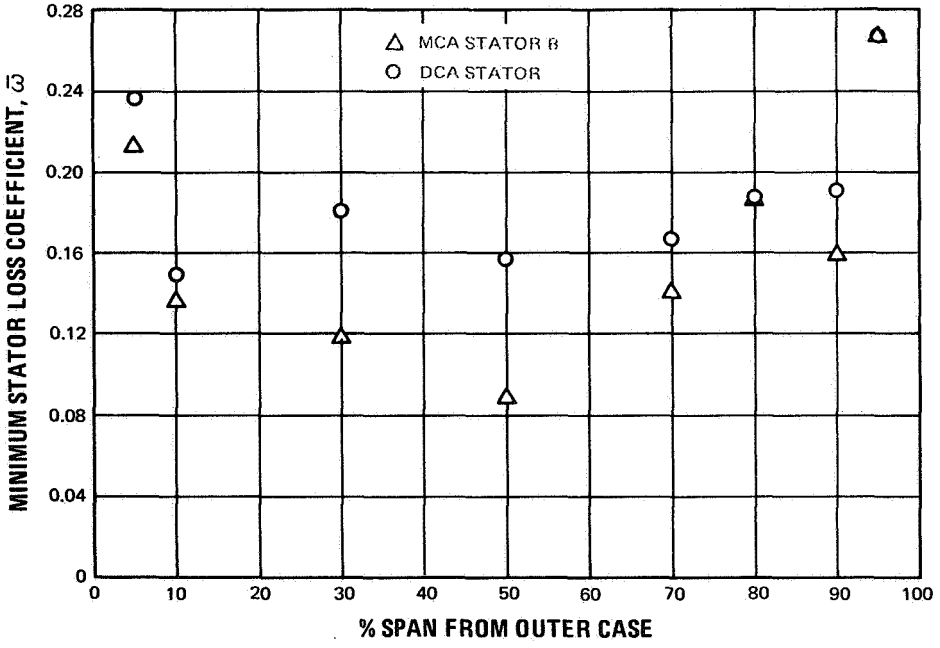

d) 120% DESIGN SPEED

Figure 25 Minimum Stator Loss Coefficient vs. Percent Span

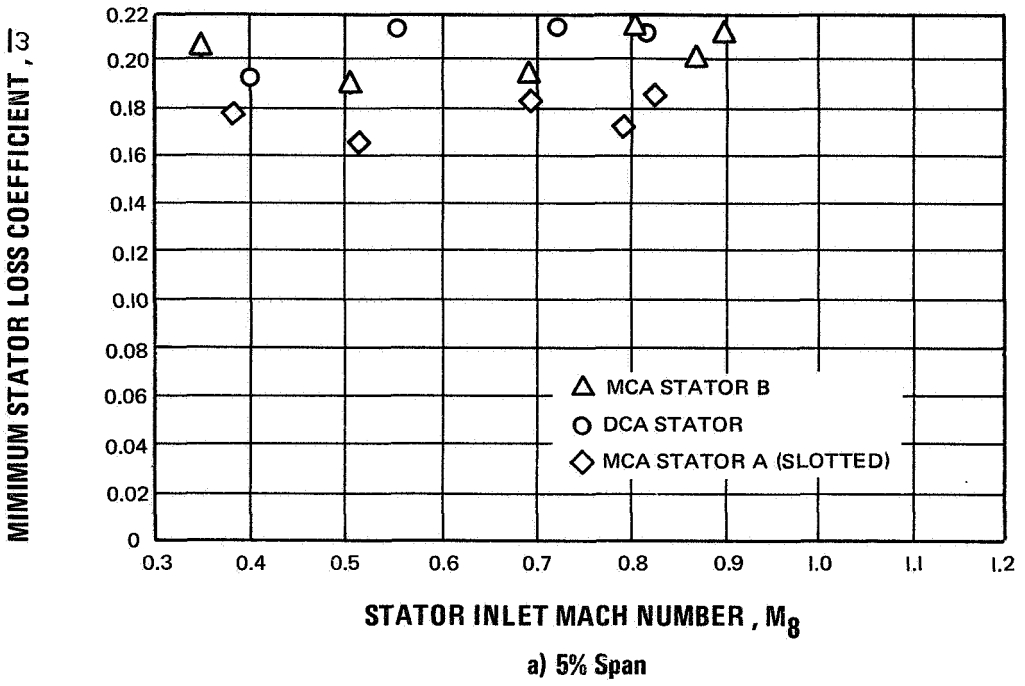

a) 5% Span

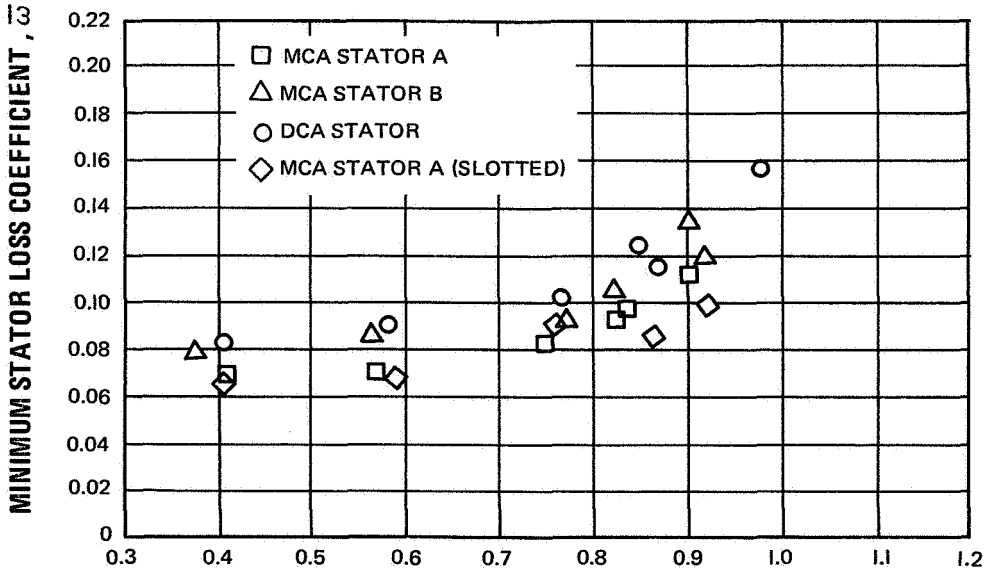

b) 10% Span

Figure 26 Minimum Stator Loss Coefficient vs. Stator Inlet Mach Number

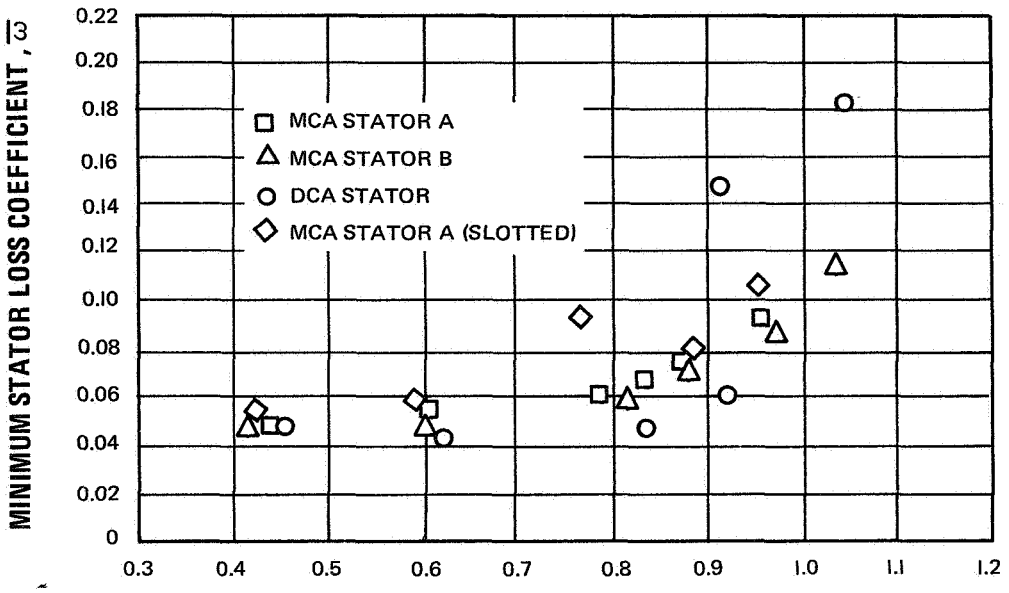

c) 30% Span

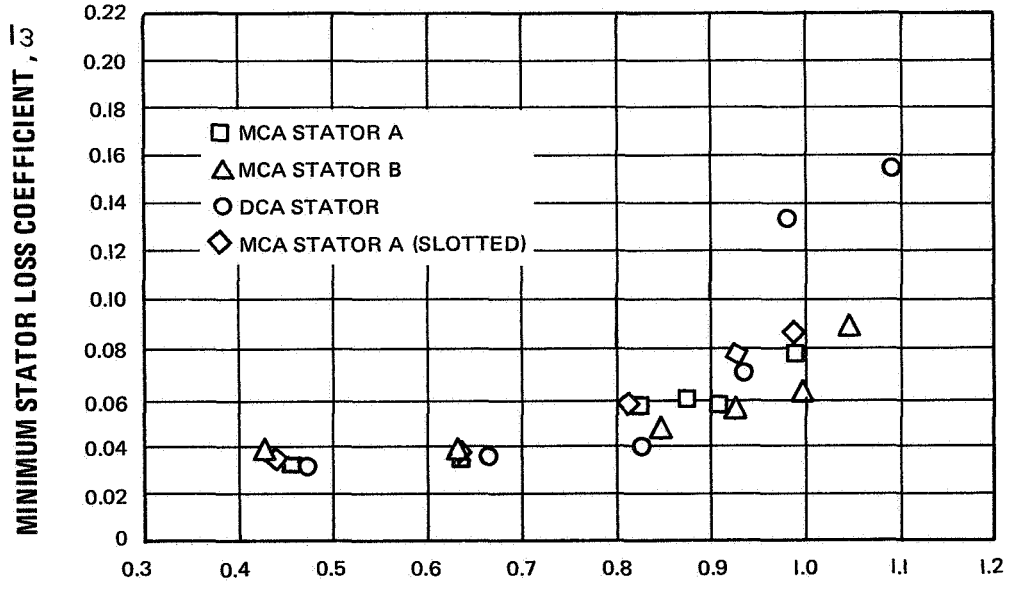

d) 50% Span

Figure 26 Minimum Stator Loss Coefficient vs. Stator Inlet Mach Number

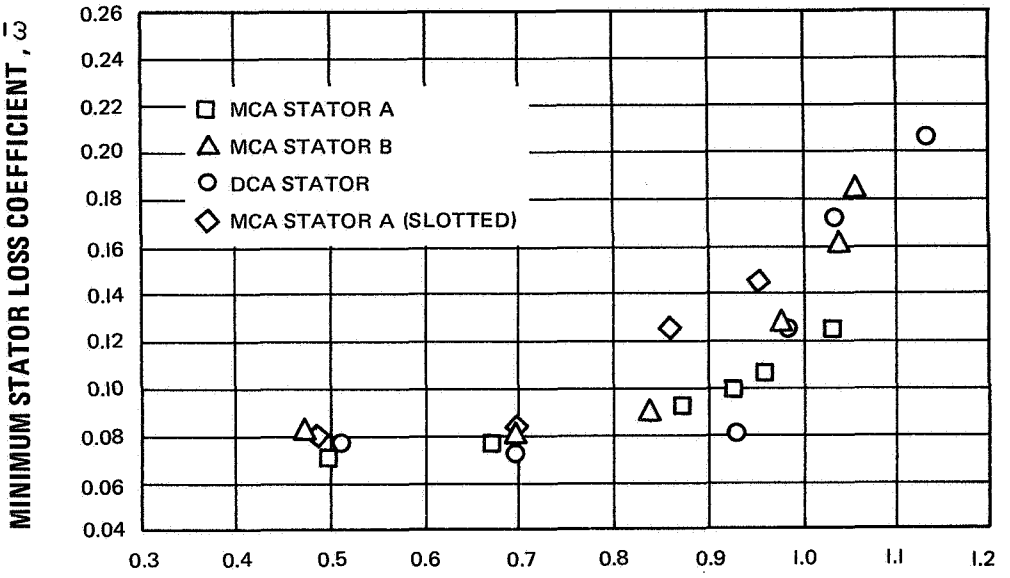

e) 70% Span

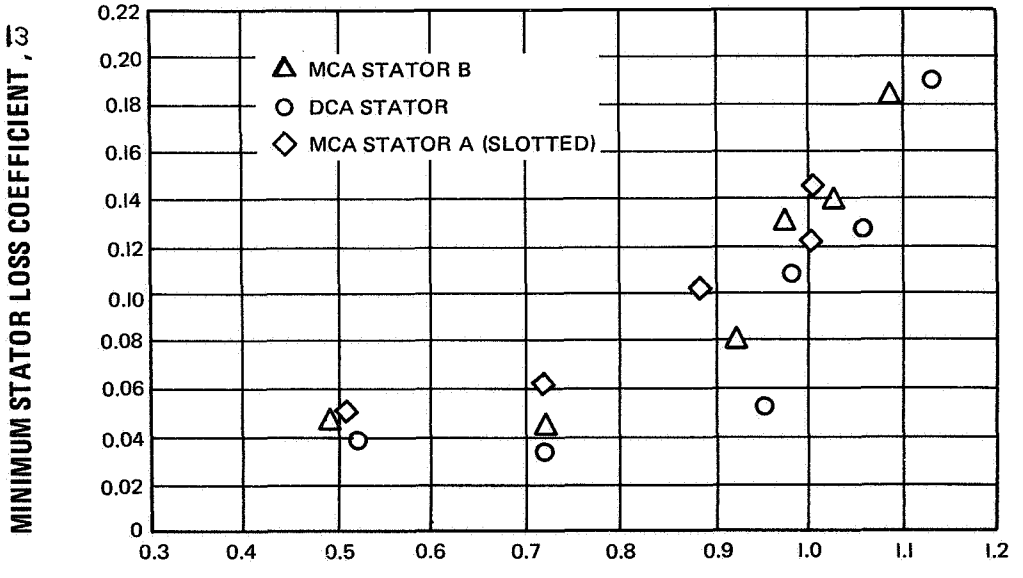

f) 80% Span

Figure 26 Minimum Stator Loss Coefficient vs. Stator Inlet Mach Number

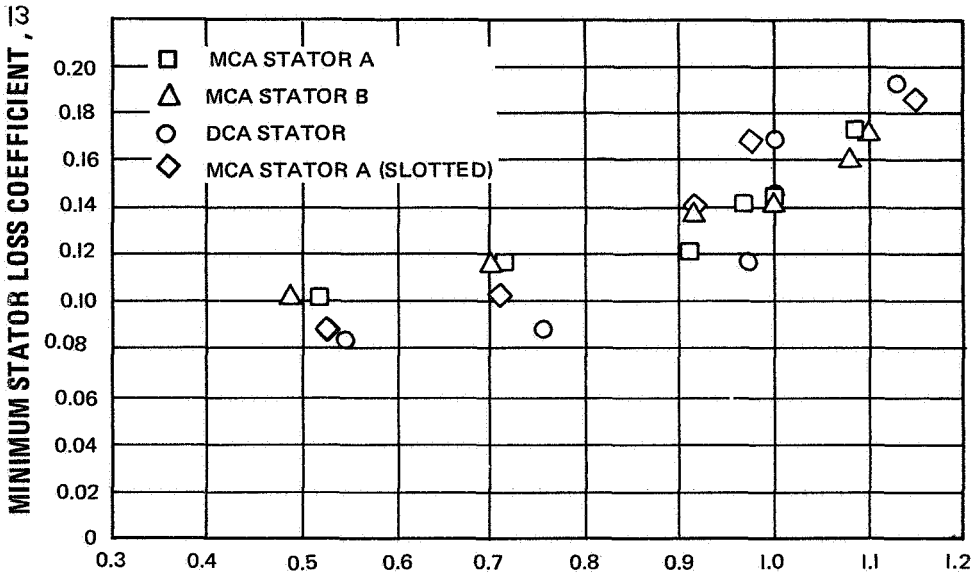

g) 90% Span

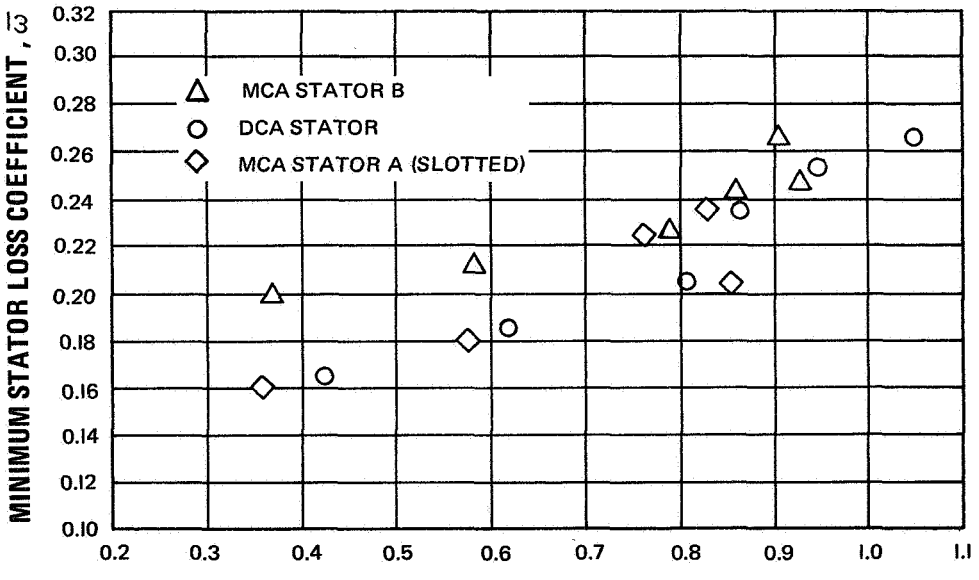

h) 95% Span

Figure 26 Minimum Stator Loss Coefficient vs. Stator Inlet Mach Number

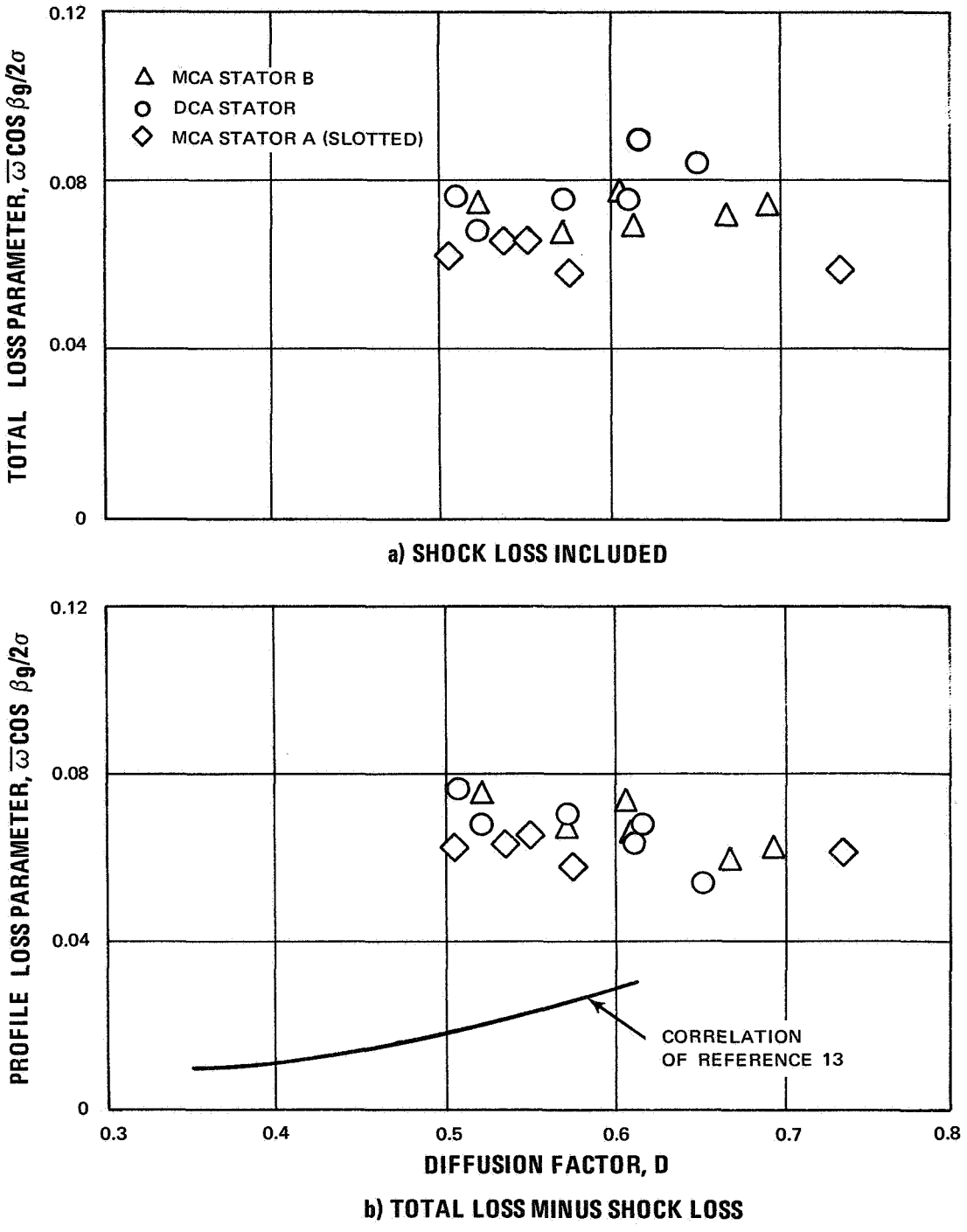

Figure 27 Minimum Stator Loss Parameter vs. Diffusion Factor, 5% Span

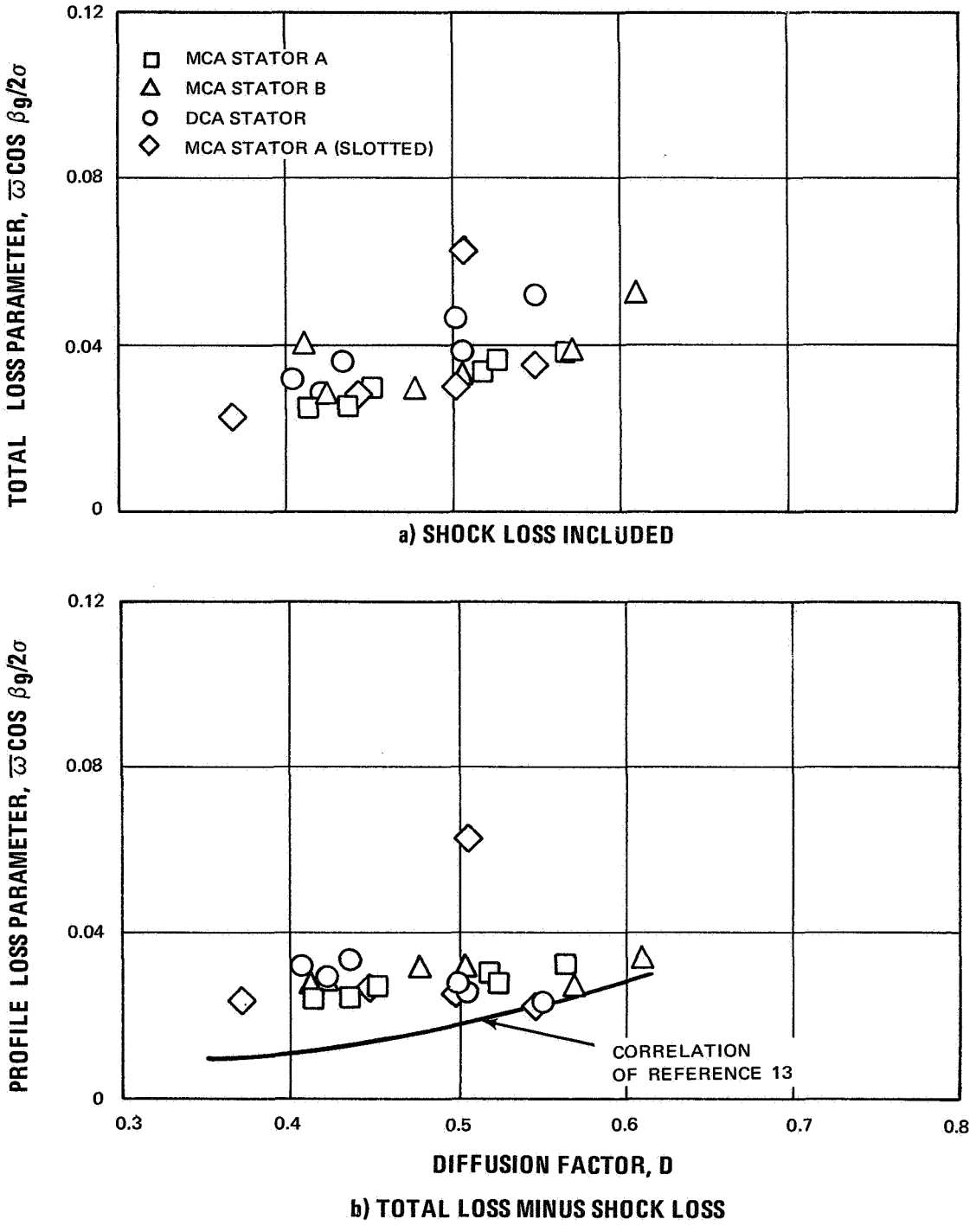

Figure 28 Minimum Stator Loss Parameter vs. Diffusion Factor, 10% Span

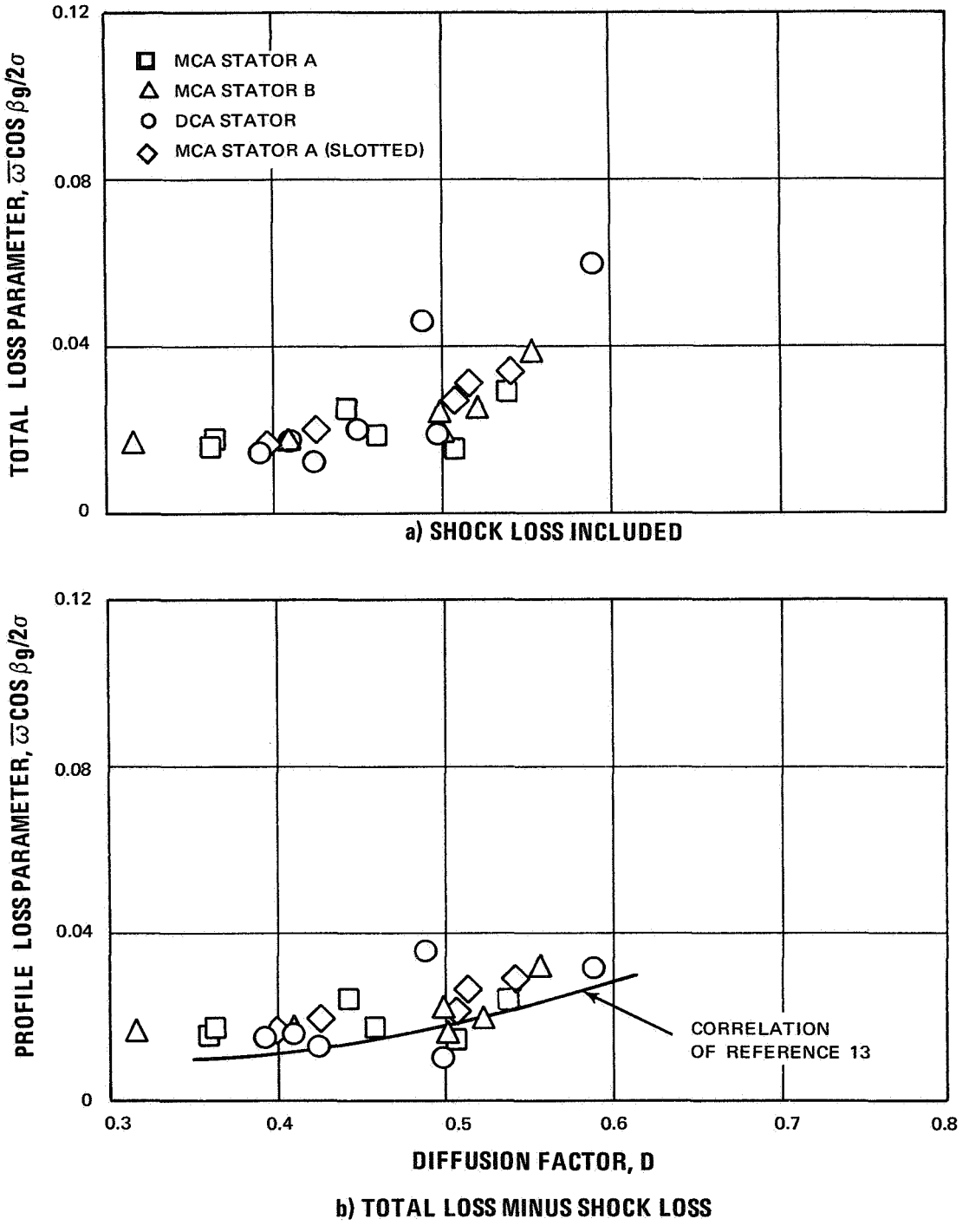

Figure 29 Minimum Stator Loss Parameter vs. Diffusion Factor, 30% Span

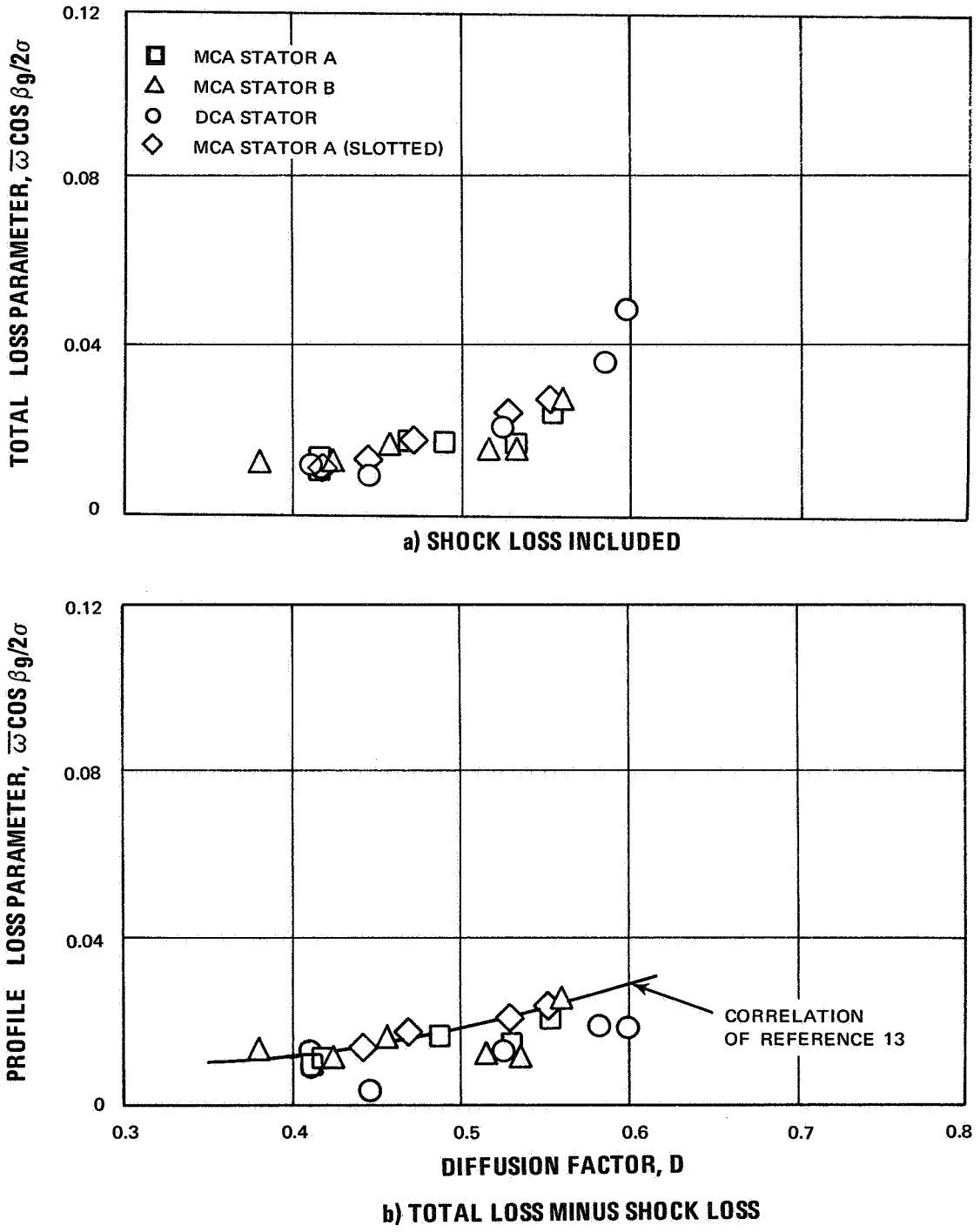

Figure 30 Minimum Stator Loss Parameter vs. Diffusion Factor, 50% Span

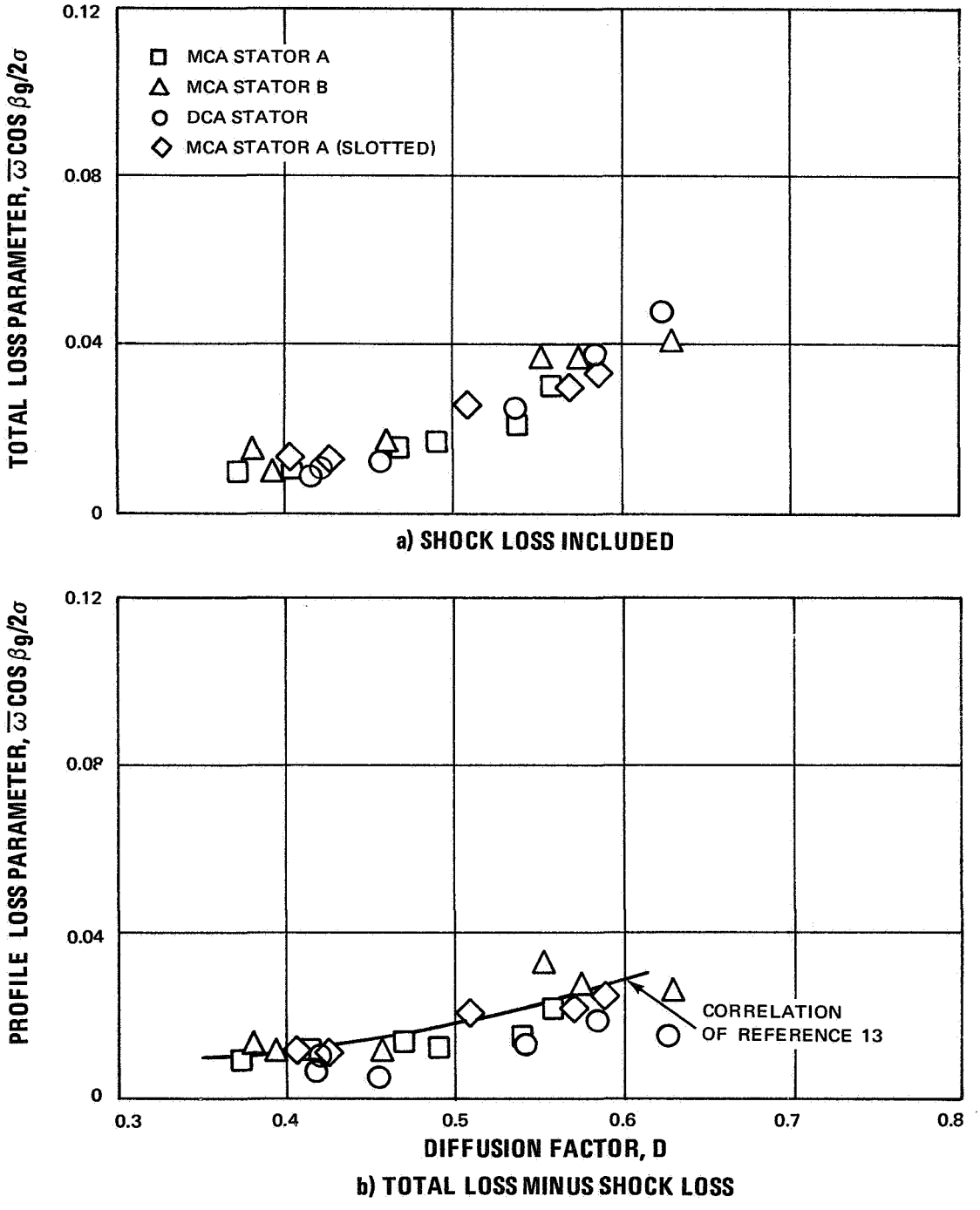

Figure 31 Minimum Stator Loss Parameter vs. Diffusion Factor, 70% Span

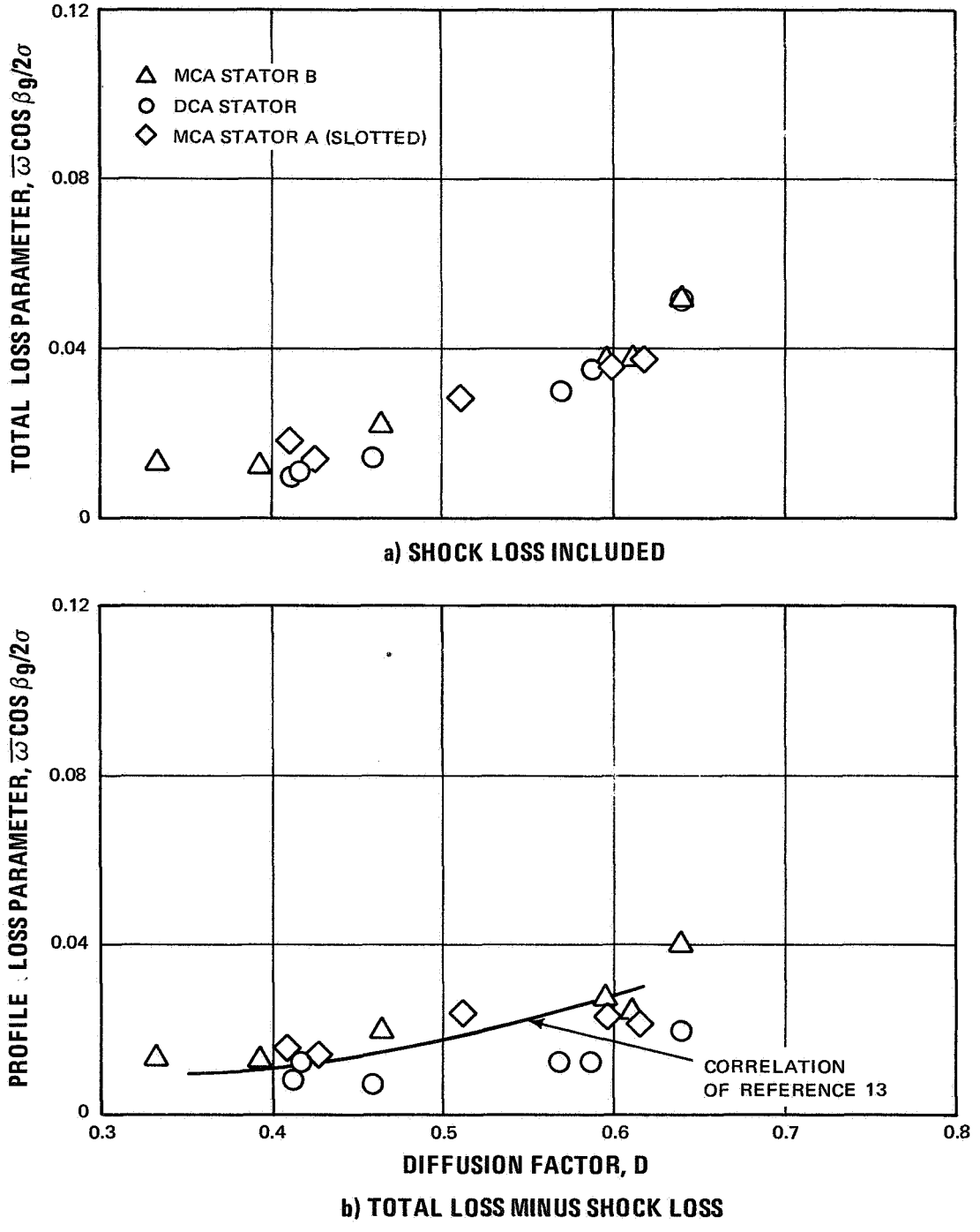

Figure 32 Minimum Stator Loss Parameter vs. Diffusion Factor, 80% Span

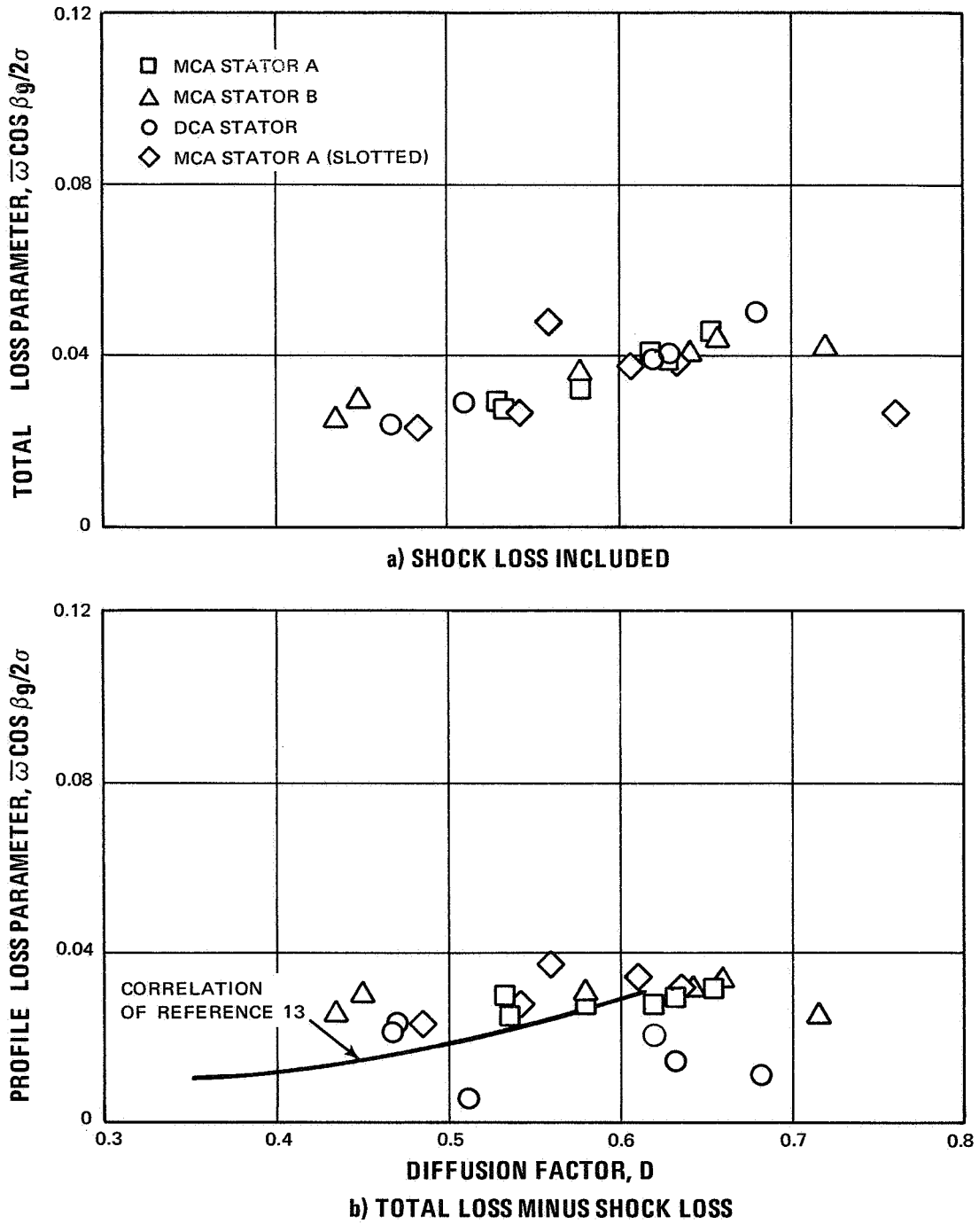

Figure 33 Minimum Stator Loss Parameter vs. Diffusion Factor, 90% Span

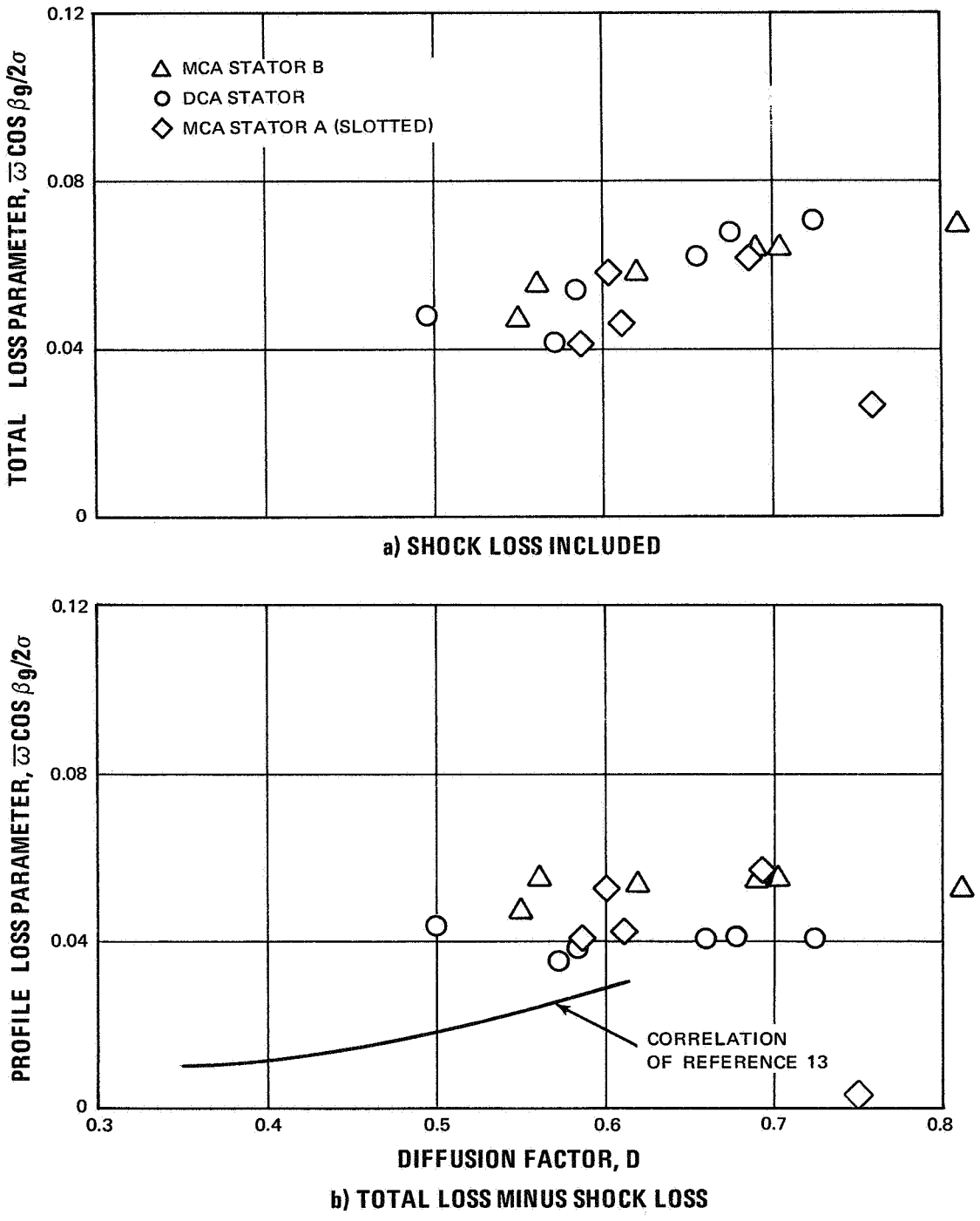

Figure 34 Minimum Stator Loss Parameter vs. Diffusion Factor, 95% Span

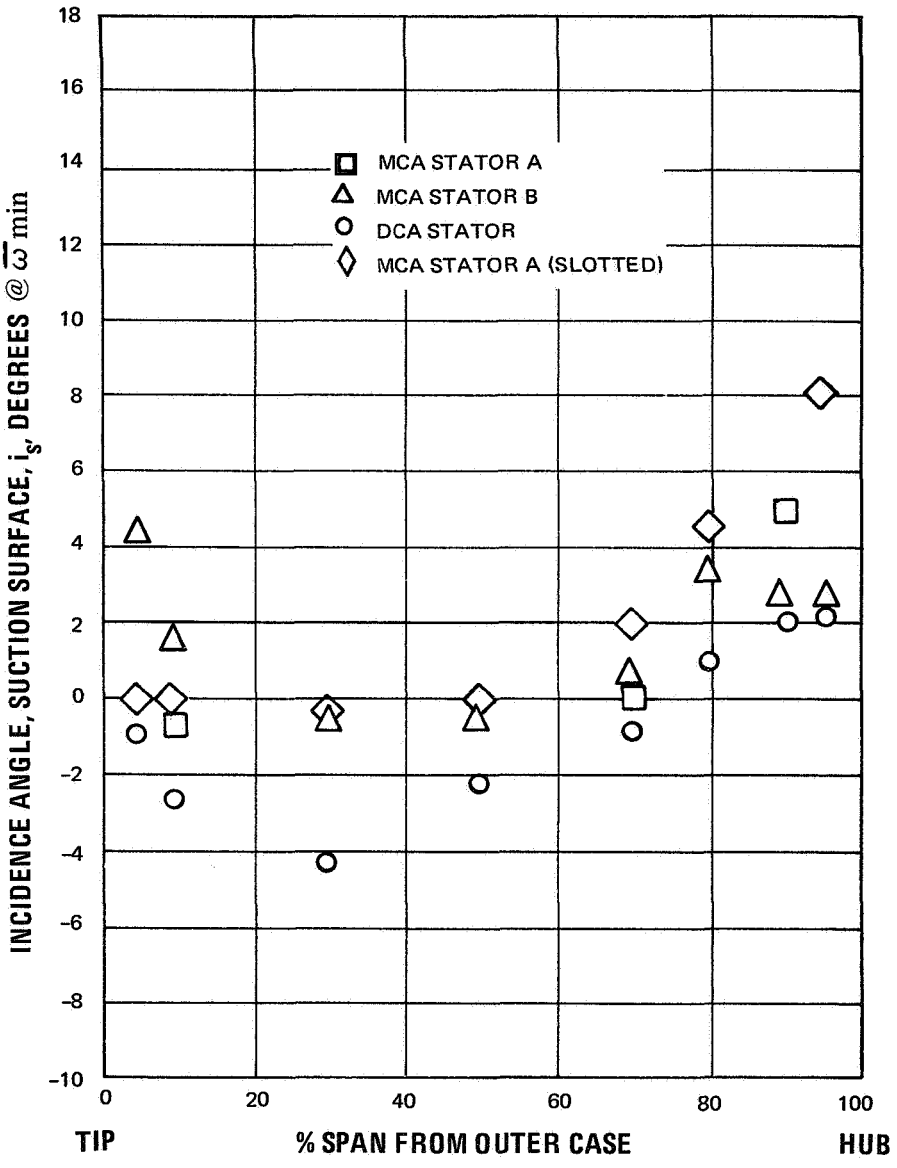

Figure 35 Incidence Angle to the Suction Surface at Stator Minimum Loss vs. Percent Span, 100% Design Speed

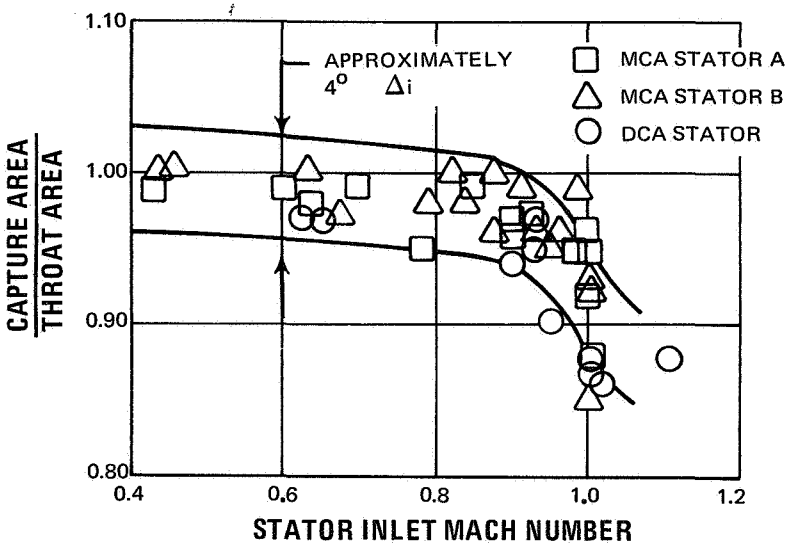

Figure 36 Ratio of Capture Area to Throat Area at Minimum Loss vs. Stator Inlet Mach Number

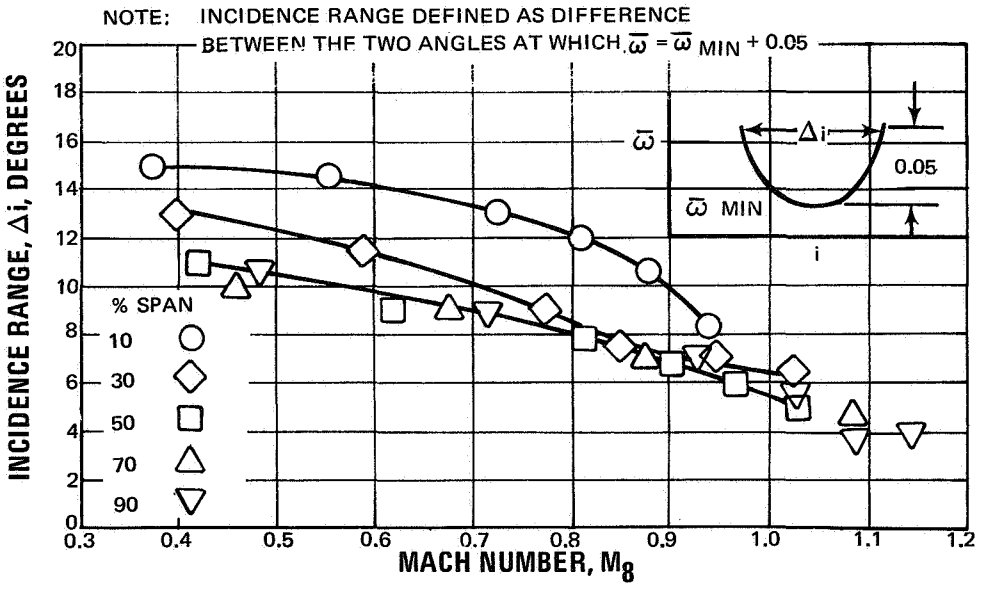

Figure 37 Incidence Range of MCA Stator B vs. Mach Number

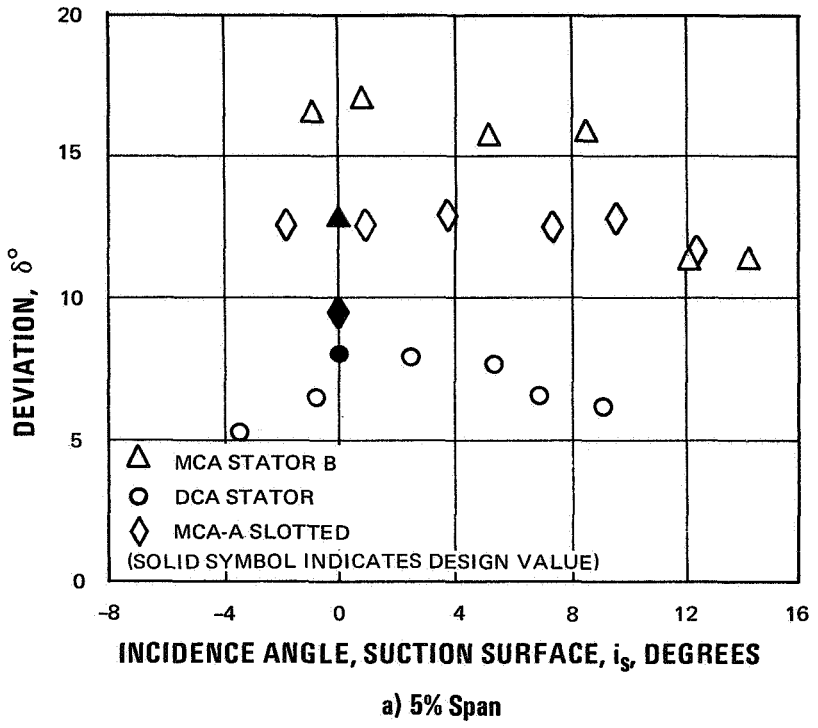

a) 5% Span

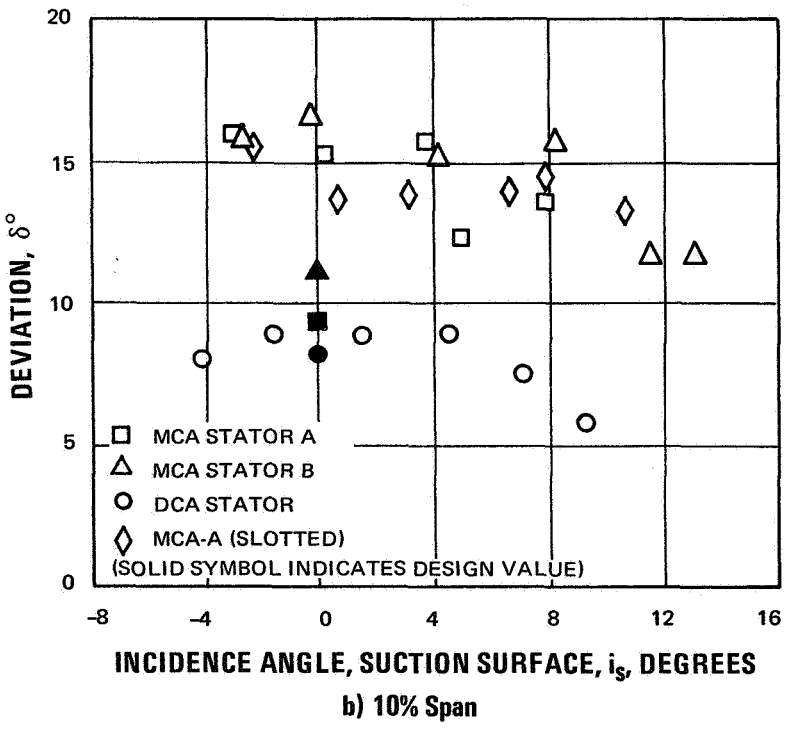

b) 10% Span

Figure 38 Stator Deviation vs. Incidence, 100% Design Speed

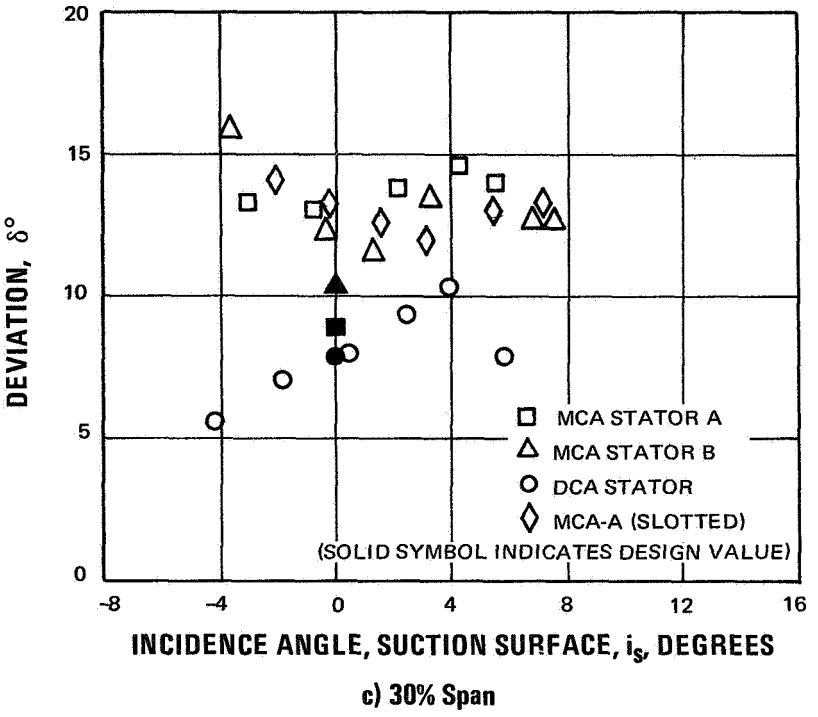

c) 30% Span

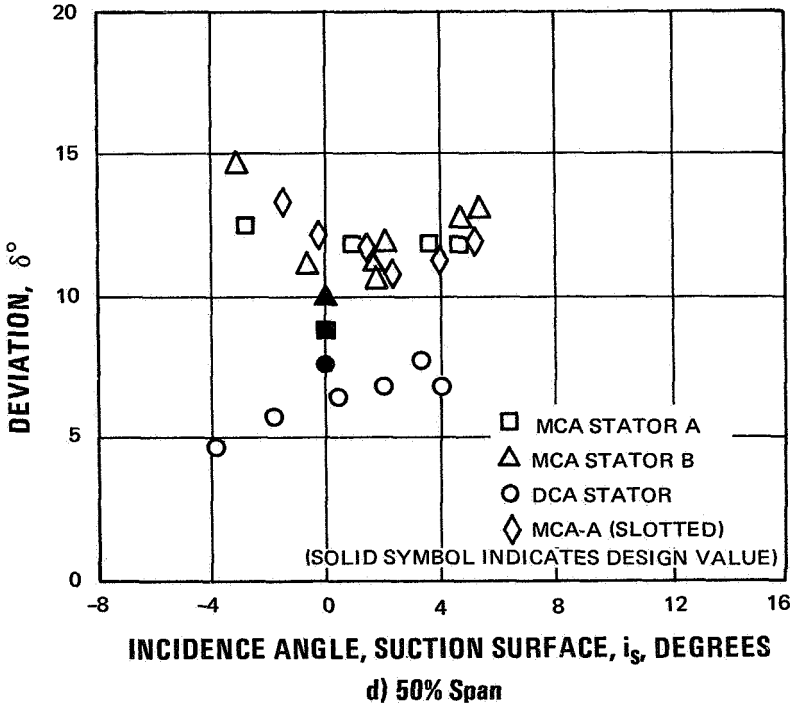

d) 50% Span

Figure 38 Stator Deviation vs. Incidence, 100% Design Speed

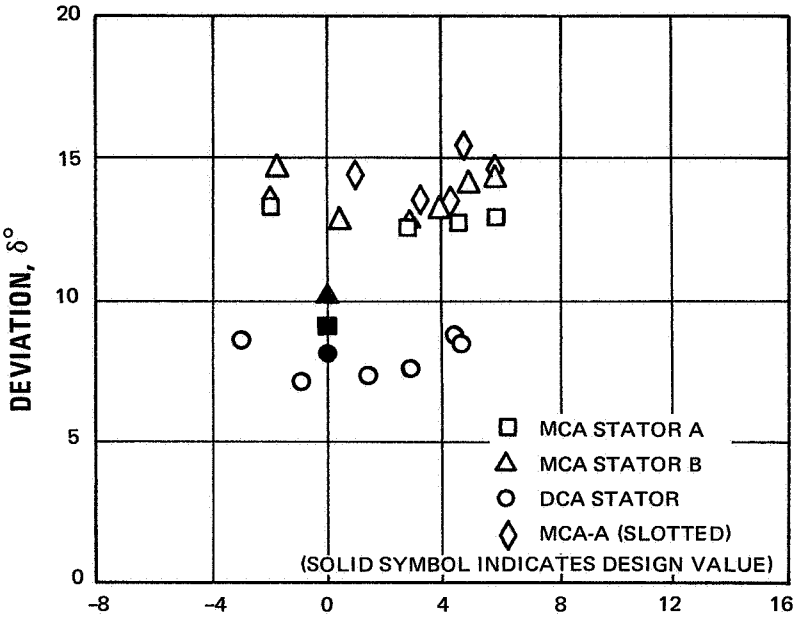

e) 70% Span

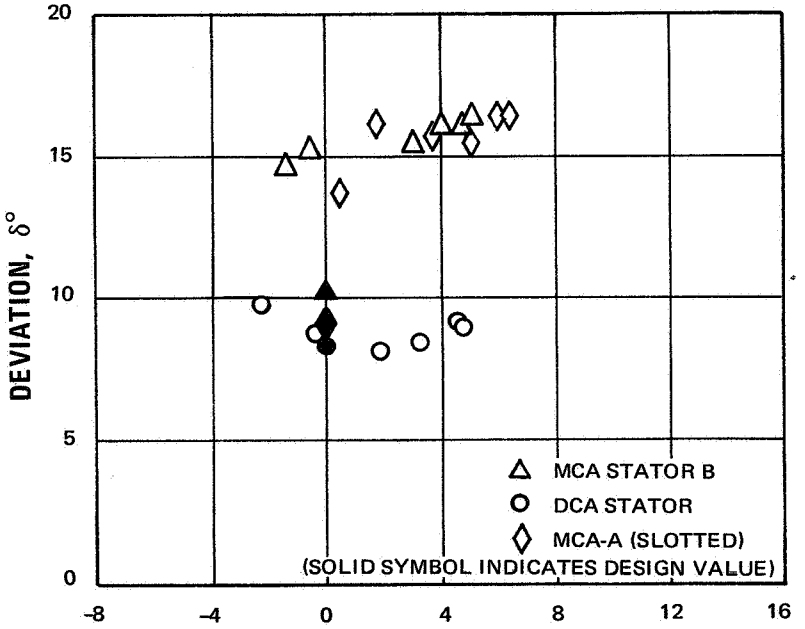

f) 80% Span

Figure 38 Stator Deviation vs. Incidence, 100% Design Speed

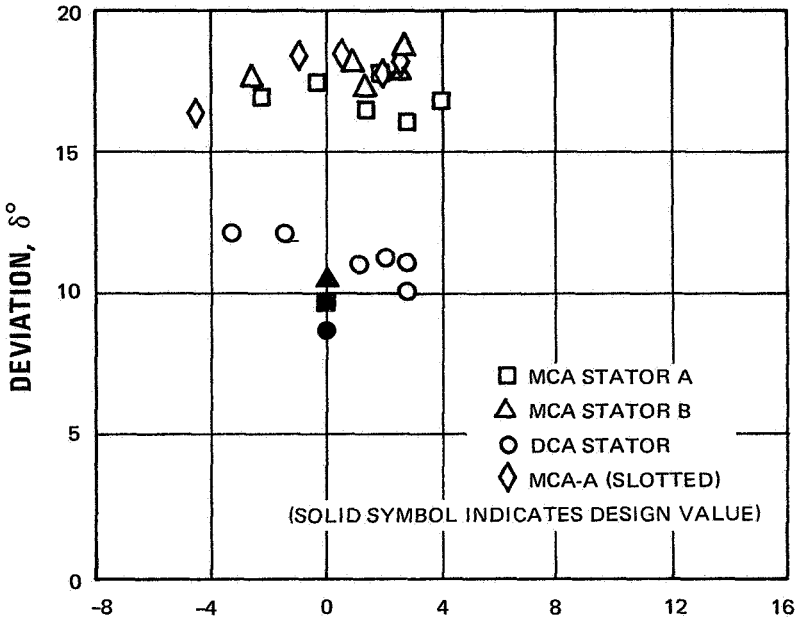

g) 90% Span

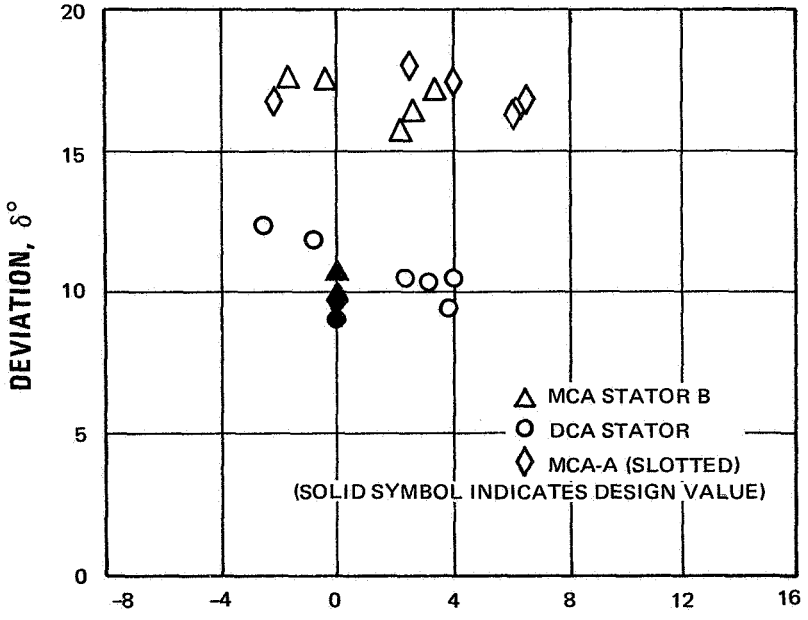

h) 95% Span

Figure 38 Stator Deviation vs. Incidence, 100% Design Speed

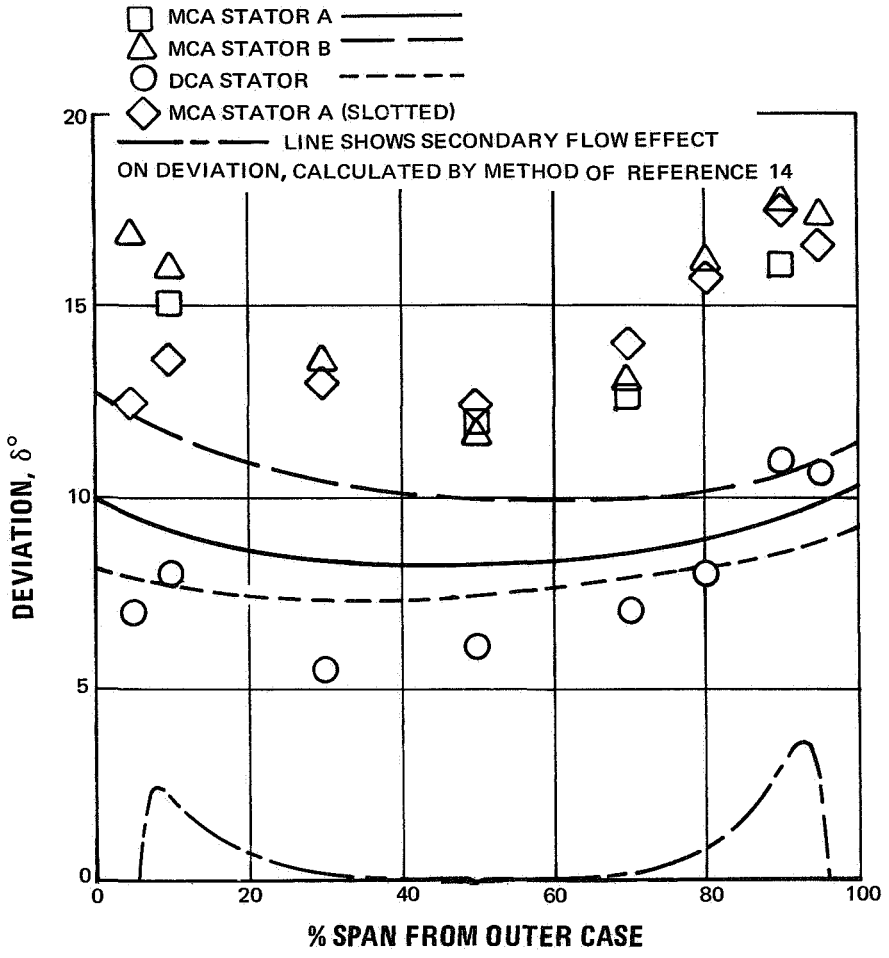

Figure 39 Deviation Angle at Stator Minimum Loss vs. Percent Span, 100% Design Speed

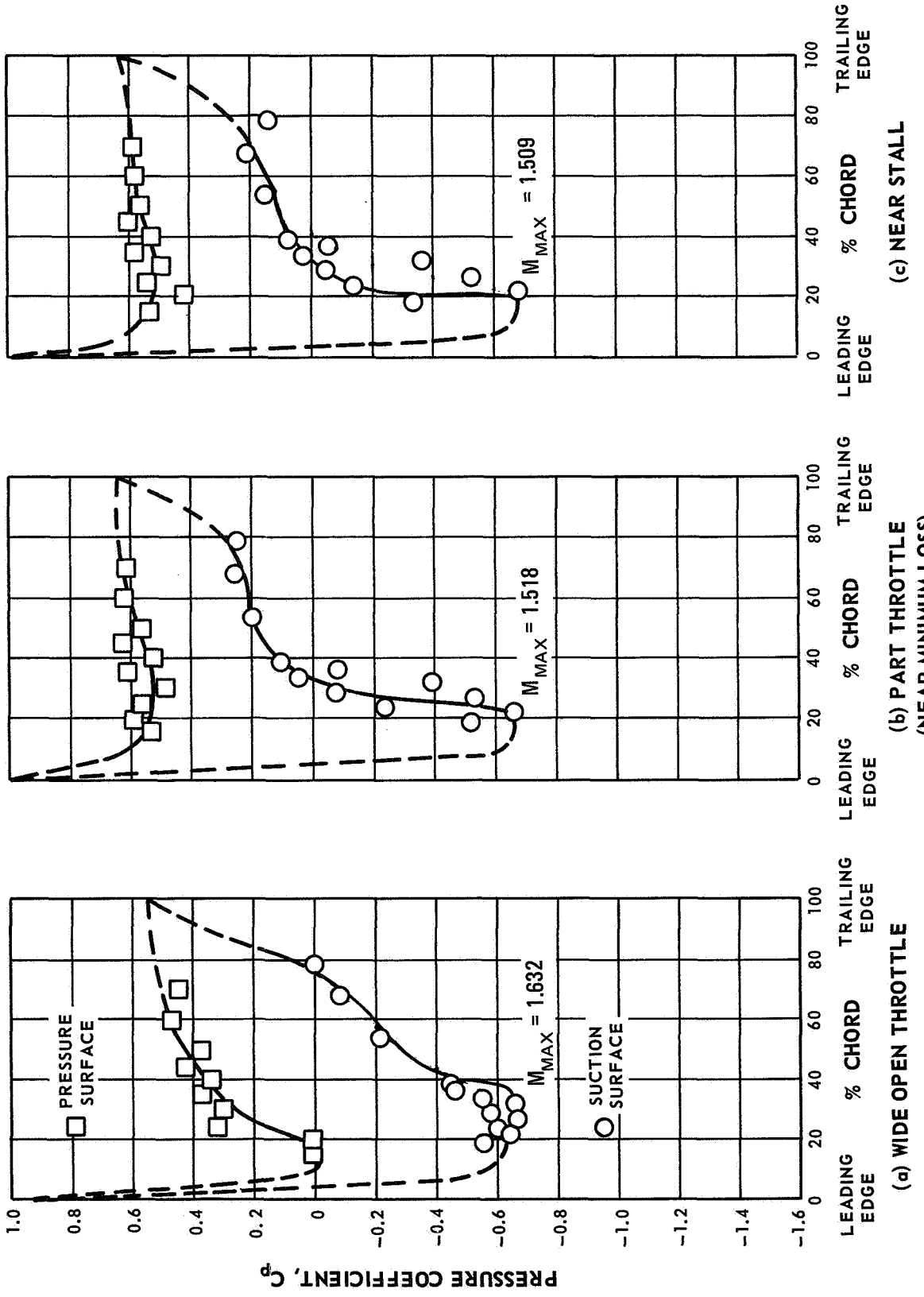

Figure 40 DCA Stator, Pressure Coefficient (C_p) vs. Percent Chord, 100% Design Speed, 90% Span

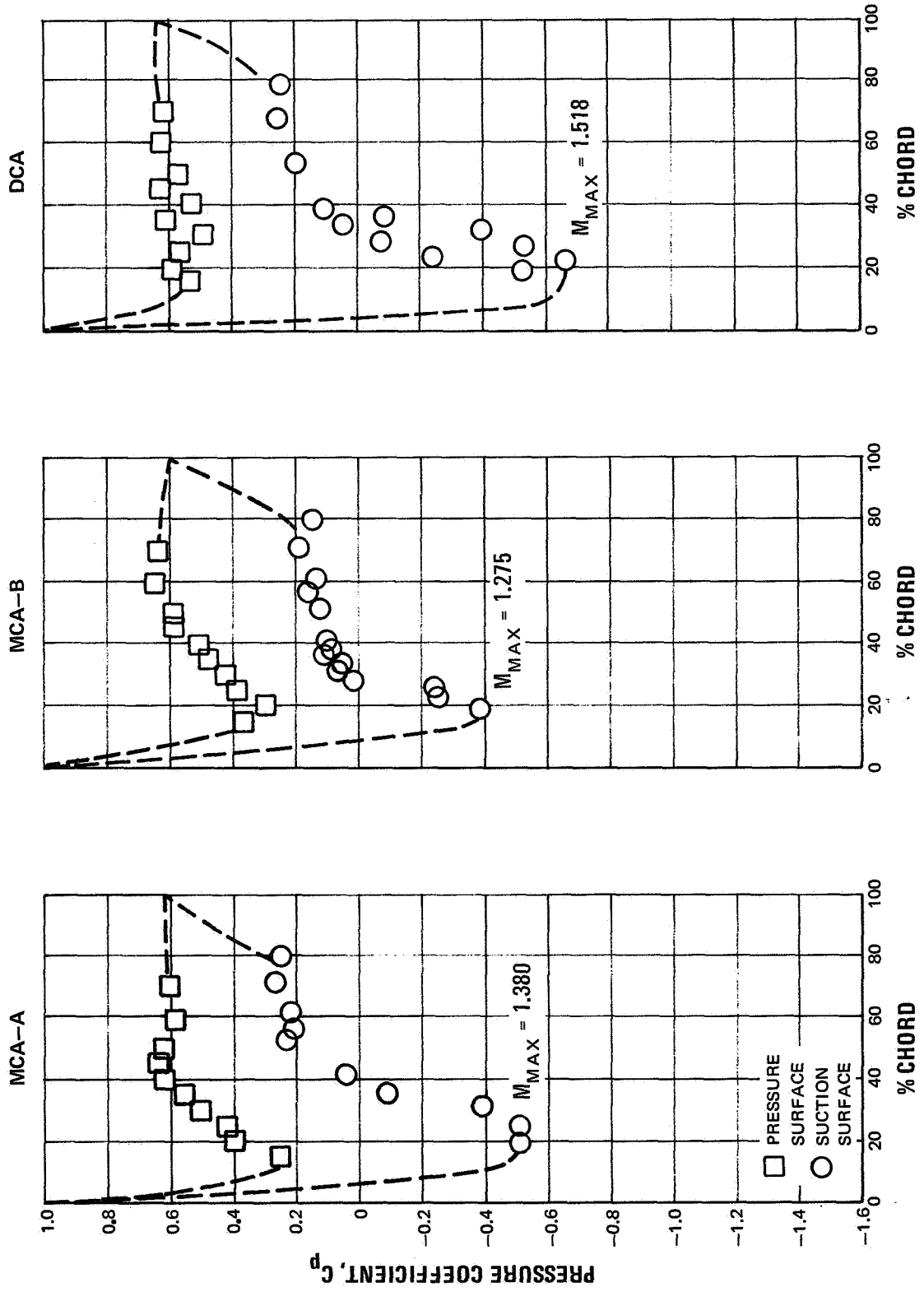

Figure 41 Stator Pressure Coefficients vs. Percent Chord, Near Design Incidence, 100% Design Speed, 90% Span

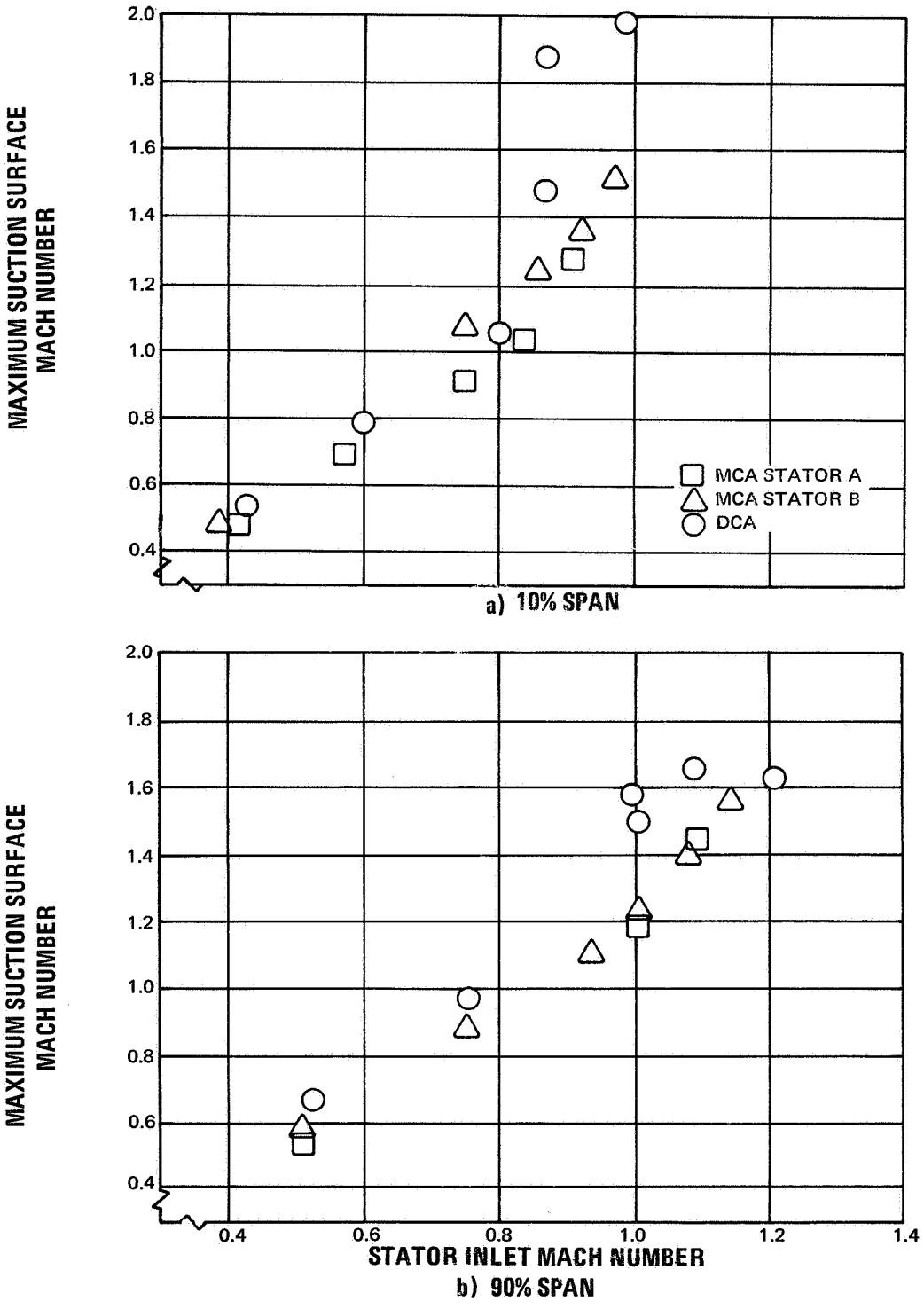

Figure 42 Maximum Suction Surface Mach Number vs. Stator Inlet Mach Number for Minimum Loss Data Points

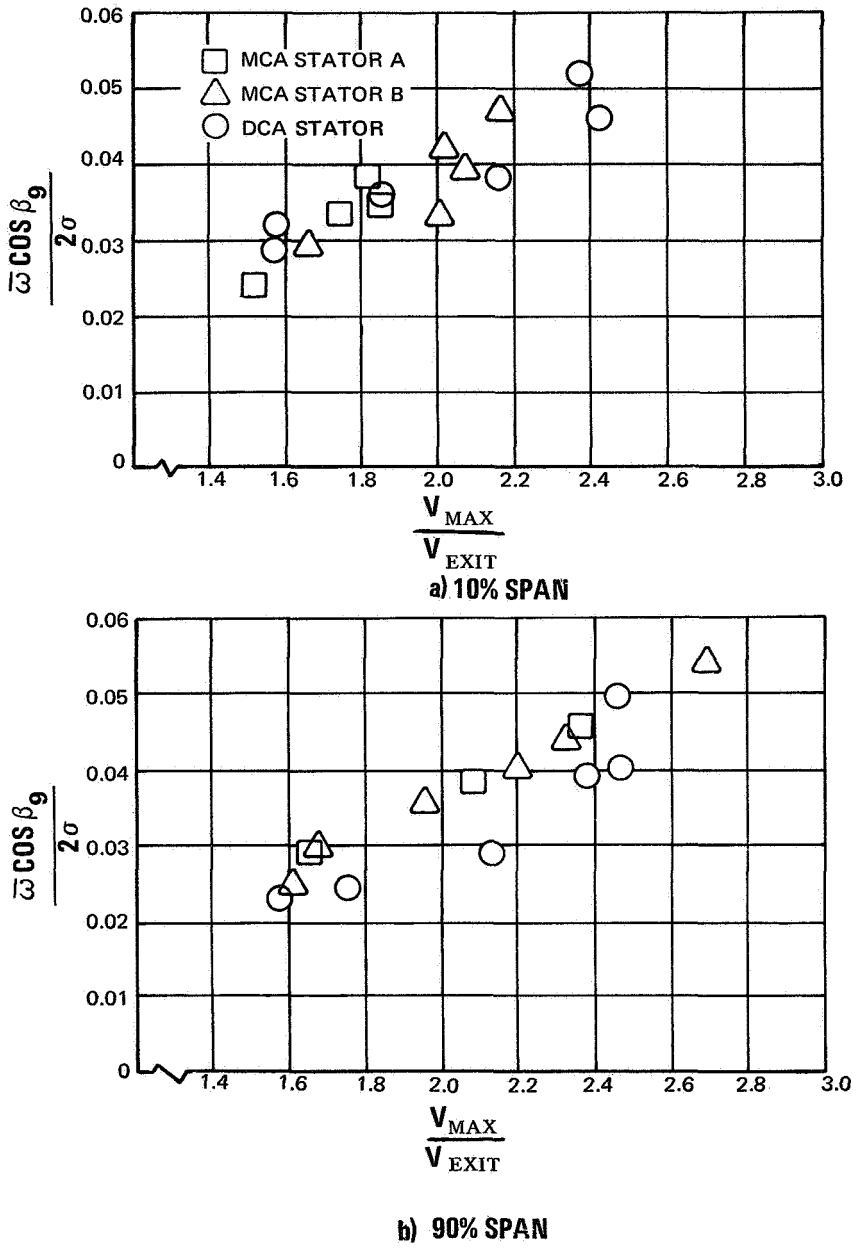

Figure 43 Stator Loss Parameter vs. V_{max} /V_{exit} for Minimum Loss Data Points

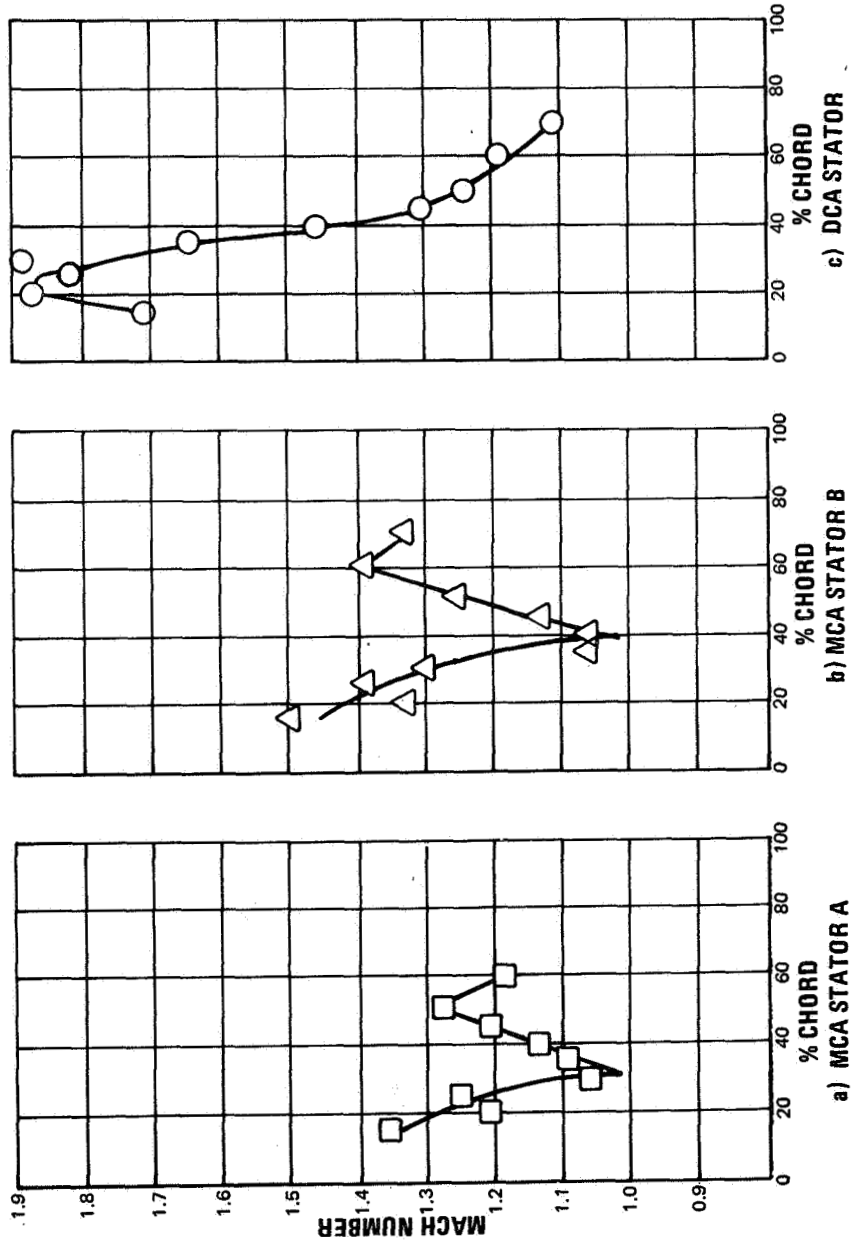

Figure 44 Stator Suction Surface Mach Number Distributions, 110% Design Speed, 10% Span, Open Throttle

DISTRIBUTION LIST

1. NASA Lewis Research Center
   21000 Brookpark Road
   Cleveland, Ohio 44135
   Attention:

Report Control Office Mail Stop 5-5	(1)	C. L. Ball Mail Stop 5-9	(1)
Technical Utilization Office Mail Stop 3-19	(1)	L. Reid Mail Stop 5-9	(1)
Library Mail Stop 60-3	(2)	J. H. DeFord Mail Stop 77-3	(1)
Fluid System Components Division Mail Stop 5-3	(1)	S. Lieblein Mail Stop 54-6	(1)
Pump and Compressor Branch Mail Stop 5-9	(6)	C. L. Meyer Mail Stop 60-4	(1)
A. Ginsburg Mail Stop 5-3	(1)	J. H. Povolny Mail Stop 60-4	(1)
M. J. Hartmann Mail Stop 5-9	(1)	A. W. Goldstein Mail Stop 7-1	(1)
W. A. Benser Mail Stop 5-9	(1)	J. J. Kramer Mail Stop 7-1	(1)
D. M. Sandercock Mail Stop 5-9	(1)	W. L. Beede Mail Stop 5-3	(1)
L. J. Herrig Mail Stop 5-9	(1)	C. H. Voit Mail Stop 5-3	(1)
T. F. Gelder Mail Stop 5-9	(1)	J. H. Childs Mail Stop 60-4	(1)
E. E. Bailey Mail Stop 5-9	(1)		

DISTRIBUTION LIST (Cont'd)

2. NASA Scientific and Technical Information Facility (6)
P. O. Box 33
College Park, Maryland 20740
Attention: NASA Representative

3. FAA Headquarters
800 Independence Ave. S.W.
Washington, D. C. 20553
Attention: Brig. General J. C. Maxwell (1)
F. B. Howard (1)

4. NASA Headquarters
Washington, D. C. 20546
Attention: N. F. Rekos (RAP) (1)

5. U. S. Army Aviation Material Laboratory
Fort Eustes, Virginia
Attention: John White (1)

6. Headquarters
Wright Patterson AFB, Ohio 45433
Attention: J. L. Wilkins, SESOS (1)
S. Kobelak, APTP (1)
R. P. Carmichael, SESSP (1)

7. Department of Navy
Bureau of Weapons
Washington, D. C. 20525
Attention: Robert Brown, RAPP14 (1)

8. Department of Navy
Bureau of Ships
Washington, D. C. 20360
Attention: G. L. Graves (1)

9. NASA-Langley Research Center
Technical Library
Hampton, Virginia 23365
Attention: Mark R. Nichols (1)
John V. Becker (1)

DISTRIBUTION LIST (Cont'd)

10. Boeing Company
Commercial Airplane Division
P. O. Box 3991
Seattle, Washington 98124
Attention: C. J. Schott MS80-66 (1)

11. Douglas Aircraft Company
3855 Lakewood Boulevard
Long Beach, California 90801
Attention: J. E. Merriman (1)
Technical Information Center C1-250

12. Pratt & Whitney Aircraft
Florida Research & Development Center
P. O. Box 2691
West Palm Beach, Florida 33402
Attention: R. A. Schmidtke (1)
H. D. Stetson (1)
J. M. Silk (1)
W. R. Alley (1)
R. W. Rockenbach (1)
B. A. Jones (1)
B. S. Savin (1)
J. A. Fligg (1)

13. Pratt & Whitney Aircraft
400 Main Street
East Hartford, Connecticut
Attention: A. W. Stubner (1)
W. D. Harshbarger (1)
P. Tramm (1)
M. J. Keenan (1)
B. B. Smyth (1)

14. Allison Division, GMC
Department 8894, Plant 8
P. O. Box 894
Indianapolis, Indiana 46206
Attention: J. N. Barney (1)
R. H. Carmody (1)
G. E. Holbrook (1)
B. A. Hopkins (1)
Library (1)

DISTRIBUTION LIST (Cont'd)

15. Northern Research and Engineering
219 Vassar Street
Cambridge 39, Massachusetts
Attention: R. A. Novak (1)
K. Ginwala (1)

16. General Electric Company
Flight Propulsion Division
Cincinnati 15, Ohio
Attention: J. W. Blanton J-19 (1)
W. G. Cornell K-49 (1)
J. R. Erwin J-162 (1)
E. E. Hood/J. C. Pirtle J-165 (1)
J. F. Klapproth H-42 (1)
J. W. McBride H-44 (1)
L. H. Smith H-50 (1)
S. N. Suciu H-32 (1)
J. B. Taylor J-168 (1)
Technical Information Center N-32 (1)

17. General Electric Company
1000 Western Avenue
West Lynn, Massachusetts
Attention: D. P. Edkins - Bldg. 2-40 (1)
F. F. Ehrich - Bldg. 2-40 (1)
L. H. King - Bldg. 2-40 (1)
R. E. Neitzel - Bldg. 2-40 (1)
Dr. C. W. Smith Library Bldg. 2-40M (1)

18. Curtiss-Wright Corporation
Wright Aeronautical
Woodridge, New Jersey
Attention: S. Lombardo (1)
G. Provensale (1)
J. Wiggins (1)

19. AiResearch Manufacturing Company
402 South 36th Street
Phoenix, Arizona 85034
Attention: Robert O. Bullock (1)
John H. Deman (1)

DISTRIBUTION LIST (Cont'd)

20. AiResearch Manufacturing Company
8951 Sepulveda Boulevard
Los Angeles, California 90009
Attention: Linwood C. Wright (1)

21. Union Carbide Corporation
Nuclear Division
Oak Ridge Gaseous Diffusion Plant
P. O. Box "P"
Oak Ridge, Tennessee 37830
Attention: R. G. Jordan (1)

22. Avco Corporation
Lycoming Division
550 South Main Street
Stratford, Connecticut
Attention: Clause W. Bolton (1)

23. Continental Aviation & Engineering Corporation
12700 Kercheval
Detroit, Michigan 48215
Attention: Eli H. Benstein (1)
Howard C. Walch (1)

24. Solar
San Diego, California 92112
Attention: P. A. Pitt (1)
Mrs. L. Walker (1)

25. Goodyear Atomic Corporation
Box 628
Piketon, Ohio
Attention: C. O. Langebrake (2)

26. Iowa State University of
Science and Technology
Ames, Iowa 50010
Attention: Professor George K. Serovy
Dept. of Mechanical Engineering (1)

DISTRIBUTION LIST (Cont'd)

27. Hamilton Standard Division of
United Aircraft Corporation
Windsor Locks, Connecticut
Attention: Mr. Carl Rohrbach
Head of Aerodynamics and Hydrodynamics (1)

28. Westinghouse Electric Corporation
Small Steam and Gas Turbine Engineering B-4
Lester Branch
P. O. Box 9175
Philadelphia, Pennsylvania 19113
Attention: Mr. S. M. DeCorso (1)

29. J. Richard Joy
Supervisor, Analytical Section
Williams Research Corporation
P. O. Box 95
Walled Lake, Michigan (1)

30. Raymond S. Poppe
Building 541, Dept. 80-91
Lockhead Missile and Space Company
P. O. Box 879
Mountain View, California 94040 (1)

31. James D. Raisbeck
The Boeing Company
224 N. Wilkinson
Dayton, Ohio 45402 (1)

32. James Furlong
Chrysler Corporation
Research Office
P. O. Box 1118
Detroit, Michigan 48231 (1)

33. Elliott Company
Jeannette, Pennsylvania 15644
Attention: J. Rodger Schields
Director-Engineering (1)

DISTRIBUTION LIST (Cont'd)

34. California Institute of Technology
Pasadena, California 91109
Attention: Professor Duncan Rannie (1)

35. Massachusetts Institute of Technology
Cambridge, Massachusetts 02139
Attention: Professor Jack Kerrebrock
Director, Gas Turbine Laboratory (1)

36. General Electric Company
Aircraft Engine Group
1 Jimson Road
Cincinnati, Ohio 45215
Attention: Marlen Miller, H-50 (1)